Interaction of motion and perception in continuous attractor representations of position.

Dmitry Laptev

University College London

Thesis submitted to University College London for the

Degree of Doctor of Philosophy

ProQuest LLC
789 East Eisenhower Parkway
P.O. Box 1346
Ann Arbor, MI 48106-1346

I, Dmitry Laptev, confirm that the work presented in this thesis is my own. Where information has been derived from other sources, I confirm that this has been indicated in the thesis.

20th December 2007

Acknowledgements

I wish to thank the MRC, CoMPLEX and my supervisor Neil Burgess for funding me and providing with the opportunity to carry out this research. I also wish to thank Neil Burgess for all the support and guidance he had given me throughout the period.

I would like to express my gratitude to Peter Dayan, Richard Clement, Peter Latham, Patrick Byrne, Ali Jeewajee, Caswell Barry, Christian Doeller, John O'Keefe, Tom Hartley, John King for their advice and help with the research. I also would like to thank the administrative staff at the ICN for providing me with a work place and necessary support.

Abstract

The simple relationship of movement to position via temporal integration helps to explain some of the neural representations of position seen in the mammalian brain, such as the representations of eye-position, and of head-direction and self-location within an environment. The positional information also comes from perception, such as vision, and the two sources need not necessarily agree. I construct neuronal firing rate models (introduced in Chapter 2) that utilize both velocity and visual inputs, and test them against physiological data acquired in situations when the two inputs are put in conflict.

I start with a model of the oculomotor system (Chapter 3), in which a visual target and integration of the motion signal play distinct roles. The model represents a continuous attractor, stable and unstable regimes of which are analyzed with the latter found to correspond to different clinical disorders.

In Chapters 4 to 6 continuous attractors are used to model hippocampal systems for the representation of the animal's location within its environment. Chapter 4 describes the 'standard' model of the integration of self-motion information to maintain a representation of current location in the firing of hippocampal 'place cells'. I demonstrate the stability and invariance under translation of this representation under the model. Using this model, I then consider how abstracted sensory information concerning environmental location is combined with self-motion information to provide the representation of location (Chapter 5). The model is tested by simulation of experimental data on place cell firing in situations where both types of information are put into conflict.

Chapter 6 investigates whether the integration of self-motion and environmental information into a single coherent representation could result from a reciprocal interaction between place cells and the recently discovered 'grid cells' in Entorhinal cortex. In this model, integration of self-motion occurs between grid cells and projections from grid cells to place cells provide the self-motion contribution to place cell firing. Conversely, sensory inputs contribute to place cell firing and projections from place cells to grid cells maintain the stability of grid cell firing relative to the environment. This model is tested against experimental data on both place cell firing and grid cell firing in situations where environmental and self-motion information are put into conflict. Testable predictions for future experimental studies are generated by the model.

In Chapter 7 we discuss the relationship of our findings to other related approaches, and their implications for the neural organization of spatial behavior.

Table of contents

1. Introduction.

This thesis concerns how the mammalian brain determines the position of the eyes relative to the head and to the visual scene, and of the body relative to the external world, on the basis of internal signals related to motion and on the basis of external perceptual signals from the world. This problem is related to the famous problem of visual constancy which has interested psychologists at an abstract level for more than a century, i.e., how visual information gives rise to the percept of a stable external world despite the movements of the eye, head and body. In this context it has long been recognized, from theoretical considerations, that incoming perceptual information must be combined with internal information concerning one's own movement (e.g. Helmholtz, 1866). The last few decades have seen great progress in measuring the neurophysiological processes underlying eye movement, self-motion, and our sense of orientation and location. As a result, the opportunity now exists for gaining a quantitative understanding of the neuronal mechanisms which enable the integration of perceptual and motion-related information in determining position.

The approach I take is that of computational modeling of some of the neuronal processes supporting the determination of eye position and self-location. The particular power of the computational modeling approach is that it enables us to make quantitative predictions, due to the fact that the mechanism of interest can be precisely specified, rather than merely verbally described. Advances in our understanding of the detailed neurophysiology at work (e.g. behavioral correlates of neuronal firing, long-term synaptic potentiation, etc.) have begun to enable the development of computational models which are both faithful to the observed electrical activity of neurons and provide insights into the behaviors they generate.

Studying patterns of neuronal firing significantly helps us to understand the algorithms generating them – an advantage that the previous psychologists did not have. The firing rate models that I use are intended to capture enough of the dynamics of neuronal electrical activity needed to investigate the interaction of perceptual and motion-related information in determining location, while avoiding unnecessary details of the underlying neurophysiology. The particular level of modeling is selected in order to make contact with the neurophysiological data to be modelled, but not any of the other aspects of the data, e.g. using firing rates rather than the detailed temporal properties of firing and ignoring the details of synaptic plasticity like spike-timing dependent plasticity. Some of these are important in other models (e.g. Burgess, Barry, O'Keefe, 2007), but it is up to the modeller to decide which are the critical data for their specific model; an important choice to make, with no guarantee of that it will be the correct one.

The relatively simpler oculomotor system for the generation of fast eye movements to visual targets, known as saccades, is the subject of the first section of the thesis. The idea is first to construct a new firing rate model of the saccadic system, which is physiologically plausible and could emulate the behavior of the normal functioning system in humans. This approach allows us to test the current hypothesis about the mechanism of the saccadic system. Then, in the model able to reproduce the behavior of the normal functioning system, we can try to reproduce the behavior observed in different clinical disorders by varying certain model parameters. This allows us to investigate the possible underlying causes of those disorders.

The relatively more complex hippocampal system for representing self-location is then the focus for the main part of the rest of the thesis. The place cells in the rat

hippocampus show strong behavioral correlates by firing only when the animal visits a particular localised region of the surrounding environment (e.g., O'Keefe, 1976). Therefore these cells are chosen as the basis for our firing rate model of self location. The place cell firing is assumed to be driven by both external perceptual information and internal self-motion information. Simulations of situations when the two sources of information are put in conflict, allow us to test our hypothesis about the mechanism by which these types of information might give rise to place cell firing. Our second, more advanced, model is designed to also incorporate another, recently discovered, type of cells with spatial correlates of firing. These cells are known as grid cells, due to the fact that they fire whenever a rat enters one of an array of locations arranged in a triangular or hexagonal grid (Hafting et al., 2005). We assume that these cells provide a substrate for path integration, and interact with place cells which receive external visual inputs. The animal position is hypothesized to be determined on the basis of this interaction. This hypothesis can be investigated by testing the model against firing rate data from the experiments in which the external and self-motion information are put in conflict. Hopefully the model will also be capable of generating some predictions which then could be tested in future animal recording and behavioral studies in order to further verify, or modify, the hypothesis.

In both eye movement and self location systems, the concept of an "attractor" in the representational space of the system provides a key insight into how it behaves. It is interesting to note that, despite the different physiologies of the systems, the main features of the way the hippocampal model of self location keeps track of location following whole-body motion were derived from a model initially proposed for the generation of eye movements in the superior colliculus (Droulez and Berthoz, 1991).

This perhaps reflects the presence of the common issue of integration of motion and perception in both systems.

2. Analysis of firing rate models of neuronal networks.

In this type of model both the output from and the input to a neuron, are simply characterised by their firing rates. No attempt is made to model the details of the generation of individual action potentials. For details see Dayan and Abbott (2001).

2.1 A basic firing rate model.

2.1.1 The total synaptic current to a neuron.

A given neuron receives synaptic inputs from N other neurons in the network. When an action potential arrives at an input b (b=1to N) at time 0, it is assumed to generate a synaptic current $I_s = w_b K_s(t)$ in the soma of the postsynaptic neuron. Here w_b is the synaptic weight and $K_s(t)$ is called the synaptic kernel. The amplitude and sign of the synaptic current generated by input b are determined by w_b. For excitatory synapses, $w_b > 0$, and for inhibitory synapses, $w_b < 0$. The probability of transmitter release from a presynaptic terminal is included in the synaptic weight factor w_b in this case.

The synaptic kernel, $K_s(t) \geq 0$, describes the time course of the synaptic current generated by a presynaptic spike arriving at time $t = 0$. The synaptic kernel most frequently used in firing-rate models is an exponential, $K_s(t) = \exp(-t/\tau_s)/\tau_s$, where τ_s

is usually close to the time constant that describes the decay of the synaptic conductance. For simplicity, the same function $K_s(t)$ is used to describe all synapses. Assuming that the effects of the spikes at a single synapse sum linearly, the total synaptic current at time t resulting from a sequence of presynaptic spikes occurring at input b at times t_i is given by:

$$I_s = w_b \int_{-\infty} d\tau K_s(t-\tau)\rho_b(\tau) \tag{2.1}$$

with $\rho_b(\tau) = \sum_i \delta(\tau - t_i)$ representing the sequence of spikes fired by a presynaptic neuron b. The total synaptic current coming from all N presynaptic inputs is then obtained by summing:

$$I_s = \sum_{b=1}^{N} w_b \int_{-\infty} d\tau K_s(t-\tau)\rho_b(\tau) \tag{2.2}$$

In the firing-rate models, the actual spike sequence $\rho_b(\tau)$, generated by neuron b, is approximated by its firing rate $u_b(\tau)$, which is obtained by averaging $\rho_b(\tau)$ over multiple trials. So we have:

$$I_s = \sum_{b=1}^{N} w_b \int_{-\infty} d\tau K_s(t-\tau)u_b(\tau) \tag{2.3}$$

If we take the derivative of the above equation with respect to t, we get a dynamical expression for I_s:

$$\tau_s \frac{dI_s}{dt} = -I_s + \sum_{b=1}^{N} w_b u_b = -I_s + \vec{w} \cdot \vec{u} \tag{2.4}$$

where $\vec{w} \cdot \vec{u}$ is the dot product of the weight $\vec{w}$ and input $\vec{u}$ vectors.

2.1.2 Firing rate of the neuron.

For constant synaptic current, the postsynaptic neuron firing rate can be expressed as $r = F(I_s)$, where F is the steady-state firing rate as a function of somatic current I_s. F sometimes is taken to be a saturating function, e.g. sigmoid or Naka-Rushton (Naka and Rushton, 1966) function, which can be important in stabilising a network against excessively high firing rates.

When the total synaptic current changes over time, the firing rate does not follow these changes instantaneously. Instead, due to the properties of the neuronal membrane, the firing rate becomes a low-pass filtered version of I_s. Therefore time-dependent firing rate is often modelled as a low-pass filtered version of the steady-state firing rate:

$$\tau_r \frac{dr}{dt} = -r + F(I_s(t)) \tag{2.5}$$

The time constant τ_r here determines how rapidly the firing rate approaches its steady-state value for constant I_s, and, consequently, how closely r can follow rapid changes in $I_s(t)$.

Thus, the firing rate model consists of the pair of equations (2.4) and (2.5). If one of these two equations relaxes to its equilibrium point much faster than the other, the model can be reduced to just one equation. If, for example, $\tau_r << \tau_s$, we can assume

that $\tau_r \frac{dr}{dt} \approx 0$, and the second dynamic equation reduces to the static case $r = F(I_s(t))$. If, on the other hand, $\tau_r >> \tau_s$, we can make the approximation that the first equation reaches equilibrium instantaneously. Then we can make the replacement $I_s = \vec{w} \cdot \vec{u}$ in the equation (2.5), and the model reduces to a single equation:

$$\tau_r \frac{dr}{dt} = -r + F(\vec{w} \cdot \vec{u}) \tag{2.6}$$

We assume that in the place cell network $\tau_r >> \tau_s$ and therefore build the dynamical model of the network on the basis of the equation (2.6).

2.2 Neuronal networks that integrate their inputs.

Two of the main classes of connections between cortical neurons are feedforward and recurrent synapses. Feedforward connections bring input to a given region from another region located upstream along a particular processing pathway. Recurrent synapses interconnect neurons within a particular region that are regarded to be at the same stage along the processing pathway.

The network incorporating both, the feedforward and recurrent connectivity, can be described by the following firing-rate equation:

$$\tau_r \frac{d\vec{r}}{dt} = -\vec{r} + F(\overline{W}\vec{r} + \overline{M}\vec{u}) \tag{2.7}$$

Here $\overline{M}$ is the matrix of the feedforward connection weights from the layer of input neurons $\vec{u}$ to the layer of output neurons $\vec{r}$. The matrix component M_{ab} represents the strength of the synapse from input neuron b to output neuron a. The product $\overline{M}\vec{u}$ gives the vector with components $\sum_b M_{ab}u_b$ for $a = 1,2,\ldots,N_v$. This vector is often defined as $\vec{h} = \overline{M}\vec{u}$. Likewise, $\overline{W}$ is the recurrent weight matrix with the matrix component $W_{aa'}$ representing the strength of the synapse from the neuron a' to the neuron a in the output layer of the network.

For the linear response function F, it can be shown mathematically (see Dayan and Abbott (2001), p 245-248) that, if the recurrent synaptic weights are chosen so that one of the eigenvalues of the matrix $\overline{W}$ is exactly equal to one, $\lambda_1=1$, and all the others are less than one, the network will integrate the projection of the input vector $\vec{h}$ onto the corresponding eigenvector $\vec{e}_1$:

$$\vec{v}(t) \approx \frac{\vec{e}_1}{\tau_r} \int_0 dt' \vec{e}_1 \cdot \vec{h}(t') \tag{2.8}$$

As can be seen from the above equation, if the external input $\vec{h}$ goes to zero at some point, the network activity does not cease. The network thus sustains its activity in the absence of external input, which provides a memory for the integral of prior input. If the function F is non-linear, then the restriction for some of the eigenvalues being exactly one, and the others less than one, no longer applies, though the ability of the network to integrate feedforward inputs obviously still depends on the appropriately chosen weight matrix $\overline{W}$.

2.3 Stability of neuronal representations.

The system of coupled differential equations (2.7) provides a description of the way in which the neural network changes from one state to the next. When the left-hand side of the system (2.7) is equal to zero, there is no change in the firing rates of the network neurons over time, $d\vec{r}/dt = \vec{0}$. The dynamic variables remain at constant values and the system is said to be at equilibrium, or at a fixed point. Once at this point, the system will stay there indefinitely, unless perturbed. This fixed point can either be stable or unstable. If the point is stable, the system, when in its vicinity, will be attracted towards the point and gradually relax onto it. If the point is unstable, the system, once perturbed from equilibrium state, will be pushed further away from it.
It is important to know the stability properties of equilibrium points, since they determine the long-term behaviour of the system. Local stability analysis can be used to determine whether a fixed point is stable or unstable. This stability analysis is based on first approximating the system of nonlinear differential equations by a linear one in the neighbourhood of the system equilibrium point. This linear system is then inspected in order to determine the stability of the point.
This type of analysis can be demonstrated on the example of the following nonlinear system, comprised of two coupled ordinary differential equations:

$$\begin{aligned} \frac{dr_1}{dt} &= F(r_1, r_2) \\ \frac{dr_2}{dt} &= G(r_1, r_2) \end{aligned} \qquad (2.10)$$

where F and G can be any of a wide range of nonlinear functions of r_1 and r_2, but they must have certain properties to ensure that (2.10) will have unique solutions. Let us

assume that the nonlinear system (2.10) has an equilibrium point (r_1^*, r_2^*) for which $F(r_1^*, r_2^*) = G(r_1^*, r_2^*) = 0$. In order to approximate the nonlinear functions $F(r_1, r_2)$ and $G(r_1, r_2)$ by linear ones in the neighborhood of (r_1^*, r_2^*) we perform a Taylor expansion of the former. The Taylor expansion of the function $F(r_1, r_2)$ is:

$$F(r_1, r_2) = F(r_1^*, r_2^*) + \left.\frac{dF}{dr_1}\right|_{r_1^*, r_2^*} (r_1 - r_1^*) + \left.\frac{dF}{dr_2}\right|_{r_1^*, r_2^*} (r_2 - r_2^*) + \ldots, \tag{2.11}$$

where the dots represent higher-order terms, e.g. $\left.\frac{1}{2}\frac{d^2F}{dr_1^2}\right|_{r_1^*, r_2^*} (r_1 - r_1^*)^2$.

Since $F(r_1^*, r_2^*) = 0$, and since near equilibrium the higher-order terms contribution to the equation is negligible compared to the first-order terms, (2.11) can be approximated by a linear equation:

$$F(r_1, r_2) = \left.\frac{dF}{dr_1}\right|_{r_1^*, r_2^*} (r_1 - r_1^*) + \left.\frac{dF}{dr_2}\right|_{r_1^*, r_2^*} (r_2 - r_2^*) \tag{2.12}$$

A similar procedure can also be done for the $G(r_1, r_2)$ function. This results in the following system of two first order linear differential equations:

$$\begin{aligned} \frac{dR_1}{dt} &= AR_1 + BR_2 \\ \frac{dR_2}{dt} &= CR_1 + DR_2 \end{aligned} \tag{2.13}$$

where

$$R_1 = r_1 - r_1^*, \quad R_2 = r_2 - r_2^*, \tag{2.14}$$

and

$$A = \left.\frac{dF}{dr_1}\right|_{r_1^*, r_2^*} \qquad B = \left.\frac{dF}{dr_2}\right|_{r_1^*, r_2^*}$$
$$C = \left.\frac{dG}{dr_1}\right|_{r_1^*, r_2^*} \qquad D = \left.\frac{dG}{dr_2}\right|_{r_1^*, r_2^*} \tag{2.15}$$

The equation (2.13) can be written in vector notation as follows:

$$\frac{d}{dt}\begin{pmatrix} R_1 \\ R_2 \end{pmatrix} = \begin{pmatrix} A & B \\ C & D \end{pmatrix}\begin{pmatrix} R_1 \\ R_2 \end{pmatrix} \tag{2.16}$$

The matrix of first partial derivatives of F and G at (r_1^*, r_2^*) in (2.16) is called the *Jacobian.* The stability properties of the equilibrium point (r_1^*, r_2^*) of the system (2.16) and, accordingly, (2.10), can be determined by looking at the eigenvalues of the Jacobian. If both of the eigenvalues have negative real parts, the equilibrium is stable, and if any has a positive real part, the equilibrium is unstable.

3. Stability analysis of a model of saccadic eye movement.

This work has been accepted for publication (Laptev et al, 2006).

3.1 Introduction to saccadic eye movements and instabilities.

Saccades are the fast, conjugate eye movements which redirect gaze to bring a new part of the visual scene onto the foveal region. Saccades show a relatively invariant relationship between the size of the movement, and saccadic peak velocity and duration. In normal human subjects, the peak velocity of saccades varies from 30 to 700 deg/sec, and their duration varies from 30 to 100 msec for eye movements of 0.5 – 40 degrees in amplitude. The peak velocity progressively saturates with the saccade amplitude after about 20 degrees. (Carpenter 1988; Leigh and Zee 1999). This consistent relationship between amplitude, duration and peak velocity of saccades is termed the main sequence (Bahill et al. 1975). It can be used to judge whether a particular saccade is abnormal and to identify unknown types of eye movements as saccades. Figure 1 shows the time course of a number of human saccades of different amplitudes in the horizontal plane (saccades in other planes do not differ in their essential characteristics).

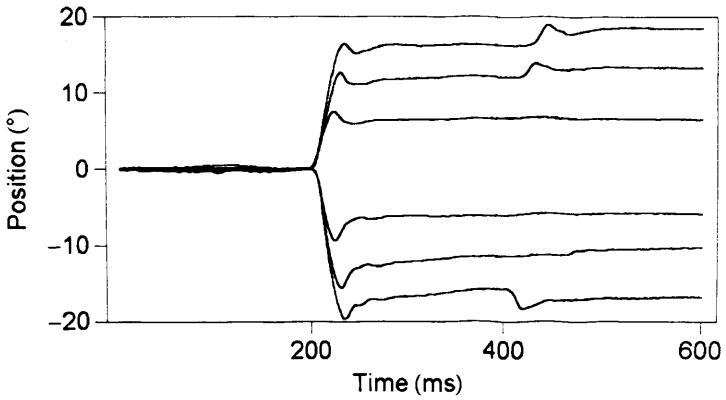

Figure 1. Saccades of different amplitudes to the left and to the right. A second, corrective, saccade can also be seen at the end of larger saccades. All the saccades in the figure are with the dynamic overshoot.

Despite the machine-like nature of most saccades, normal individuals often make anomalous saccadic eye movements. Amongst the most common anomalous movements are dynamic overshoots and square wave jerks. A dynamic overshoot occurs at the end of a saccade and consists of an overshoot followed by a small corrective saccade in the opposite direction (Abadi et al, 2000) (Figure 1). Square-wave jerks are conjugate, sporadic, involuntary, horizontal saccadic intrusions that interrupt fixation. They are comprised of a saccade that takes the eye away from the intended fixation position, followed about 200ms later by a saccade that returns the eye back to its initial fixation position (Abadi and Gowen 2004) (Figure 2).

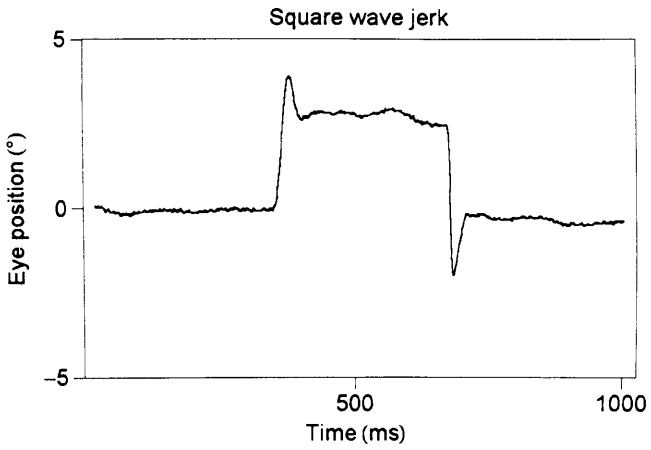

Figure 2. A square-wave jerk.

Saccadic oscillations, composed of back-to-back saccades, may be found in normal subjects as well as in patients with neurological disorders. Such saccadic oscillations are composed of multiple consecutive oppositely directed saccades, without an intersaccadic interval. This last feature distinguishes them from the square-wave jerk oscillations, in which there is typically an intersaccadic interval of about 200ms.

One of the types of these saccadic oscillations, that is observed among normal subjects, is *voluntary nystagmus*. Some individuals have the ability to generate bursts of high frequency oscillations of approximately 1 - 5° in amplitude (Ashe et al, 1991) (Figure 3).

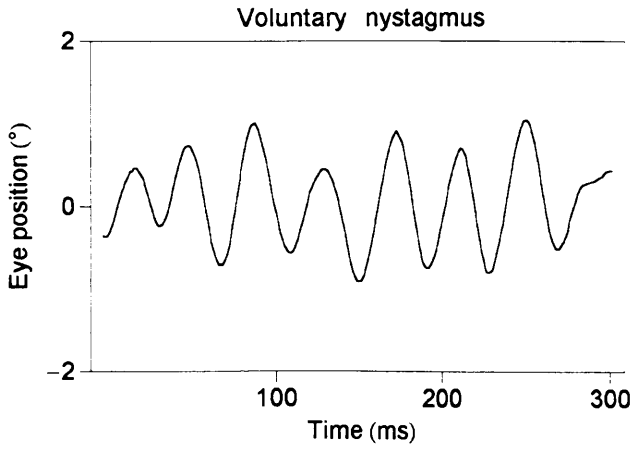

Figure 3. Voluntary nystagmus waveform.

One of the symptomatic saccadic oscillations, similar in appearance to voluntary nystagmus, is *ocular flutter*. It consists of bursts of back-to-back horizontal saccades, about 1 - 5° in amplitude, often precipitated by a change in gaze. The other symptomatic saccadic oscillation is *microsaccadic flutter*, which consists of back-to-back horizontal microsaccadic oscillations with a frequency of 15 – 30 Hz and amplitude of 0.1 – 0.5° (Ashe et al, 1991).

Inherent instabilities in the saccadic system were previously revealed by a model of the nonlinear dynamics of the system (Broomhead et al. 2000). The main criticism of this model, from a physiological standpoint, is that it does not explicitly include the action of the pause cells. In this work we investigate a role for the pause cells involving inhibition of the burst cells at the end of a saccade, and characterise the instabilities which can arise from their malfunction.

3.2 Physiology of the saccadic system.

3.2.1 Components and behavior of the saccadic system.

The eye movements are produced by six extraocular muscles that are attached to the outer wall of the eye (sclera). The medial and lateral rectus muscles produce predominately horizontal movements, the superior and inferior rectus muscles produce predominately vertical movements, and the superior and inferior oblique muscles produce mainly rotary movements. The muscles position is shown in Figure 4, which represents a transverse section through the skull. The extraocular muscles receive commands from motoneurons in the nuclei of the abducent, trochlear and

oculomotor nerves, which are located in the brain stem. The activity of these motoneurons is in turn coordinated by a distinct network of interconnected neuronal groups, which is determined by the particular type of eye movement. The saccadic system represents one of six such major preoculomotor networks and is designed for saccade generation.

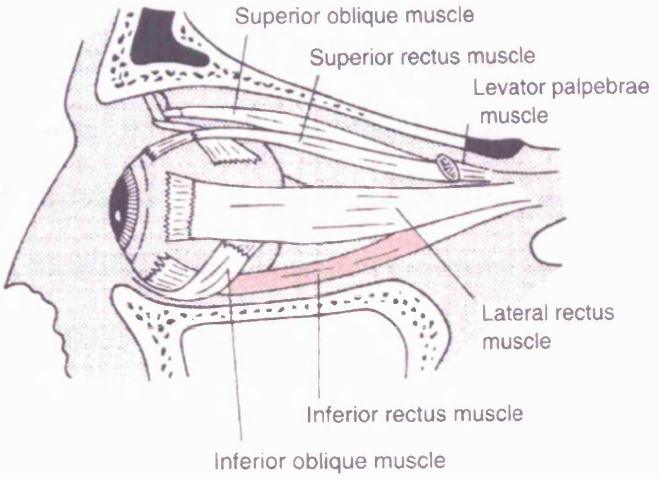

Figure 4. Transverse section through the scull, showing the extraocular muscles. The medial rectus is obscured from view by the eyeball.

The essential components of the network that generates saccades are burst neurons and omnipause neurons (Scudder et al. 2002; Sparks 2002). Burst neurons are subdivided into short-lead burst neurons and long-lead burst neurons. Short-lead burst neurons are silent during fixation and eye movements other than saccades. Just prior to and during the saccade they fire rapidly in a burst of activity. Long-lead burst neurons are also silent during steady fixation, but their firing rates increase well before the start of the saccade (up to 100 msec) and last throughout the saccade. Omnipause cells fire continuously except just before and during saccades in any direction, during which time they cease firing.

Saccades are initiated in response to signals from the visual cortex specifying the required displacement of the eyes. A brief trigger input inhibits the pause cells whereupon the short-lead burst cells start firing, initiating the saccade and further maintaining the inhibition of the pause cells. The burst of activity is subsequently integrated to produce a change in the tonic level of activity of cells in the nucleus prepositus hypoglossus. This tonic signal is required by the motoneurons for them to produce the additional force needed to hold the eye in its new position against orbital elastic restoring forces. When the required displacement has been made, the burst cells cease firing and the pause cells resume firing. The relationships between the firing patterns of the different types of neurons underlying the generation of saccades are shown schematically in Figure 5.

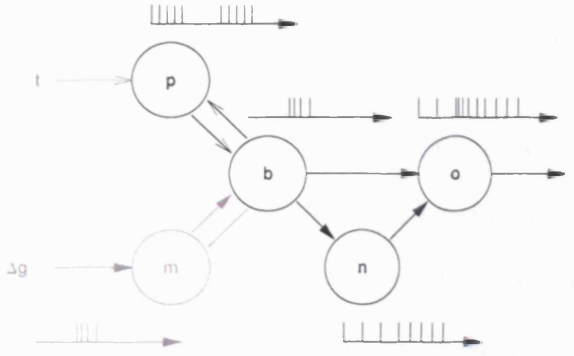

Figure 5. Schematic diagram of the brainstem circuitry involved in the generation of saccades. The pause cells (*p*) fire all the time except during a saccade. The short-lead burst cells (*b*) generate a burst of firing during the saccade. The neural integrator cells (*n*) produce a tonic change in firing rate proportional to the integral of the signal produced by the burst cells. The oculomotor neurons (*o*) produce a firing pattern equal to the sum of the burst and tonic responses. The motor error cells (*m*) fire in proportion to the difference between the actual eye position and target eye position.

Cells with this firing pattern have not been found experimentally, but the behaviour of these cells may form part of the behaviour of the long-lead burst neurons. The trigger input (t) is assumed to inhibit the pause cells at the beginning of a saccade and the input Δg specifies the amplitude of the saccade. The circuitry involved in the specification of the size and onset of a saccade is less well established and so has been shown in grey in the figure.

3.2.2 Firing rate characteristics of the short-lead burst neurons as determined experimentally.

Current knowledge of the firing characteristics of short-lead burst neurons is based on a comprehensive study conducted by Van Gisbergen et al (1981). Van Gisbergen, Robinson and Gielen recorded from short-lead burst neurons in the pontomedullary reticular formation in monkeys trained to follow jumping visual targets. They found that the firing rate of the burst cells is a non-linear, saturating function of motor error, which they defined as the difference between final and instantaneous eye position during the saccade. It was also found that individual horizontal burst neurons fire maximally when the eye makes a saccade in a particular direction. So, if a neuron fires maximally just before and during a saccade to the right, then it will be quiescent during a saccade to the left. The direction of eye movement for which a burst cell fires maximally is referred to as its 'on' direction and the opposite direction is referred to as its 'off' direction. Van Gisbergen et al investigated the responses of individual right and left burst neurons by recording their firing rates during saccades made over a range of amplitudes, and plotting the corresponding trajectories in the firing rate against motor error phase plane. It was found that, whenever the motor error is nonzero, the trajectories contract almost instantaneously to a common for saccades of all sizes curve in the phase plane and then converge slowly to the origin

along this curve (Figure 6). This means that the system expresses behavior which is similar to the behavior of slow/fast systems.

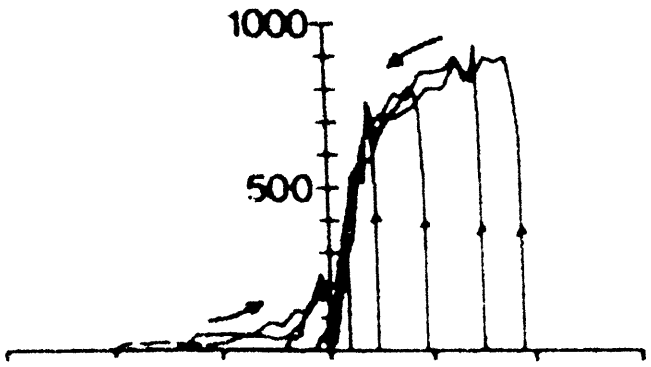

Figure 6. Relationship between the firing rate and motor error obtained from recordings of a right short-lead burst neuron during saccades of different amplitudes. The vertical axis denotes firing rate in spikes/sec while the horizontal axis denotes motor error in steps of 10 degrees.

By flipping the response curves from left burst neurons about the firing rate axis, and then averaging over all response curves, Van Gisbergen et al obtained a single curve describing the mean response of all neurons (Figure 7). In the 'on' direction, this mean burst cell response curve was observed to have the form of an increasing exponential function that saturates at large motor errors. In the 'off' direction the curve was found to be approximately zero except for a small maximum close to zero error (Figure 7). Van Gisbergen et al suggested that the 'off' response may generate a small tug at the end of the saccade in the direction opposite to that of the eye movement. They suggested it may be needed to prevent the inertia of the eye causing overshoot of the target. Later Miller and Robins (1992) demonstrated, by measuring the tension in extraocular muscles, that there is no active breaking at the end of a

saccade. Nevertheless, the 'off' response is thought to be needed to reduce the firing rate of agonist motoneurons at the end of a saccade in order to slow down the eye (Abadi et al, 2000).

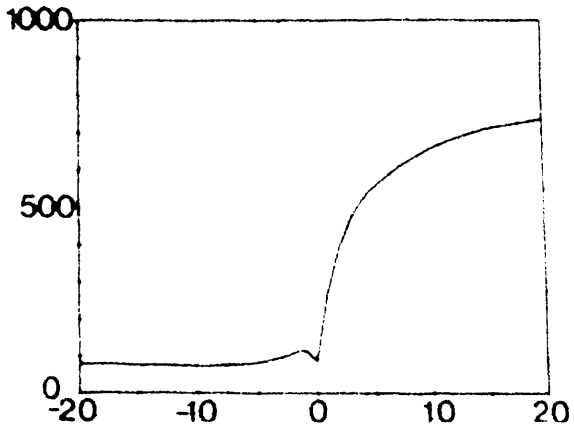

Figure 7. Mean short-lead burst neuron response curve obtained by Van Gisbergen et al. The vertical axis denotes firing rate in spikes/sec while the horizontal axis denotes motor error in degrees.

3.3 Broomhead et al's modeling of the saccadic system.

A model of the behaviour of the circuitry underlying the generation of saccades can be based directly on experimentally determined quantitative relations between the firing patterns of the different neurons. The firing rate of the short lead burst cells is a non-linear, saturating function of the difference between final and instantaneous eye position during the saccade, a quantity which is referred to as the motor error (Van Gisbergen et al. 1981). With the provisional assumption that the long lead burst neurons encode the motor error *m*, the coupling between the short and long lead burst

neurons can be described by a system of slow/fast differential equations (Broomhead et al, 2000):

$$\begin{aligned} \varepsilon \frac{db}{dt} &= -b + f(m) \\ \frac{dm}{dt} &= -b \end{aligned} \tag{3.1}$$

where $f(m)$ is a function that defines the curve of burst cell firing b against the dynamic motor error m and ε is a small positive number. In effect, whenever the dynamic motor error is nonzero, the state of the system relaxes rapidly onto the curve $b = f(m)$. This curve represents the nullcline of the system, since $db/dt = 0$ along it. The system then evolves according to $dm/dt = -b$. The result of this is that b and m decrease to zero along the curve $f(m)$. The origin is thus a unique stable equilibrium of the system, which corresponds to the endpoint of the burst signal of the saccade. The role of the multiplier ε is to constrain the dynamics of the burst cells onto the burst cell firing rate nullcline. As ε is made smaller, the system moves more rapidly onto the nullcline and follows it more closely. The parameter ε determines how quickly the burst cells respond to the dynamic motor error signal, with the response time decreasing as ε is decreased.

A more realistic version of the model included separate populations of neurons responsible for leftward and rightward saccades (Broomhead et al, 2000). In this bilateral model, the function used to describe the firing rate of a given population is described by a sum of two different functions, one describing the 'on' response (the response in the direction of maximal firing) and the other the 'off' response. The left

and right populations of burst neurons are assumed to be mutually inhibitory, to ensure that co-contraction does not occur. The equations for the bilateral model of burst generation are:

$$\begin{aligned} \varepsilon \frac{dr}{dt} &= -r + \gamma r l^2 + f(m) \\ \varepsilon \frac{dl}{dt} &= -l + \gamma l r^2 + f(-m) \\ \frac{dm}{dt} &= -(r - l) \end{aligned} \qquad (3.2)$$

$$\text{with } f(m) = \begin{cases} \alpha'(1 - e^{-m/\beta'}) & \text{if } m \geq 0 \\ -\frac{\alpha}{\beta} m e^{m/\beta} & \text{if } m < 0 \end{cases}.$$

Here r and l are the firing rates of the right and left burst neurons respectively and $\gamma \geq 0$ is a parameter which represents the strength of the mutual inhibition. The functional form of each mutual inhibition term is taken to be quadratic in the activity of the inhibiting neuron. If the mutual inhibition is linear, then one can subtract the equation for the left burst neurons from that of the right burst neurons to reduce the model to the original set of equations (3.1). The function f was selected to include both an on response term with $m \geq 0$ and an off response term with $m < 0$, as found experimentally (Van Gisbergen et al, 1981). Alternative forms of the on and off responses can be specified by the values of the parameters α, β, α' and β'.

3.4 A new model of the saccadic system.

In order to enable the investigation of the effect of omnipause cells malfunctioning on saccadic system behaviour, the omnipause cells are represented explicitly. The pause

cells are assumed to inhibit the burst cells and to be inhibited in turn by the burst cells, because the level of polarisation of the pause cells has been found to match the burst cell firing pattern during saccades (Scudder et al, 2002). As yet, a function which describes the firing pattern of the pause cells has not been derived directly from experimental data. Part of the problem is that the variables which determine the firing of the pause cells have not been reliably identified. In the early control theory models pause cell firing was described by a constant unit function which was switched to zero by a trigger input. A more realistic description was introduced by Gancarz and Grossberg (1998) who modeled the behaviour of the pause cells with a Naka-Rushton function of the motor error. We have used a similar function but have made it depend on the difference between the firing rates of the left and right burst cells rather than the motor error, because the omnipause neurons are known to be inhibited by the burst cells. The following function describes the omnipause cell behaviour in the model:

$$p(r-l) = 1 - \frac{(r-l)^2}{5^2 + (r-l)^2} \tag{3.3}$$

This function depends only on the absolute value of the difference between the left and right burst neurons, which means that the omnipause cells are inhibited whenever one of the left or right populations of burst cells is firing strongly. The parameter 5 specifies how close the firing rates of the two populations of burst cells have to be before the inhibition of the pause cells ceases. This value was found to ensure cessation of the inhibition at the end of the saccade and was not varied in subsequent numerical simulations. In order to ensure that activity in the pause cells completely inhibits the burst cells they are assumed to inhibit the burst cells by a shunting

inhibition mechanism. We have followed the lead of Gancarz and Grossberg (1998) again in using a power function of the pause cell activity to describe the inhibition. Numerical simulation revealed that a power of at least 8 was required to ensure complete inhibition of the burst cells by the pause cells at the end of a saccade, and this parameter value was used in all subsequent calculations.

The new model for the saccadic burst generator consists of four equations:

$$\begin{aligned}
\varepsilon \frac{dl}{dt} &= -l + (1 - \alpha u)^8 (f(-m - \gamma r)) \\
\varepsilon \frac{dr}{dt} &= -r + (1 - \alpha u)^8 (f(m - \gamma l)) \\
\frac{dm}{dt} &= -m - (r - l) \\
\varepsilon \frac{du}{dt} &= -u + p(r - l)
\end{aligned} \tag{3.4}$$

where u is the firing rate of the pause cell population.

In this model the parameter α, where $0 \leq \alpha \leq 1$, can be used to scale down the normal firing level of the omnipause neurons in order to simulate malfunctioning of these cells: as α is decreased the degree of inhibition of the burst cells by the omnipause neurons falls. The parameter γ, where $\gamma > 0$, can be used to alter the strength of the mutual inhibition between the burst cells: increased values of γ correspond to a higher level of inhibition. The parameter ε was fixed at 0.002 for this study.

The sigmoidal function f in this model was a logistic function:

$$f(x) = \frac{\kappa}{1 + \lambda e^{-\mu(x - 2.5)}} \tag{3.5}$$

where κ, λ and μ are all positive parameters. The left and right medium-lead burst neuron responses in this model are represented by two logistic functions, overlapping around the origin. The amount of overlap was set at 2.5 degrees. This value is an assumption for which there is no direct experimental evidence, but which received support from the subsequent finding of an off response of the burst cells within the range found in neurophysiological recordings (Van Gisbergen et al, 1981) (see *Origin of off response* in 3.5.1). In order for both sets of burst cells to be silent when the motor error is zero, the pause cells act to inhibit the burst cells when they are equally active at the origin. The values for the parameters of f were selected empirically so that durations and peak velocities of the saccades of different amplitude simulated with the model followed the main sequence (Bahill et al, 1975; Lebedev et al, 1996). The following parameter values gave the best fit $\kappa = 567$, $\lambda = 2.048$ and $\mu = 0.566$. We have used a logistic function, which is continuously differentiable at the origin, rather than a Naka-Rushton function with an odd exponent, which is not, to simplify the stability analysis of the system.

The oculomotor plant acts as a sequence of two low pass filters, one with a slow time constant T_1 and one with a fast time constant T_2. Optican and Zee (1984) estimated $T_1 = 0.15$s and $T_2 = 0.012$s.

$$\begin{aligned} \dot{p} &= v \\ \dot{v} &= -\left(\frac{1}{T_1} + \frac{1}{T_2}\right)V + \frac{-p + n + (r - l)}{T_1 T_2} \end{aligned} \tag{3.6}$$

The behaviour of the neural integrator was also shown to be linear and can be modeled by a first order low-pass filter with a time constant T_n. This time constant

has been found experimentally to be 25 s in the normal oculomotor system (Optican and Zee, 1984).

$$\frac{dn}{dt} = -\frac{1}{T_n}n + (r - l) \tag{3.7}$$

The neural integrator and the oculomotor plant parts of the saccadic system are downstream from the pulse generating mechanism and therefore do not affect its stability.

3.5 Stability analysis explains the occurrence of pathological oscillations.

3.5.1 The origin of the off response.

Our first finding was that with incorporation of the pause cells, during normal saccades the burst cells develop off and on responses similar to the ones found experimentally by Van Gisbergen et al (1981), as illustrated in Figure 8. The off response arises from the overlap of the burst cell response functions at the origin, instead of from a separate term in the response function, as in the Broomhead et al (2000) model. This validates our representation of the burst cell response function as a more physiologically plausible sigmoidal function.

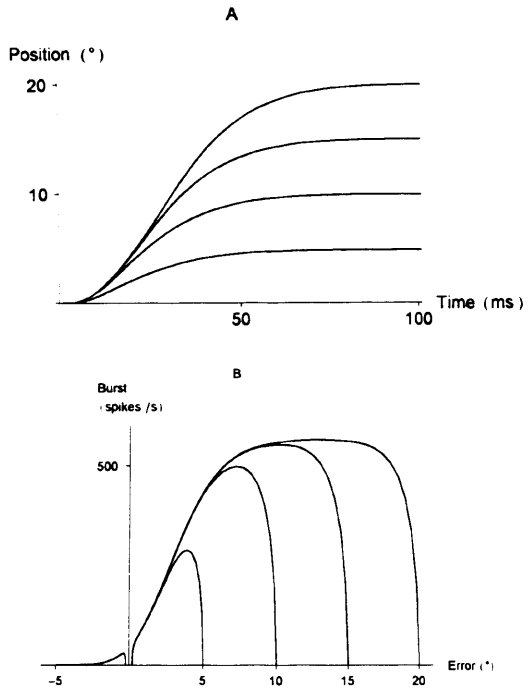

Figure 8. Time course of simulated saccades of different sizes, together with the behaviour of burst cells whose on directions are in the direction of the saccade. In these simulations $\alpha = 1$ and $\gamma = 0.01$.

3.5.2 The local stability of fixation.

In a normal saccadic system steady fixation is a stable equilibrium. A standard technique for analysing the stability of a system in an equilibrium state is to calculate the eigenvalues of the linearised system as a parameter is changed. If any of the real parts of the eigenvalues change sign then the system changes behaviour at that value of the parameter. In order to investigate what effect pause cells malfunctioning may have on an otherwise normally functioning saccadic system, we gradually decrease α from 1 to 0 in our model over a range of values of mutual inhibition γ. With the value of mutual inhibition $\gamma = 0.01$ used to simulate normal saccades, the system has a stable equilibrium for all levels of pause cell activity. With increased mutual

inhibition between the burst cells oscillations developed. For example, with $\gamma = 0.1$ the system undergoes a Hopf bifurcation at $\alpha = 0.025$ during which the stable equilibrium at the origin becomes unstable and a stable limit cycle is formed. This bifurcation is revealed by a change of sign of the real parts of a pair of complex eigenvalues (Wilson, 1999), as shown in Figure 9.

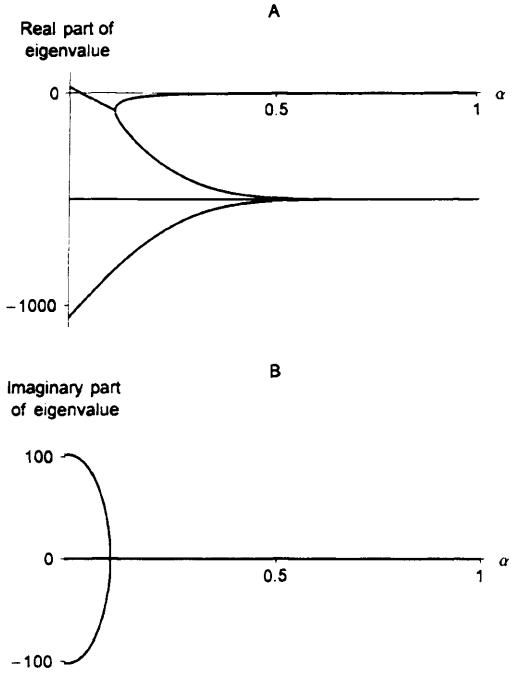

Figure 9. (A) Real parts of the four eigenvalues of the Jacobian for the saccade generator equations (3.4). (B) Imaginary parts of the four eigenvalues of the Jacobian, two of which are always equal to zero. The real parts of a pair of the eigenvalues cross the origin at $\alpha = 0.025$. In these simulations $\gamma = 0.1$.

3.5.3 The range of amplitudes and frequencies of oscillations.

The types of saccadic oscillations produced by the model were investigated numerically by varying the strength of the burst neurons inhibition by the omnipause neurons and the strength of the mutual inhibition between the burst cells. As

illustrated in Figure 10, the highest frequency of oscillation was 20 cycles per second and occurred with low pause cell inhibition and low mutual inhibition. The lowest frequencies were around 3 cycles per second and occurred with high mutual inhibition. The oscillations which arise just after a Hopf bifurcation has occurred will be sinusoidal; with larger values of the bifurcation parameter, relaxation oscillations occur. Whilst the low amplitude oscillations in Figure 10 are pendular in shape the higher amplitudes have an exponential profile which is not consistent with back-to-back saccades. The largest amplitudes were up to 6 degrees and occurred with low pause cell inhibition and high mutual inhibition.

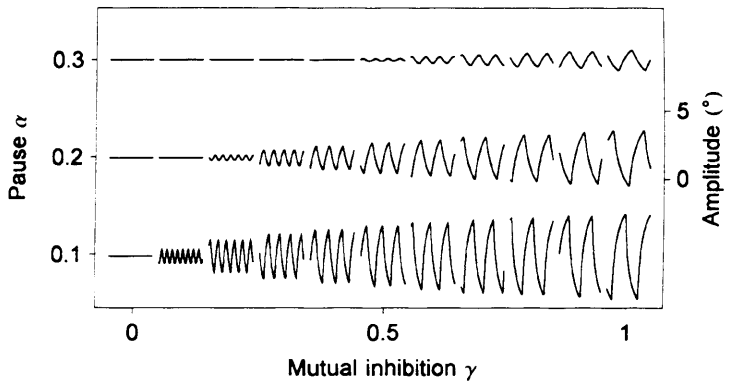

Figure 10. Illustration of the types of saccadic oscillations which can be obtained from the model by altering the effectiveness of the pause cells (α) and the mutual inhibition (γ) between the burst cells. Each segment is 0.5 seconds long.

3.6 Discussion.

Inherent instabilities in the saccadic system were previously revealed by a model of the nonlinear dynamics of the system (Broomhead et al, 2000, Akman et al, 2005). The main criticisms of the previous model are that it did not explicitly include the

pause cells and that it relied on the 'off' response of the burst neurons being abnormally large for the oscillations to occur. We have addressed the first of these criticisms by developing a more physiologically plausible model, which explicitly contains the omnipause neurons. This model demonstrates that burst neurons with overlapping sigmoidal response functions do indeed show 'on' and 'off' responses similar to the ones found experimentally (Van Gisbergen et al, 1981), when inhibited by the pause cells. The second criticism arose from the concern that the assumption that only the 'off' response of the burst neurons is affected, while the 'on' response remains normal, may not be physiologically realistic. Recently, post saccadic inhibitory rebound (Ramat et al, 2005) has been proposed as a plausible physiological mechanism for generating off responses independently of the on response, which makes the second criticism less valid. To be physiologically realistic the mutual inhibition between the burst neurons must act via inhibitory burst neurons. If the revised model described here was extended to include a pair of inhibitory burst neurons then pathological off responses could be simulated by manipulation of the response function of the inhibitory neurons. In this study we have concentrated on the instabilities that can arise when the on and off responses are not independent but arise from the same underlying sigmoidal response function.

As is shown in this work, by varying the strength of the burst neurons inhibition by the omnipause neurons and the strength of the mutual inhibition between the burst cells, the model can generate periodic oscillations within a frequency range 3 – 20 cycles per second and amplitude range 0 - 6 degrees. Thus, the model can generate oscillations with the amplitudes observed in microsaccadic flutter (0.1 – 0.5 degrees), as well as in voluntary nystagmus and ocular flutter (1 – 5 degrees). The model frequency range also fully covers that observed in voluntary nystagmus and ocular

flutter, and partially covers the range of frequencies seen in microsaccadic flutter (15 – 30 degrees).

Models of the oculomotor system have usually been described in terms of block diagrams. Apart from the advantage of simplicity of construction, given the ready availability of powerful simulation packages, such models deliver easy-to-understand explanations of some aspects of saccadic disorders in terms of structural damage to the system. However, such models include so many offset and slope parameters that it is not feasible to carry out an exhaustive enumeration of all the possible behaviours of the models. This makes it difficult to assess how much the behaviour of a given model depends on the choice of a specific set of parameters. An advantage of the nonlinear dynamics approach is that only a few equations and parameters are required to describe the behaviour of the system. Alternative models of the development of microsaccadic oscillations attribute them to a delay in the action of the pause cells (Zee and Robinson, 1979) or to a combination of mutual inhibition between the burst cells and an excessive off response from the burst cells (Broomhead et al, 2000, Ramat et al, 2005). One method of assessing these models is to compare the range of oscillations found as the delay and inhibitory strength of the pause cells, and the level of mutual inhibition of the burst cells, are systematically varied. The range of frequencies associated with microsaccadic oscillations and flutter is 6 to 30 Hz (Ashe et al, 1991, Ramat et al, 2005). Ramat et al (2005) have argued that to achieve this range of frequencies through delays in feedback would require an implausibly large range of neural time constants. The model described in this paper gave oscillations of up to 20 Hz in frequency, which suggests that an additional neural mechanism such as post saccadic inhibitory rebound is necessary to account for the entire range of saccadic oscillations found clinically. Our results suggest that the most realistic

waveforms are found with levels of pause cell inhibition and burst cell mutual inhibition which are just over the borderline for stability. This may make good physiological sense as it suggests that normally the firing levels of the pause cells are just enough to suppress the burst cells but no more. As the constant firing of the pause cells requires energy, keeping their level of activity as low as possible will save on energy usage.

A model of the dynamics of the saccadic system enables standard stability analysis techniques to be used to discover how instabilities can develop. Analysis of the equations of our earlier nonlinear dynamics model revealed that jerk nystagmus, in which there is an accelerating slow drift away from the point of fixation followed by a saccade in the opposite direction, can develop by a sequence of a pitchfork followed by a pair of Hopf bifurcations producing left and right beating oscillations (Akman et al, 2005). In the current model a Hopf bifurcation occurs directly at the equilibrium. The significance of the difference between these two patterns of bifurcations is that in the first case the subsequent oscillations are asymmetric whereas in the latter case they are symmetric. In physiological terms the implications of this finding are that microsaccadic oscillations are generated by alternate firing of the left and right burst cells, with the peak of the firing occurring when the error signal is least, whereas in jerk nystagmus the peak firing rates of the burst cell occur when the error signal is maximal. Incorporating a pair of inhibitory burst neurons in the current model to allow pathological off responses to be simulated would allow oscillations to develop directly through a Hopf bifurcation and also through a pitchfork followed by a Hopf bifurcation. This would give rise to a system able to generate nystagmus waveforms as well as microsaccadic oscillations.

In conclusion, the importance of a bifurcation analysis of a model is that it reveals the range of underlying instabilities in the model, which can lead to pathological eye movements without any structural damage. As has been appreciated in other fields of movement research (Verdaasdonk et al, 2004), a comprehensive stability analysis is required to understand the range of behaviours that a motor system can produce, and to assess the likely outcome of manipulation of system parameters. Recently, Ramat et al (2005) provided convincing arguments that the level of activity of the pause neurons can be reduced in normal subjects by a variety of manipulations including blinks, convergence and most reliably by a combination of a small saccade and a large vergence movement. Such manipulations may form the basis of approach to experimental neurology in which the underlying mechanisms of an oscillation, which on its own could arise from a number of causes, can be determined from the way in which the oscillation changes with systematic experimental manipulations.

4. Modeling integration of self-motion by hippocampal place cells.

4.1 Path integration.

The term 'path integration' was first proposed by Mittelstaedt and Mittelstaedt (1973) for the ability of an agent to keep track of its current location, on the basis of idiothetic information alone, relative to its starting point as it moves around. Arthropods in the Mittelstaedt and Mittelstaedt (1973) study were able to return

straight home after a random search excursion under conditions that were designed to exclude all external cues. Mittelstaedts then concluded that this capability must be based on the integration and storage of the animal's own movements. The term 'spatial updating', on the other hand, refers to a more extended version of path integration, which also includes the ability to keep track of other locations within the environment, on the basis of idiothetic information alone (Byrne et al, 2007).

The fact that hippocampal lesions impair spatial navigation (e.g. Morris et al, 1982) implies that the hippocampus might have something to do with path integration. More specifically, Whishaw et al (2001) claimed, on the basis of their rat lesion studies, that hippocampal damage impairs path integration. However, hippocampus does not appear to be required for the simplest form of path integration, known as 'homing' (Alyan and McNaughton, 1999). More likely, the hippocampus is required for the more complex spatial updating, and possibly also for integrating path integration with sensory inputs (Etienne and Jeffery, 2004). In this chapter I show, through the development of a biologically plausible neural network model, how hippocampal place cells may perform path integration. The issue of integrating sensory and path integration inputs by the hippocampal place cells is addressed in the next chapter, by extending the model to include sensory inputs.

4.2 The hippocampus.

The hippocampus became a focus for the study of spatial cognition following the discovery of place cells in the hippocampi of freely moving rats by O'Keefe and Dostrovsky (1971). Since then cells with other spatial correlates of firing have been

found in surrounding neocortical areas. The functional anatomy of the hippocampus and surrounding areas, and the paradigm of single unit recording in freely moving rodents is briefly reviewed in Figures 11-14.

Figure 11. The anatomical organization of the rat hippocampus and surrounding cortical areas. The hippocampus proper is a sausage-shaped structure lying under the neocortex (shown in blue, above). It is formed from two interlocking sheets of cells: a sheet of granule cells (the 'dentate gyrus', DG) and a sheet of pyramidal cells divided into two regions (CA3 and CA1). The sheet of pyramidal cells broadens out through the regions known as subiculum (S), pre- and para-subiculum (pS) and medial and lateral entorhinal cortex (mEC and lEC), becoming six layered neocortex. Place cells are found in regions CA1 and CA3, head-direction cells and place-by-direction cells are found in presubiculum and grid cells in medial entorhinal cortex. Adapted from Burgess and O'Keefe (2003).

Figure 12. Approximate numbers of principal (projection) cells in various regions of the rat hippocampal formation (including the hippocampus proper, subiculum and entorhinal cortex), and major projections are shown. Note the extensive recurrent projections within area CA3. Adapted from Burgess and O'Keefe (2003).

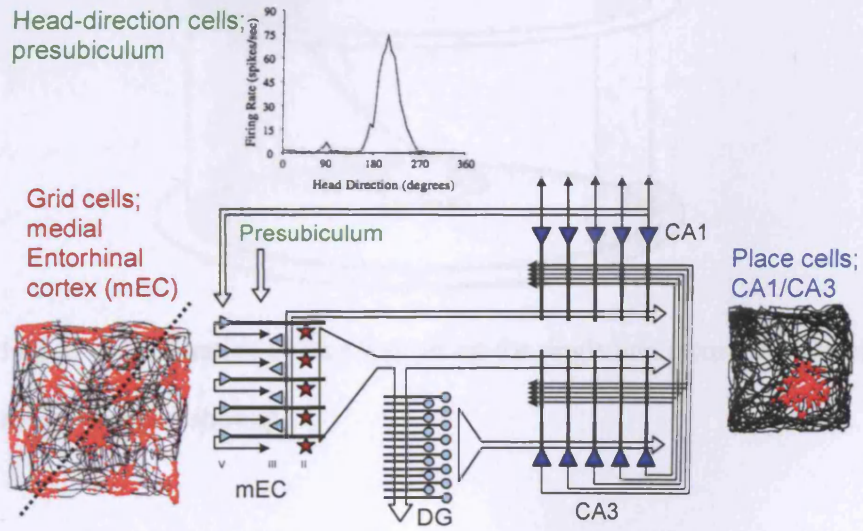

Figure 13. Schematic anatomy and spatial correlates of cell firing around the hippocampal formation. Head-direction cells in the presubiculum fire according to the animals' head direction (above). Place cells in the hippocampus fire according to the location of the animal (right: black line shows the path of a rat exploring a square box, red dots show the locations at which a place cell fired an action potential). Grid

cells in medial entorhinal cortex firing whenever a rat enters one of an array of locations arranged in a triangular or hexagonal grid (left: black line shows the path of a rat exploring a square box, red dots show the locations at which a place cell fired an action potential). Figure kindly provided by Neil Burgess.

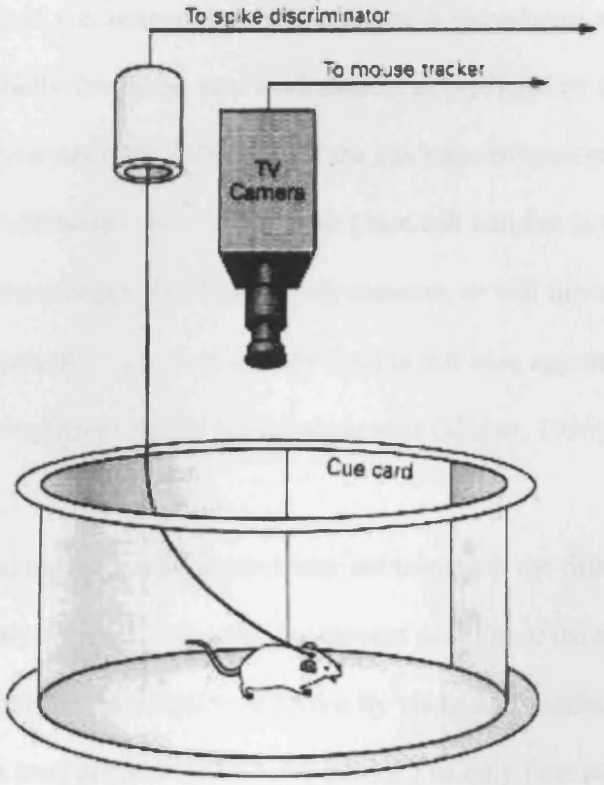

Figure 14. Illustration of a typical set-up for single unit recording in freely moving rodents (mouse shown).

4.3 Navigational neurons.

The hippocampus has been shown to be involved in spatial memory in rodents, as well as in primates and humans. Neurons in areas CA3 and CA1 of the rat hippocampus exhibit location specific firing (O'Keefe and Dostrovsky, 1971;

O'Keefe, 1976). Pyramidal cells in those areas fire only when the animal visits a particular localised region of the surrounding environment. The cells are known as the place cells and the localised region as their place field. Collectively these place cells provide a population code for spatial position. A neural representation ('cognitive map') of a particular environment is formed in such a way (O'Keefe and Nadel, 1978). If you change the shape and size of the original environment, the place cells will initially fire in the new environment as predicted by the Boundary Vector Cell model (Hartley et al, 2000). But if the environments are more radically different, e.g. made of different material, the same place cell will fire in different places (as defined by boundaries) in different environments, or will fire in one and not in the other environment. Thus, each environment in this case appears to be represented by the unique 'cognitive map' in the hippocampus (Muller, 1996).

As the animal moves around a particular environment, the firing pattern of place cells is continuously updated, reflecting the current position of the animal. This continuous shifting of neural representation is driven by visual and vestibular inputs, and takes place even in total darkness (O'Keefe, 2007). The only time when a complete cessation of location-specific place cell firing is seen, is when the animal is being forcefully held still.

Another interesting type of cells, closely related to the place cells, is the head-direction cells. These cells, mainly located in postsubiculum and limbic thalamus, signal the instantaneous head direction of the animal in the horizontal plane in a world-centered reference frame (Taube et al, 1990a; Taube et al, 1990b). Similarly to the place cells, the internal representation of head direction, maintained by these cells, is updated continually with the head movement of the animal, even in the absence of

visual inputs (McNaughton et al, 1991; Mizumori and Williams, 1993). The head-direction system relies on familiar landmarks in order to reset or calibrate itself (Goodridge and Taube, 1995).

Cells that combine the properties of the head-direction and the place cells have also been found in the presubiculum (Cacucci et al, 2004). These cells, like the place cells, have a preferred location, at which they are most active. But their response also depends on the current head direction of the animal, i.e. they are not unidirectional like the place cells. The following figure illustrates responses of these cells:

Figure 15. Firing of place by head-direction cells is modulated by both location and head direction. *A*. Locational firing-rate maps for the place by head-direction cell TPD f3. Central firing-rate map is direction independent. Surrounding rate maps show locational firing for specific head directions only (in 45° bins). Black numbers refer to peak firing rates (Hz), and blue numbers in blue boxes refer to the mean rate

of the dark blue area of the map (Hz). All maps are individually autoscaled. *B.* Directional polar plot showing that the cell TPD f3 fires maximally when the rat faces southwest. Number refers to peak firing rate. *Bottom right*: Directional dwell-time polar plot (seconds). *C.* Locational and directional firing-rate maps of four representative place by head-direction cells. For each cell, the locational firing-rate map (*left*, white number refers to peak firing rate and blue number is as in *A*) and the directional polar plot (*right*) are shown. The *bottom right* of each rate polar plot indicates the directional dwell-time polar plot (seconds). Adapted from Cacucci et al (2004).

4.4 Recurrent network models of path integration (PI).

4.4.1 Continuous attractor and Mittelstaedt models.

A characteristic anatomical feature of the CA3 region of the hippocampus is the extensive recurrent connections between its pyramidal cells (Amaral and Witter, 1989). The presence of recurrent connections suggests that the network is subject to stable attractor dynamics, which means that place cell activity patterns correspond to the stable equilibria states of a potential CA3 attractor network. A number of researchers to date have taken an attractor dynamics approach to modelling the behaviour of the recurrent networks, notably head direction (Skaggs et al, 1995; Zhang, 1996; Stringer et al, 2002a) and place cell networks (Samsonovich and McNaughton, 1997; Redish and Touretzky, 1998; Kali and Dayan, 2000; Stringer et al, 2002b). These networks are referred to as 'continuous attractor' networks, since they can stably maintain patterns of firing of their neurons corresponding to any location in a continuous physical space: one-dimensional in the case of head direction

cells forming a 'line attractor' (see Figure 16), and two-dimensional in the case of place cells, where we have a whole Cartesian plane of stable fixed points (a 'plane attractor').

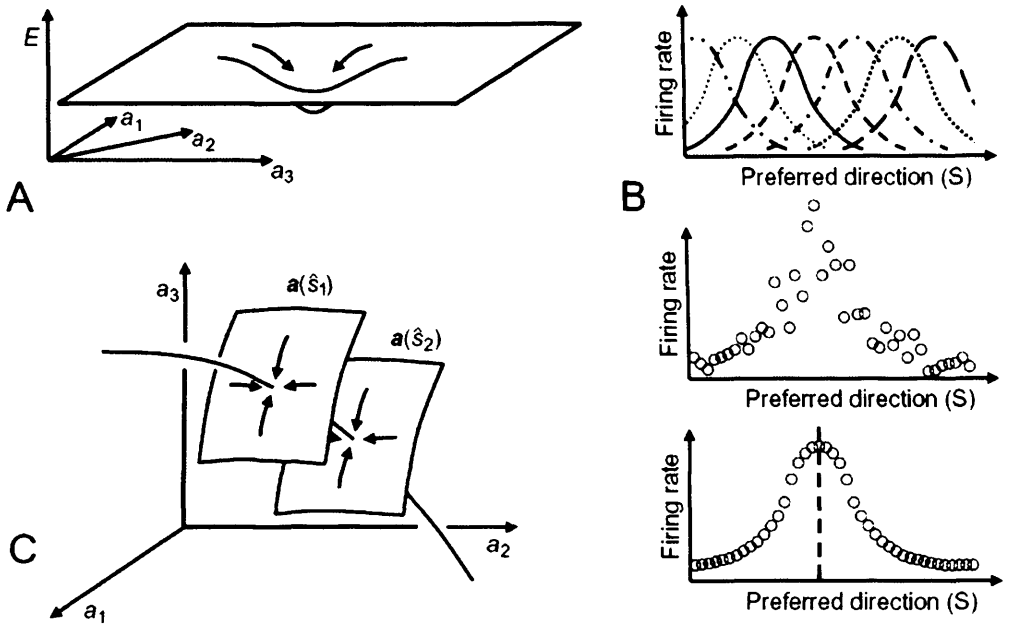

Figure 16. Point attractors, line attractors and the encoding of head-direction. A) A point attractor for neural activity is a pattern of activity (a1, a2, a3..) into which other nearby patterns of activity will evolve under the dynamics of the system (i.e. the connection weights and rules for updating activation values). In the Hopfield (1982) model it is thought of as a minimum energy state by analogy with physical systems. B) A population of head direction cells (Taube et al., 1990a,b) encode the rat's head direction, each firing maximally for a single preferred direction (S; top plot). For a given head direction, the pattern of activity across the population of head-direction cells will resemble a noisey bump when the cells are laid out along the x axis according to their preferred direction (middle plot). A continuous attractor for neural activity can be formed by appropriate recurrent connectivity between the cells. Connections between pairs of cells have weights that are symmetrical and depend

only on the difference between the two cells' preferred directions: cells with more similar preferred directions having stronger connections. These connections constrain the pattern of activation to form a smooth bump, reducing noise and allowing more accurate decoding of head-direction (bottom). C) The set of allowed smooth bump-shaped patterns of activation form a "line attractor". Each actual head direction (S1, S2..) will give rise to a pattern of activation that will converge to a point on the line attractor: providing an estimate of the head direction ($\hat{S}1$, $\hat{S}2$..). Under the dynamics of the system, patterns of activation along the line can move to other patterns along the line, but patterns off the line will converge onto it. Adapted from Burgess (2006).

Samsonovich and McNaughton (1997) and Stringer et al (2002b) incorporated a path integration mechanism in their models, which allows the models to keep track of their location using idiothetic inputs alone. See also Redish and Touretzky (1998). In order to function, these models have two main requirements: that the strength of connections between CA3 place cells decreases proportionate to the distance between their preferred locations; and that there exists a population of appropriately connected 'shifter cells' with spatially constrained firing that is also modulated by agent's speed and head direction. The former of these requirements, in conjunction with appropriate feedback inhibition, can lead to the creation of a stable activity pattern in CA3 neurons. The latter requirement is necessary for that pattern to shift so as to track the agent's position.

Taking a completely different approach, Mittelstaedt (2000) constructed a "triple-loop" model of path control by head direction and place cells. Extending some of his earlier work with arthropods, this model provides an engineering solution to the problem of path integration for comparison with neurophysiological data, rather than

explicitly simulating neuronal firing itself. The basic principal was of control loops – altering behaviour to minimize the differences between: the current heading and the desired heading (the "compass" loop, involving head-direction cells); the current path integrator coordinates and its reference value (the "path" loop); and the path integrator's reference value and the current goal location (determining the location where search terminates, the "place" loop, involving place cells, and specified by the non-spatial cues present at the goal location). Interestingly, Mittelstaedt makes the point that the place cells are the output of the path integration system, rather than embodying it as they do in Samsonovich and McNaughton's model. In addition, he notes that the different loops may act independently: thus allowing some aspects of PI to occur in the absence of the "place" loop. For example, homing to a recently visited location might be supported by using two "path" loops, one reset at the start of the outward trajectory and the other reset at the start of the return journey – without need to use the "place" loop and non-spatial cues identifying the goal location. Overall, this model represents an examination of the hippocampal role in path integration from a different point of view (arthropod PI) and at a different level of analysis (control system engineering) from our approach.

4.4.2 Place cell tuning curves.

The place cell tuning to location often has a shape close to the shape of a Gaussian function (Hartley et al, 2000). Therefore in our model we use the following formula for the place cell tuning curve:

$$f(x - x_i, y - y_i) = A_p \exp[-(s_i)^2 / 2\sigma_p^2] \qquad (4.1)$$

where $s_i = \sqrt{(x - x_i)^2 + (y - y_i)^2}$ is the distance between the current location of the agent (x, y) and the preferred location of cell i (x_i, y_i), at which it fires maximally. σ_p^2 is the variance of the place field and A_p is the peak firing rate of the place cell (both assumed to be the same for all place cells in the model for simplicity).

The activation pattern over the population of place cells, arranged so that each one's location corresponds to its preferred location (i.e. same location, different cell) is basically equivalent to the place cell tuning curve (i.e. same cell, different location) (Zhang, 1996). In the real brain the place cells are not topologically arranged according to their preferred location, but appear to be rather randomly distributed. Nevertheless, if one imagines the place cells as laid out on the Cartesian grid corresponding to the coordinates of their preferred locations (x_i, y_i), one can see a bump-shaped activity pattern defined by (4.1), that is centered at the neuron i with the preferred location closest to the current position of the agent, i.e. $x \approx x_i$ and $y \approx y_i$. Further in the report I will refer to the implicit 2D space represented by the set of activities of these neurons as the 'state space' of the system.

4.4.3 The basic mechanism of activity shifting.

If there are only recurrent connections between the place cells (no external inputs), their dynamics can be described by the following equation (4.2). The equation describes how a neuron's firing rate depends on the net input to it – see the equation (2.5) in Chapter 2.

$$\tau \frac{dr_i}{dt} = -r_i + F\left(\sum_j W_{ij} r_j\right) \tag{4.2}$$

Here r_i is the firing rate of the place cell i, τ is the place cell time constant, W_{ij} is the weight of the recurrent connection from the place cell j to the place cell i and F is the response function of the place cells.

Stable solutions to equation (4.2) obey:

$$r_i = F\left(\sum_j W_{ij} r_j\right) \tag{4.3}$$

We want the stable firing rates of place cells to be of the form of $f(x - x_i, y - y_i)$ in the equation (4.1). Substituting $r_i = f(x - x_i, y - y_i)$ into the equation (4.3), we get the following equation for the stable solutions:

$$f(x - x_i, y - y_i) = F\left(\sum_j W_{ij} f(x - x_j, y - y_j)\right) \tag{4.4}$$

And this should be true for any choice of (x_i, y_i), which means that our system should be translation-invariant. For this to be the case, the average synaptic weight W_{ij} between two neurons with favorite locations s_i (x_i, y_i) and s_j (x_j, y_j) has to be solely a function of the distance $(s_i\text{-}s_j)$, i.e. $W_{ij} = W_{i\text{-}j}$, see e.g., Dayan and Abbott (2001).

If the system, defined by (4.2) and (4.4), receives an external input, which is proportional to the derivative $f'(x - x_i, y - y_i)$, it is possible to show (for a linear F) that the stable bump of activity, given by $f(x - x_i, y - y_i)$, will shift in the state space of the agent with speed proportional to the magnitude of the input.

We consider the one-dimensional case, i.e. movement along x direction (y is constant). The derivative of the function $f(x - x_i)$ with respect to x at the point x_i

can be approximated through the f values for the neighboring neurons by the centered difference rule:

$$f'(x-x_i)=\frac{f(x-x_{i+1})-f(x-x_{i-1})}{2\Delta x} \tag{4.5}$$

where Δx is the distance between the favourite locations of any two neighbouring neurons (Droulez and Berthos, 1991; Byrne and Becker, 2004).

If we think of $D_{i,(i+1)}= 1/(2\Delta x)$ and $D_{i,(i-1)}= -1/(2\Delta x)$ as the differential synaptic weights onto the neuron i from its two neighbouring neurons along the x axis, the external input that is proportional to $f'(x-x_i)$ can be represented as $\lambda\sum_j D_{i-j}f(x-x_j)$. Here $\overline{D}$ is the matrix of the differential connection weights and λ is the proportionality coefficient. Then, assuming that the bump preserves its shape during the movement, we get the following equation for the system with the recurrent and differential pathways:

$$\tau\frac{d}{dt}f(x-x_i)=-f(x-x_i)+\sum_j W_{i-j}f(x-x_j)+\lambda\sum_j D_{i-i}f(x-x_j) \tag{4.6}$$

The first two terms on the right cancel out due to the translation invariance of the system, and, by evaluating the derivative on the left of the equation, we get:

$$\tau f'(x-x_i)\frac{dx}{dt}=\lambda f'(x-x_i) \tag{4.7}$$

where $f'(x-x_i)$ cancel out: $\tau\frac{dx}{dt}=\lambda \Rightarrow \frac{dx}{dt}=\frac{\lambda}{\tau}\Rightarrow x=\frac{\lambda t}{\tau}$, giving:

$$r_i = f(x - x_i) = f\left(\frac{\lambda t}{\tau} - x_i\right) \tag{4.8}$$

Thus, the system shifts the activity pattern with the velocity determined by λ, or, in other words, an externally generated 'velocity signal'. $\lambda(t)$ will be integrated over time such that the represented location moves consistently with it (performing 'path integration').

4.4.4 Recurrent connection weights.

Stringer et al (2002b) have provided a model of Hebbian associative learning of the recurrent connections in CA3 during the exploration of novel environments by the agent. The model generated a recurrent weight profile which is very close in its shape to the Gaussian function of the distance between the favorite locations of the presynaptic and the postsynaptic neurons. Since there is a body of evidence for synaptic plasticity in the CA3 recurrent collateral pathways (Debanne et al, 1998), it is reasonable to assume that the real recurrent weight profile is similar to the one generated by the Stringer et al model. Therefore we adopt the following Gaussian function to represent the profile in our model:

$$W(x_i - x_j, y_i - y_j) = A_w \exp[-(s_{i-j})^2 / 2\sigma_w^2] \tag{4.9}$$

where $s_{i-j} = \sqrt{(x_i - x_j)^2 + (y_i - y_j)^2}$ is the distance between the preferred locations of the cells i (x_i, y_i) and j (x_j, y_j), σ_w^2 represents the broadness of the profile and A_w is the weight normalization factor.

As can be seen from (4.9), the strength of the synaptic weight between any two neurons depends only on the distance between them in the state space s_{i-j}. Thus, our recurrent weight matrix supports the stable solutions equation (4.4).

4.4.5 The response function.

If we have a sufficient density of coverage of the represented space by the place cells, we can approximate the equilibrium equation (4.4) by its continuous form, replacing the sum over preferred locations (x_j, y_j) weighted by a Gaussian function W of the distance between (x_i, y_i) and (x_j, y_j) by the 2D-convolution:

$$f(x,y) = F(f(x,y) * W(x,y)) = F\left(\int_{-\infty}^{\infty} \int_{-\infty}^{\infty} w(x-X, y-Y) f(X,Y) dX dY \right) \qquad (4.10)$$

Since both W and f are Gaussian, it can be shown mathematically that the result of their convolution is another 2D-Gaussian, with the variance $\sigma^2 = \sigma_w^{\,2} + \sigma_p^{\,2}$. In order for the equations (4.10) and (4.4) to be true, our response function F has to be a power function of the form:

$$F(x) = (x)^n , \qquad \text{where } n = \frac{\sigma_p^{\,2} + \sigma_w^{\,2}}{\sigma_p^{\,2}} \qquad (4.11)$$

In the case when $\sigma_p^{\,2} = \sigma_w^{\,2}$, F is simply a square function ($n = 2$). On the other hand, if $\sigma_p^{\,2} >> \sigma_w^{\,2}$, the function is close to linear.

We can think of this function as of a non-saturating region of the Naka-Rushton function, which is considered to provide a reasonably good description of neuronal

responses. We thus assume that our model always operates in a non-saturating regime, which by itself appears to be a reasonable assumption. If we consider the case when $\sigma_p^2 = \sigma_w^2$, the equation (4.4) becomes:

$$f(x - x_i, y - y_i) = \left(\sum_j W_{ij} f(x - x_j, y - y_j) \right)^2 \tag{4.12}$$

and this is a solution to (4.2) for all neurons, i.e. all preferred locations (x_i, y_i) and for all locations of the agent (x, y).

4.4.6 Stabilizing the attractor network.

Now we have a continuous family of equilibrium points, which is necessary for us in order to implement plane attractor dynamics. But, as it is possible to see from (4.12), the equilibrium points are unstable. The slightest deviation from the equilibrium state will either result in the infinite growth of the activity bump or its decay towards zero (another, stable equilibrium point of the system), depending on the direction of initial deviation from the unstable equilibrium state.

In order to make $f(x - x_i, y - y_i)$ a stable family of equilibrium solutions, we modify the system (4.2) by introducing into it negative feedback inhibition. We assume the inhibition to be shunting, consistent with the action of shunting GABA synapses (Wilson, 1999). Doiron et al (2000) have shown that the shunting inhibition has a divisive, rather than subtractive, effect on the firing rates of the pyramidal cells when the latter operate at frequencies below 40 Hz. Since the place cells have been found to operate in the range of 5 – 15 Hz, we implement a divisive inhibition in our model. The inhibition is performed through the action of a single, global inhibitory neuron,

which is assumed to have a linear response function for simplicity. This neuron receives equally strong synapses from all the place cells in the network and provides equal negative feedbacks to all of them as well, broadly consistent with the very large dendritic and axonal spread of basket cells. Thus, our system becomes:

$$\tau \frac{dr_i}{dt} = -r_i + \left(\sum_j W_{i-j} r_j \Big/ Jv \right)^2$$

$$\tau_v \frac{dv}{dt} = -v + \gamma \sum_j r_j \qquad (4.13)$$

where v is the firing rate of the global inhibitory neuron, τ_v is its time constant, γ is the strength of the synapse from any place cell onto the inhibitory neuron and J is the synaptic strength of the negative feedback.

To make our model simpler to analyze, we assume that the time constant of the inhibitory neuron is much smaller than τ of the place cells, and therefore could be approximated by zero. This makes v always equal to $\gamma \sum_j r_j$ and enables us to reduce the system of equations (4.13) by one, giving:

$$\tau \frac{dr_i}{dt} = -r_i + \left(\sum_j W_{i-j} r_j \Big/ J\gamma \sum_j r_j \right)^2 \qquad (4.14)$$

4.4.7 The path integration mechanism.

To enable our system (4.14) to perform path integration, we add to it differential synaptic pathways in a way similar to the linear case described above. For that

purpose we assume that there are four distinct groups of place by head-direction cells in the hippocampus. The tuning curve of the place by head-direction cell *i* is defined as follows:

$$f(x-x_i, y-y_i, \theta-\theta_i) = f(x-x_i, y-y_i)\left|\cos(\theta-\theta_i)\right|_+ \tag{4.15}$$

where $f(x-x_i, y-y_i)$ is the tuning curve of the place cell *i*, $\left|\cos(\theta-\theta_i)\right|_+$ is a rectified cosine function and θ_i is the preferred head direction of the place by direction cell *i*. The equation (4.15) can also be seen as a response curve of a normal place cell, which is modulated at the level of its dendrites by an input from a head-direction cell. In fact, to be more accurate, we need the direction of bodily movement of the rat, rather than its head direction, in order to perform path integration. For the purpose of modeling we simply assume that the two are the same, though this, of course, is not always true.

One of the four groups is comprised of the cells with the preferred head direction of 0 degrees, another – 90 degrees, a third – 180 degrees and a fourth – 270 degrees. Thus, each place cell *i* has a corresponding place by direction cell *i*, with the same favorite location, in each of the four groups.

Apart from the differential connections, we also introduce an external (feedforward) input h_i to the place cell *i* into the model. This input is supposed to represent visual signals to the place cells. And our model becomes:

$$\tau \frac{dr_i}{dt} = -r_i + \left((\sum_j W_{i-j} r_j + V \sum_j D^1_{i-j} r^1_j + V \sum_j D^2_{i-j} r^2_j + V \sum_j D^3_{i-j} r^3_j + V \sum_j D^4_{i-j} r^4_j + h_i) / J\gamma \sum_j r_j \right)^2 \quad (4.16)$$

where $r_j^n = r_j \cos|\theta - \theta^n|_+$,

with n = 1,2,3,4 and $\theta^n = 0°, 90°, 180°, 270°$ correspondingly, is the firing rate of the place by direction neuron j from the group n. W_{i-j} is the weight of the recurrent connection from the place cell j to the place cell i and D^n_{i-j} is the weight of the differential connection from the place by direction neuron j from group n to place cell i. V is the speed and θ is the direction of the agent's movement. h_i is the visual input to the place cell i.

The weight matrices $\overline{D^1}$ and $\overline{D^3}$ are set up to compute the activity derivative along the x axis, in positive and negative directions respectively, analogous to (4.6), while $\overline{D^2}$ and $\overline{D^4}$ are tuned to perform the same operation along the y axis of the state space of the agent. According to the matrices, each of the place by head-direction neurons makes a negative projection onto one of its neighboring (in the state space) place cells and a positive projection onto another one.

However, as our simulations later showed, the negative projection is not necessary – just one positive projection from each place by head-direction cell onto one of its neighbouring place cells is sufficient for the model to perform path integration. Therefore, in order to be physiologically realistic, in our simulations (see Chapter 5) we use a version of (4.16) where $D_{i,(i+1)} = 1/(2\Delta x)$ and $D_{i,(i-1)} = 0$ in $\overline{D}$ (see Eq. 4.6). The strength of the differential synaptic connections is modulated by the agent's speed of movement, i.e. the network contains neurons that perform multiplicative

operations on their inputs (Byrne and Becker, 2004). Such neurons have been postulated in models of visual cortex (Mel, 1993; Mel, 1994). On the other hand, there is a possibility that the inputs are provided by the place by head-direction cells and that the firing rate of these cells is also modulated by movement speed, i.e. place by head-direction by speed neurons. This type of neuron is currently being searched for by different research groups.

5. Modeling environmental and self-motion influences on place cell firing.

The firing of place cells seems to represent the location of the rat, and there are at least two types of information which could be used to determine location. These are perceptual information from the environment and internally generated information concerning the rat's own movements. The inevitable accumulation of errors by any system for path integration, including the continuous attractor models referred to above, requires that perceptual environmental information is required to maintain the representation of location in register with the environment. In the absence of such information, behavioural measures of path integration demonstrate the rapid increase in error with movement. For example, a hamster attempting to return to its nest in total darkness will have near-random heading directions after performing 5 full rotations (Etienne, Maurer and Seguinot, 1996). Equally, although place cell firing is maintained in darkness (becoming slightly less precise; Markus et al., 1994), it is possible that the stability of firing depends on input from uncontrolled trial-specific cues in the olfactory, acoustic or tactile domains. Thus, removal of all olfactory cues

within a uniform cylindrical environment coincided with the abolition of spatially specific place cell firing (Save, Nerad, Poucet, 2000).

Previous continuous attractor models of path integration, as well as the model of Mittelstaedt, did not incorporate sensory inputs, and thus were not biologically realistic, since they could not properly emulate the behaviour of the real system for spatial updating. Kali and Dayan (2000) built an attractor network model of allocentric spatial memory, based on recurrently interconnected place cells that receive feed-forward connections from entorhinal cortex neurons. They assume that entorhinal neurons' activity is driven by both spatial and path integration inputs, but they do not model the path integration source of information explicitly. Instead, in certain simulations they modulate entorhinal cell activity in such a way as to account for possible PI inputs. During their simulations of O'Keefe and Burgess' (1996) experiments (see the next section), they assume that visual inputs dominate, and apply no PI modulation to entorhinal cell activity. The entorhinal cells in this case receive only sensory inputs, determined by the agent's distance from each of the four walls of the enclosure, as well as his head direction. The model correctly describes those place fields from O'Keefe and Burgess's (1996) data that follow the transformation of the environment, but does not capture the behaviour of those place cells that remain fixed with respect to one wall or develop a second place field after stretching of the environment.

Any realistic model of place cell firing needs to include perceptual information from the environment in addition to mechanisms for path integration. Indeed, the presence of error in both perceptual and self-motion information indicate that place cell firing represents a compromise between two types of unreliable information. The relative

influence of external perceptual information and internal self-motion information will likely depend on the precise behavioural and environmental circumstances of the rat. In this chapter we consider the mechanisms by which these types of information might give rise to place cell firing, and how they might interact. In the next section we consider a model of the perceptual influences on place cell firing to complement the continuous attractor models of path integration. In the following sections we go on to consider the interaction between the two types of information, focussing on experimental situations designed to put them in conflict so as to be able to evaluate their relative influences on place cell firing.

5.1 Boundary Vector Cell (BVC) model of environmental input to place cells.

In order to investigate the nature of the environmental inputs driving place cell activity, changes to the shape or topography of an environment have been used. Comparing recordings from the same cell made in rectangular environments of varying shape and size, O'Keefe and Burgess (1996) noticed that the location of peak firing typically maintained a constant position to the nearest walls. In addition to this, several fields were stretched along the axes in expanded environments, and some even became bimodal. See Figure 17. O'Keefe and Burgess proposed, based on these findings, that place cells receive inputs that are tuned to respond to the presence of a barrier at a given distance along a given allocentric direction, with sharper tuning at shorter distances. Other studies (see Barry et al, 2005) also suggest that impediments to movement, such as the walls of the environment, a free standing barrier or a sheer drop, play a key role in defining place cell firing. Moreover, Cressant et al (1997)

demonstrated that small objects within the environment did not influence place cell firing when they were isolated, but did when they were put in line to form an extended barrier.

Figure 17. Example of the firing fields ('place fields') of a place cell as a function of the rat's location within a rectangular box in 4 different configurations of shape and size (sides vary between 66 or 122cm). Adapted from O'Keefe and Burgess (1996). Hot colours show higher firing rates. Plots are auto-scaled, peak firing rates vary between 3 and 7Hz).

Inspired by the above experimental findings, Hartley et al (2000) developed the Boundary Vector Cell model of place cell firing. In this model place cell activity is driven by feed-forward inputs from putative BVCs whose firing is determined by the presence of extended barriers (e.g. walls, large objects and impassable drops). A

particular Boundary Vector Cell fires maximally when a barrier is encountered at the BVC's preferred distance and allocentric direction from the rat (Figure 18, *left*).

The receptive field of each BVC is assumed to be a product of two normalised Gaussians, one a function of distance, the other of allocentric direction. The distance tuning is narrow for cells which have a peak response to boundaries near the rat and gradually widens with the distance. This is consistent with the rat being able to judge shorter distances more accurately and means, in accordance with this, that BVCs tuned to shorter distances exert more influence on place cell firing than the ones tuned to longer distances. The angular extent (σ_{ang}) of all fields is assumed to be the same. Thus, the receptive field g_i for a BVC i whose response is greatest to a boundary at distance d_i and bearing ϕ_i relative to the rat's location is given by:

$$g_i(r,\theta) = \frac{\exp[-(r-d_i)^2/2\sigma_{rad}^2(d_i)]}{\sqrt{2\pi\sigma_{rad}^2(d_i)}} \times \frac{\exp[-(\theta-\phi_i)^2/2\sigma_{ang}^2]}{\sqrt{2\pi\sigma_{ang}^2}} \qquad (5.1)$$

where σ_{ang} is constant, and the radial extent σ_{rad}, which controls distance tuning, varies linearly with distance: $\sigma_{rad}(d_i) = (d_i/\beta + 1)\sigma_0$. Here, σ_0 and β are constants determining, respectively, the radial extent of fields at zero distance and their rate of increase with distance.

A section of wall at distance r and bearing θ subtending an angle $\delta\theta$ at the rat contributes:

$$\delta f_i = g_i(r,\theta)\ \delta\theta \qquad (5.2)$$

to the firing rate f_i of Boundary Vector Cell i. For each location (x,y) in the environment, the contribution of all boundaries to the firing of BVC i is determined by integrating (5.2) over θ. This process can be repeated for all locations (x,y) to give the BVC i firing field within the environment. As a result, each BVC has a firing field that follows the boundary of the environment at its favored direction and distance (Figure 18, *right*).

Figure 18. *Left.* A Boundary Vector Cell fires maximally when a barrier is encountered at its preferred distance and allocentric direction from the rat (bar charts on the left represent the cell firing rate). *Right.* Each BVC has a firing field that follows the boundary of the environment at its favored direction and distance (shown in a small and a large square). A place cell firing rate is modeled as the thresholded

sum of two or more BVC firing fields (shown in two bottom rows). Adapted from Hartley et al (2000).

Each place cell receives input from a selection of n BVCs ($n \geq 2$). The place cell's firing rate $F(x,y)$ is modeled as proportional to the thresholded linear sum of the BVC inputs it receives (Figure 18, *right*):

$$F(x,y) = A\Phi\left(\sum_{i=1}^{n} f_i(x,y) - T\right) \tag{5.3}$$

where the threshold T and a weighting parameter A are constants, and Φ is the Heaviside function (i.e. $\Phi(x) = x$ if $x > 0$, $\Phi(x) = 0$ otherwise). Firing does not depend upon the rat's heading and the direction tuning of all BVCs is determined relative to the same allocentric reference frame (assumed to be provided by the head direction system).

Place cell responses generated by the BVC model are similar to the ones obtained experimentally. When geometric changes of the environment take place, the behavior of simulated place cells is similar to that observed by O'Keefe and Burgess (1996), see Hartley et al (2000). The majority of cells maintain their position relative to nearby walls, while some stretch, some become bimodal and a smaller number turn on or off, in appropriate proportions. The model also provides an explanation for the place cell behavior when more radical changes to the environment are introduced (Hartley et al, 2000; Barry et al, 2006).

5.2 Experimental effect of conflicting environmental and PI inputs: Gothard et al (1996b).

Gothard et al (1996b) conducted a study in which populations of hippocampal neurons were recorded simultaneously in rats shuttling on a track between a movable reward site, mounted in a sliding box, at one end and a fixed reward site at the opposite end. On each trial, the box was randomly moved to one of five equally spaced locations, thereby creating mismatches with the originally learned relationships of the box to other cues in the environment (Figure 19). The movement of the box took place while the rat ran toward the fixed reward site, and each time the rat returned to the box in its new position. Along a journey, the same cells were active, in the same order, regardless of the location of the box, although elements of the sequence of place fields on the full track were sometimes omitted.

Figure 19. *A*, Linear track (188 X 8 cm) with the five equally spaced (22 cm apart) box locations used as the start or end point of each journey. *B* shows the five types of outbound journeys, labeled *box1 out*, *box2 out*, etc. *C* shows the five types of inbound journeys. Adapted from Gothard et al (1996b).

The principal finding was that when a mismatch existed between the internal spatial representation and real-world coordinates, defined by external cues, a dynamic correction process took place. For small mismatches, the internal representation, after some initial delay, was translated through intervening states, faster than the actual speed of rat, until the internal representation caught up with true coordinates. In case of large mismatches, however, the internal representation jumped abruptly to the new

position, skipping the intervening coordinates. For intermediate mismatches, a mixture of the two effects was observed.

The internal spatial representation was quantified in terms of population vectors. Then the similarity of the population activation on the full-length journey to the population activation on each of the four types of shortened journeys was tested by correlating point by point the population vectors computed for each spatial location. The results of these correlation procedures for two rats are represented graphically in Figure 20, adapted from Gothard et al (1996b). As the location of the high correlation areas (red ridges in the figure) shows, the population firing patterns at the beginning and end of the journeys (i.e. in the vicinity of the box and fixed food cup) were always similar regardless of the journey type. The correction always took place after some initial time delay, which was longer for the longer journeys and shorter for the shorter ones. After the delay, the bump was usually rapidly translated through the intermediate stages until it was closely aligned with the landmarks corresponding to the end of the track the rat was approaching. The shorter the track was compared to the original one, the more rapid was the correcting translation of the bump. For the journey types 4 and 5 the discontinuity of the ridges can be seen (Figure 20), which is due to the 'jumping' of the bump through the intermediate stages.

Based on the results of this work and also of their earlier study (Gothard et al, 1996a), in which rats shuttled between a box and a pair of landmarks placed variably in a large arena, Gothard et al proposed that firing of the place cells is controlled by a competitive interaction between path integration and external sensory input, primarily vision.

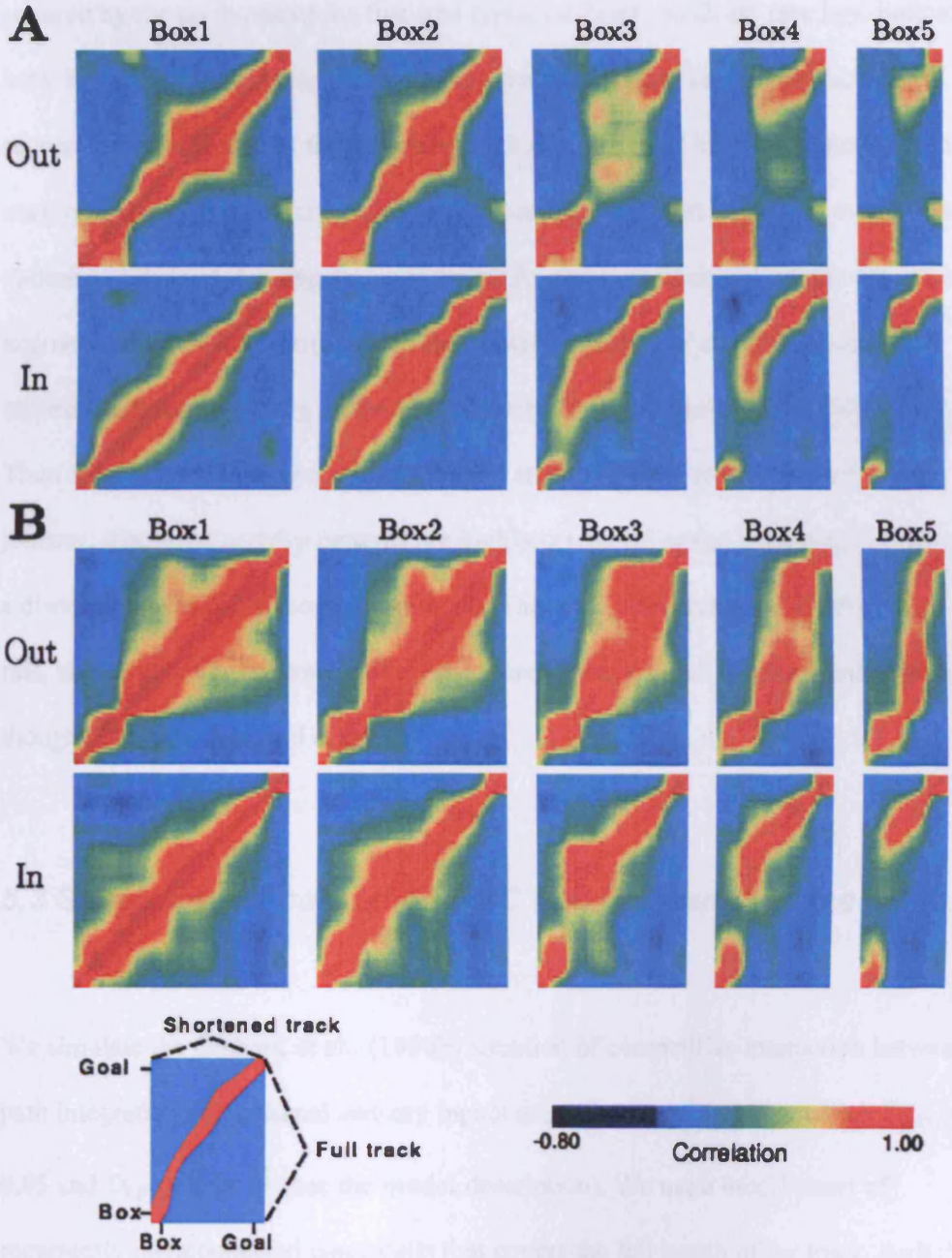

Figure 20. Population vector correlations between the pattern of firing on the full track and on the shortened track for two rats, A and B. For each rat, population vector correlations are shown for the outbound journeys (top five plots) and inbound journeys (bottom five plots). For each correlation plot, the vertical axis corresponds to the full track, whereas the horizontal axis corresponds to the length of the track

covered by the rat in one of the five trial types, i.e. box1, box2, etc (see key, bottom left). Highly correlated firing patterns between one location on the full track and a second location on one of the shortened tracks are indicated in *red.* The first plot in each row is a spatial autocorrelation of the population vectors on the full track, with values of 1.0 along the diagonal. For the rat A, when the track was greatly shortened, e.g. on box4-out trial (fourth plot to the right), the pattern of activity remained correlated at the beginning of the trial when the rat was in the vicinity of the box. Then there is an area of low correlation and an abrupt jump to the final part of the journey, where the activity patterns are highly correlated again, indicating that there is a discontinuous shift in the representation. The rat B, in contrast to the other seven rats, showed continuous transition of the representation on all the outbound journeys, though not on the inbound ones.

5.3 Simulation of combined BVC and PI input to place cells.

We simulate the Gothard et al., (1996b) situation of competitive interaction between path integration and external sensory inputs using the model (4.16) in which $D_{i,(i+1)}$= 0.05 and $D_{i,(i-1)}$= 0 in $\overline{D}$ (see the model description). We use a 86x21 sheet of recurrently interconnected place cells that covers the full length of the track, such that the beginning of the track corresponds to the column 11 of the place cell sheet, and the end of the track to the column 76 of the sheet. Thus, at the start, the population activity bump is centered at the place cell which occupies 11^{th} position in the sheet, both horizontally and vertically. The time constant τ is set to 0.05, the strength of the synapse from any place cell onto the inhibitory neuron γ to 0.04, and the synaptic strength of the negative feedback J to 0.123. All the simulations were done in

MATLAB 7.1, using differential equation solver 'ode45'. This takes the initial state of all the firing rates, a constant running speed (V = 5) and orientation ($\theta = 0$; i.e., along the track), the (constant) connection weight values, and iterates equation 4.16, determining which time points to the sample itself. Note that these parameter values were chosen to illustrate the model's behaviour – the dependence of behaviour on parameter values is explored more systematically in the more complete place cell-grid cell model (later).

When simulated without any external input, the model generates a stable activity profile of a Gaussian shape (Figure 21). This activity profile can be sustained indefinitely without any external inputs (although may move around a little bit if the firing is noisy), which is in agreement with the persistence of place cell activities in total darkness (although some people think that persistent firing depends on odor cues, see Save, Nerad, Poucet, 2000). The activity bump position is updated by the model in accordance with the specified values of speed and movement direction.

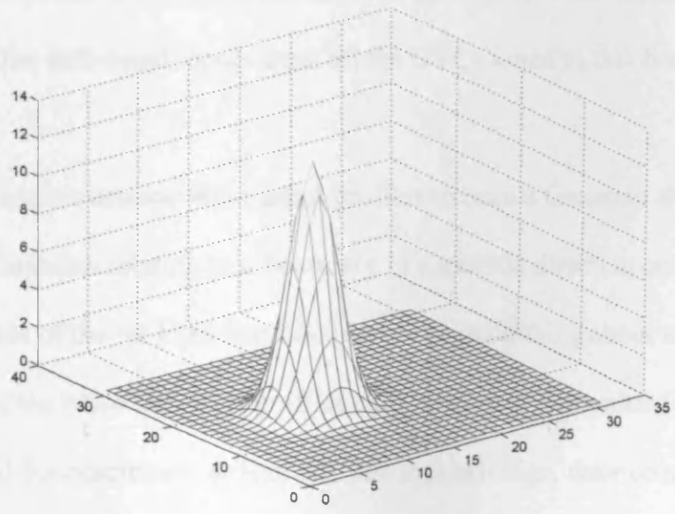

Figure 21. The Gaussian activity profile is kept stable without any external inputs.

5.3.1 The shape of the Boundary Vector Cell inputs.

In order to simulate interactions of visual inputs with the path integration mechanism, in situations similar to those studied by Gothard et al, we must specify the BVC input to place cells. Every place cell in our model is assumed to receive inputs from up to four orthogonally tuned BVCs, each of which has directional tuning perpendicular to one of the up to four surrounding boundaries. In different simulations, we consider inputs from only one boundary (the one ahead of the rat when running on a linear track, or all four walls when foraging freely in a rectangular box, see below). Each of these BVC inputs to a place cell is assumed to have a preferred distance matching the distance from the centre of the place field to the boundary in the BVC's preferred direction (in the standard, or familiar environment, i.e., before any deformation of the environment has taken place).

The position of the place cell activity bump in the state space, representing the environment, is thus controlled by the sets of BVC inputs, each associated with a boundary in a specific direction. Each set of these inputs, or an "input profile", is composed of the individual inputs from all the BVCs tuned to that boundary.

In our modelling we assume these input profiles to have a Gaussian shape, with the mean of the Gaussian relating to a boundary in a specific direction occurring at the current distance of the rat from that boundary. The good thing about such a Gaussian shape is that even when two such profiles shift relative to each other (e.g., when the environmental boundaries are deformed), and thus misalign, their combined input (i.e. their sum) still remains focused and relatively symmetric, if the relative displacement is not too great (i.e. a reasonable overlap is preserved). And this is the case even if the two Gaussians considerably differ in magnitude and variance. We need the combined

input profiles to stay relatively focussed, otherwise it will be impossible for visual inputs to control the position of the place cell activity bump.

On the other hand, if we assume Gaussian shape for individual BVC tuning curves, rather than for the overall input profile from a boundary, the resulting overall input profiles will not be Gaussian such that the sum of two displaced input profiles will be less likely to control the position of the activity bump. Although in the case of single place cells a Gaussian BVC curve may give a reasonable fit, as in O'Keefe and Burgess (1996), it does not work so well for a large group of cells.

In order to reduce a number of parameters, and thus to make fitting easier, we assumed that the amplitude and variance of these Gaussian profiles vary linearly with the distance from the boundary to which a given BVC is tuned (corresponding to the decreasing influence of more distant boundaries). The following linear equations gave a reasonably good fit to the stretching and squashing observed in the most recent experiment using four walls to form a variable shaped rectangular boundary (Barry et al., 2007; see Section 6.3.3 for simulations of these data): $A(d_i) = 1.218 - 0.0042d_i$; $\sigma(d_i) = 21.5 + 0.1011d_i$, where A is the amplitude, σ is the standard deviation and d_i is the mean of a profile.

Then we decomposed a set of firing profiles, described by these equations and spanning 160m, into a set of tuning curves for individual BVCs distributed through that distance. The equation (5.4) for the shape of each individual BVCs response, as a function of its preferred distance d_i then was found to give a remarkably good fit to the overall profile, i.e. to provide the description of how the shape of BVC curves changes with the tuning distance:

$$h_i(x) = A(d_i)\exp\left(\frac{-(x-d_i)^2}{2(\sigma(d_i)+a(x-d_i))^2}\right) \quad (5.4)$$

where $a = 0.1086$. Both A and σ vary linearly with preferred distances of BVCs: $\sigma(d_i) = 21.5 + 0.1011d_i$, while $A(d_i) = (1.218 - 0.0042d_i)$ for the simulations of free foraging in rectangular boxes (see above and Section 6.3.3 below).

The tuning curves of our BVCs are similar to those proposed by Hartley et al (5.1), with the main difference being that the variance of a particular (otherwise Gaussian) curve is not constant, but instead is a linear function of the distance from the peak of the curve. See Figure 22. This makes our curves skewed, so that the side oriented towards the boundary of interest is steeper than the one oriented away. Such a shape seems to be physiologically plausible, since shorter distances are easier to estimate.

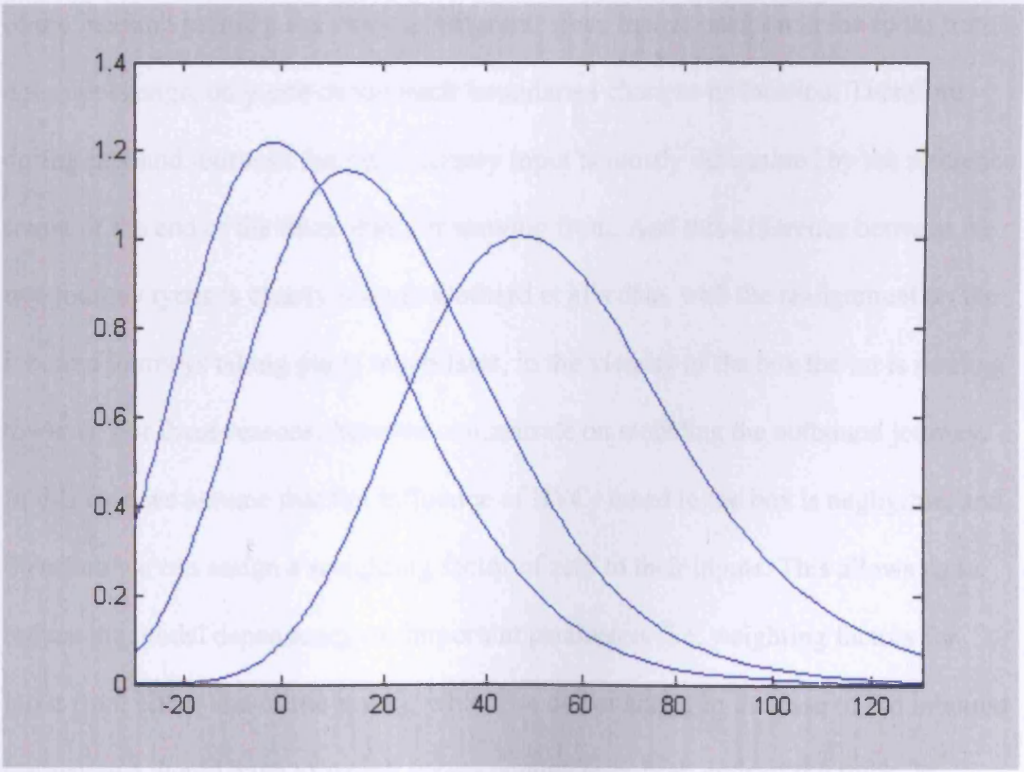

Figure 22. The shape of the BVC tuning curves in the combined model. Note the slight asymmetry, as the variance increases linearly with the distance of the rat from the boundary relative to the distance at which the BVC is tuned to fire maximally.

5.3.2 Simulation of the Gothard et al. (1996b) place cell experiment.

In Gothard et al.'s (1996b) experiment, there is a considerable difference between outbound and inbound journeys. In the case of the outbound journey, a change in the box location results in a change of the starting rat position relative to the entire room. On its journey from the box, the rat presumably does not see the box. Although rats apparently have a field of view of 330 degrees, the box is right behind the rat and is sufficiently small. And when the rat runs, it has to concentrate on the path in front of it. This allows us to assume that inputs from BVCs tuned to the box are negligible compared to the ones coming from BVCs tuned in the opposite direction. In the case of the inbound journey, the story is different, since the rat position in the room frame does not change, only one of the track boundaries changes its location. Therefore during inbound journeys the rat's sensory input is mostly determined by the reference frame of the end of the track that it is moving from. And this difference between the two journey types is clearly seen in Gothard et al's data, with the realignment on the inbound journeys taking place much later, in the vicinity of the box the rat is running towards. For these reasons, here we concentrate on modeling the outbound journey. In this case we assume that the influence of BVCs tuned to the box is negligible, and therefore we can assign a weighting factor of zero to their inputs. This allows us to reduce the model dependency on important parameters (i.e. weighting factors for input from either end of the track), which we do not know. In the case of the inbound journey, we would have to weigh inputs coming from both ends of the track. In

addition, no manipulations are made to boundaries on either side of the track, so we also ignore any BVCs tuned to the lateral directions. Thus, h_i in our model (4.16) represents an input to the place cell i from the BVC i, which is tuned to the boundaries in front of the rat, and is given by (5.4). To make up for the reduced number of BVCs, we triple the amplitude of the BVCs tuned to the one direction considered so that: $A(d_i) = 3(1.218 - 0.0042d_i)$.

During simulations the initial starting position of the rat was changed in such a way as to emulate the Gothard et al experiment. The behavior of the model resembled in a number of ways the behavior described by Gothard et al. Thus, during small mismatches, the activity bump was translated through intermediate positions until its location was in agreement with the external inputs provided by the BVCs tuned to the approaching end of the track. The speed of translation depended on the mismatch magnitude, with larger mismatches resulting in more rapid translations (Figure 23, *top*). When the mismatch was large, the activity bump dissolved in its initial position and reappeared in a 'correct' one, in line with Gothard et al findings (Figure 23, *bottom*). For intermediate mismatches, a combination of the two effects sometimes took place, which was also noted by Gothard et al. (1996b).

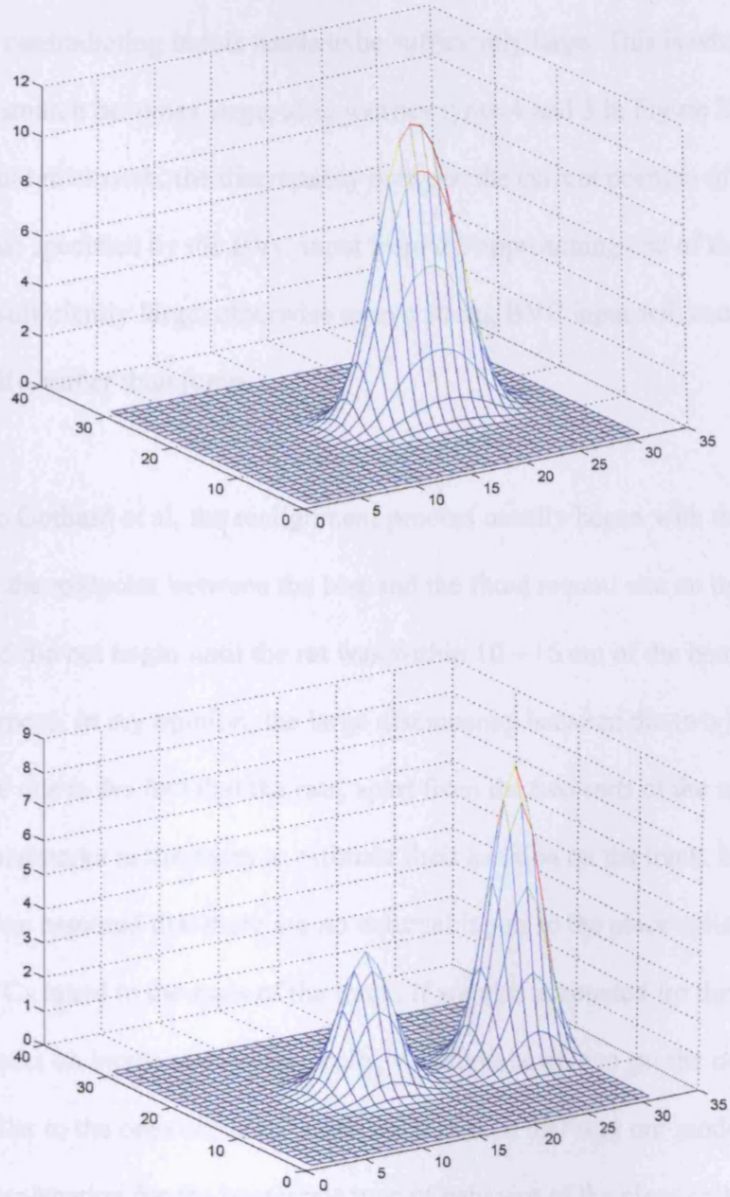

Figure 23. *Top*: A rapid activity bump translation through intermediate stages in order to clarify a moderate mismatch between visual and path integration inputs. The bump elongation is due to a hysteresis effect caused by the rapidity of translation. *Bottom*: The activity bump 'jumps' through intermediate stages if the discrepancy between visual and path integration inputs is large.

In order for the bump to make a jump to a new location, the difference in magnitude between the contradicting inputs needs to be sufficiently large. This is what happens when the mismatch becomes large, as in journey types 4 and 5 in Figure 20. Apart from the signal mismatch, the discrepancy between the current position of the activity bump and that specified by the BVC input from the approaching end of the track also needs to be sufficiently large, otherwise even a strong BVC input will cause the bump to shift rapidly, rather than jump.

According to Gothard et al, the realignment process usually began with the rat approaching the midpoint between the box and the fixed reward site on the outbound journeys, and did not begin until the rat was within 10 – 15 cm of the box on the inbound journeys. In my opinion, the large discrepancy between the two journeys appears to be due to the fact that the rats, apart from the two ends of the track, also used other landmarks in the room to estimate their location on the track. In our simulations we assumed that there are no external inputs to the place cells other than from the BVCs tuned to the ends of the track. If we also accounted for the effect of other landmarks on inputs to the place cells, we might be able to get the delay patterns similar to the ones observed experimentally. In that way our model could provide an explanation for the hysteresis type of behavior of the place cells observed by Gothard et al, which they suggested was due to the fact that the path integration mechanism normally dominates the update process.

The issue of time delay before the beginning of realignment was also addressed by Redish et al (2000). Following their experimental studies, they concluded that deterministic explanations of place cell firing as a consequence of external cues are insufficient, and that temporal dynamics of change from previous activity states needs

to be taken into account. This is certainly true, though hardly can provide an explanation for the difference in delays between the outbound and inbound journeys.

Below are shown simulation results, generated by equations (4.16) and (5.4), for the original length of the track (160cm: the length of track used by Gothard et al., outside of the moveable starting box) and three equally spaced shortened versions: 134cm, 107cm and 80cm (Figure 24).

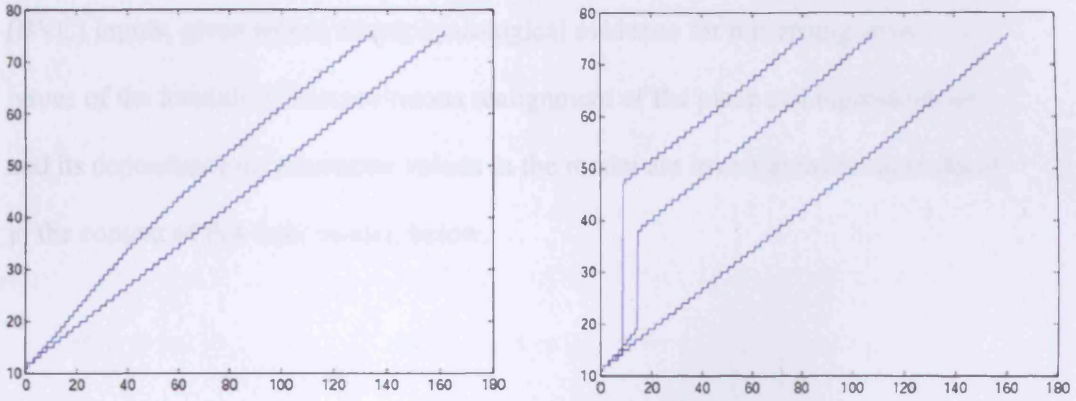

Figure 24. Realignment of the simulated place cell representation of location as track length varies. Plots show position on the track on the *x* axis and of the relevant place cells ordered by their location of peak firing on the full length track on the *y* axis. The 11th place cell in columns 11-76 have peak firing locations evenly distributed along the full length track. The blue line shows where each of these place cells (labeled by its column number) has its peak firing location on the track. Left plot shows the full length track (160cm) and the next longest track configuration. Right plot shows the full length track and the two shortest track configurations. Note the smooth transition shown on the left and the 'jump' shown on the right.

The model shows gradual realignment of the place cell representation of location when the track is slightly shortened, and a sudden jump when the track is shortened

significantly. See Figure 24. However, for the parameter values used above, the transition to the reference frame of the box ahead of the rat occurs much earlier on the track than was seen by Gothard. This indicates that either the relative strength of the input from BVCs is too high compared to the input received via recurrent connections, or weighted too much in favour of the cues ahead of the rat, or that the time constant τ of the system is too short compared to the running speed V. However, rather than tuning the parameters of this model further, I develop it into a model with the mechanism for PI explicitly separated from the place cells and their perceptual (BVC) inputs, given recent neurophysiological evidence for this arrangement. The issues of the location of discontinuous realignment of the place cell representation, and its dependence on parameter values in the model are investigated in more detail in the context of this later model, below.

6. Integration of environmental and self-motion information: a reciprocal interaction between Entorhinal grid cells and place cells?

Subsequent to the development of the continuous attractor models of place cell firing, and to the start of my own simulations, an experimental discovery was made which appears to provide a significant insight into the issues considered above. In this chapter we consider the implications of this discovery for the interaction of path integrative and perceptual influences on the brain's representation of self-location.

That is, we consider how the work in the previous chapter should be updated in the light of this discovery.

6.1 Entorhinal grid cells.

In 2005, Hafting and colleagues discovered a new type of cell with a spatially-specific firing pattern in the medial entorhinal cortex (mEC), which they called grid cells. Each of these cells fires in multiple locations in an environment, such that the locations can be perceived as nodes of a regular grid of equilateral triangles spanning the whole environment (Figure 25, *left*, *middle*). Neighbouring grid cells have been found to have the same grid spacing and orientation relative to the environment. Yet they all appeared to have different phases, such that the grid nodes of one grid cell were shifted relative to the grid nodes of its neighbouring cell, suggesting that the whole environment was covered by the nodes of a local cell group with a common grid spacing and orientation (Figure 25, *right*). Each cell appears to preserve a shape and size of its grid firing pattern unchanged throughout environments of different shapes and sizes. At the same time the orientation of the grid is controlled by polarizing visual landmarks in each environment, in the same way as the head-direction cells (Taube, 1998). As well as the orientation, the phase of the grid also remains constant throughout multiple exposures to the same environment, and so is also probably anchored to external landmarks. The spacing and field sizes of the grid cells located more dorsally/ventrally in the mEC differ, gradually increasing with increasing depth from the postrhinal border.

Figure 25. *Left*. Plots of spike locations (*red*) along the rat's trajectory (*grey*) of three neighboring grid cells. *Middle*. Firing rate maps of these three grid cells. *Right*. *Above*: The spike locations of the three cells shown in different colors (*red, green and blue*). *Below*: The locations of peak firing rates for the three cells (*labeled by numbers*). Adapted from Hafting et al (2005).

6.2 Modeling the PI input to place cells via grid cells and the environmental input to grid cells via place cells.

6.2.1 The PI input to place cells via grid cells.

The fact that the grid cells preserve the shape and size of their grids despite removal of visual cues, suggests a path integration mechanism is responsible for maintenance of the grid structure. That the mEC is directly involved in path integration is also suggested by the disruption of return paths (Parron et al, 2004) and spatial search patterns (Steffenach, 2005) during navigation of rats with entorhinal lesions.

Since, similar to the CA1 and CA3 areas of the hippocampus, recurrent connections are also present in the mEC (Lingenhohl and Finch, 1991; Germroth et al, 1991; Dhillon and Jones, 2000), it is reasonable to suggest that a grid-cell-based path integration mechanism would be similar to the one proposed above which is based on recurrent connections between the place cells. Hafting et al. (2005) also point out that the mEC receives direct inputs from the head-direction cells of the postsubiculum, having in this respect an anatomical advantage over the place cells which do not.
At the same time, according to Hafting et al (2005), the fact that neighbouring grid cells have constant spacing, field size and orientation of grids, as well as variable grid phasing, suggests that conjunctions of active neurons are repeated periodically as the rat moves over a surface. The basic operation of such grid-cell-based path integrating mechanism is explained in Figure 26, adapted from O'Keefe and Burgess (2005).

Figure 26. Schematic of grid-cell-based path integration mechanism (for simplicity demonstrated using a cluster of just nine grid cells). **A)** Connections between grid cells that have aligned grid-like firing patterns with conjunctive phases (see *b*). The connections from one cell (black in the middle) are shown with black arrows. The cell has connections to each of its neighbours that are modulated by inputs from head direction cells (grey lines), each of which is tuned to one of the six directions from the central cell to its neighbours. The modulation can take place at the level of target neuron dendrites, or at the level of the grid cell providing the shifting input, which in this case would be a grid by head-direction cell (by analogy with the place by head-direction cells). A modulation by the rat's speed is also required analogous to the first model. **B)** The locations of peak firing of the grid cells from *a*, as well as two additional ones (for full coverage), are shown. The grey arrow shows the direction of rat's movement. **C)** *Top row:* An activity bump shifting through the population of topologically organized place cells when the rat moves as shown in B. *Bottom row:* Activity propagating through the nine grid cells whose firing patterns are shown in *b* (firing rate of each cell is shown by a bar above it). These nine cells are repeatedly used to provide path integration along any trajectory in any environment.

Thus, as can be seen, the proposed grid-cell-based mechanism of path integration is similar to the place-cell-based one, with the difference that a particular grid cell receives inputs from six surrounding grid cells, modulated by the rat's movement direction, instead of four in the case of place cells. The number of cells is also limited (with n=9 being the smallest possible number), and the cells are cyclically organized providing a number of path integration circuits. Similar proposed mechanisms have recently been implemented and shown to be sufficient to provide a path integration signal (Fuhs and Touretzky, 2006; McNaughton et al., 2006). However, while

acknowledging the need for perceptual inputs from the environment to stabilize the grid cell firing patterns, these previous studies did not attempt to describe or simulate these inputs, or their interaction with path integration, in any detail.

Since grid cells fire in multiple locations in the environment, the grid-cell-based path integration mechanism by itself is insufficient to allow navigation to specific previously visited locations. The place cell activity, on the other hand, can enable accomplishment of such a task (e.g. Burgess et al, 1994). Therefore it is reasonable to suggest that the grid cells provide driving inputs to the place cells. A particular place cell in such a set up would receive connections from all the grid cells, with various grid orientations and spacing, that happen to be active near to the place field in a particular environment. The connection weights could be a Gaussian function of the preferred locations of the place and grid cells, similar to the recurrent connections between the place cells (Eq. 4.9). The combined input from all the grid cells connected to a particular place cell will be maximal at the centre of the place field and will decay with increasing distance from it, since the inputs from grids of different orientations and scale will no longer converge (see Figure 27, adapted from O'Keefe and Burgess (2005)).

6.2.2 The environmental input to grid cells via place cells.

Place cells, in turn, are also expected to provide inputs to grid cells, based on similar principles, i.e. the connection strength being a Gaussian function of the preferred locations of the grid and place cells (Eq. 4.9). This is needed in order to anchor the grid-like responses of grid cells to the environment. This cannot be achieved by providing sensory inputs, e.g. from the BVCs, directly to grid cells, since their

responses are not tied up to one specific location in the environment like those of place cells. But what cannot be done directly, can be done via place cells, since each grid cell is expected to be linked to all those place cells with which it happened to fire in the same place during initial exposures to the environment (Figure 27). These same connections, i.e. from a place cell to neighbouring (in the state space) grid cells, also serve the purpose of registering together different clusters of grid cells, each having a specific grid orientation and spacing. This is needed in order to maintain a stable relationship between them, and cannot be achieved by connecting those clusters directly since grid cells fire in multiple locations in an environment, so that the firing of 2 grid cells from different clusters might only overlap at a single location.

Figure 27. The schematic shows how sets of grid cells with different orientations of their grid-like firing patterns would allow place-cell-based navigation. Inputs from place cells to grid cells provide means of registering the grid cell firing patterns to external landmarks and to each other. Note that the different orientations of grid

shown here have not been found – grid orientations seem to be constant within a rat (Barry et al., 2007).

6.2.3 The grid cell – place cell model.

In order to model the behavior of the navigation system based on the reciprocal interactions between place cells and grid cells, we assume that inputs to place cells are provided by three sets of grid cells, all with the same grid orientation, but different grid scaling and 441 cells in each.

The proposed system is represented by the following set of equations:

$$\tau\frac{dr(g^1)_i}{dt}=-r(g^1)_i+\left((\sum_j W_{i-j}r(g^1)_j+V\Phi(|\theta-0^\circ|)a^1r(g^1)^W+V\Phi(|\theta-60^\circ|)a^1r(g^1)^{SW}+V\Phi(|\theta-120^\circ|)a^1r(g^1)^{SE}\right.$$

$$\left.+V\Phi(|\theta+180^\circ|)a^1r(g^1)^E+V\Phi(|\theta+120^\circ|)a^1r(g^1)^{NE}+V\Phi(|\theta+60^\circ|)a^1r(g^1)^{NW}+\sum_j P^1_{i-j}r(p)_j)/J\gamma\sum_j r(g^1)_j\right)^2;$$

$$\tau\frac{dr(g^2)_i}{dt}=-r(g^2)_i+\left((\sum_j W_{i-j}r(g^2)_j+V\Phi(|\theta-0^\circ|)a^2r(g^2)^W+V\Phi(|\theta-60^\circ|)a^2r(g^2)^{SW}+V\Phi(|\theta-120^\circ|)a^2r(g^2)^{SE}\right.$$

$$\left.+V\Phi(|\theta+180^\circ|)a^2r(g^2)^E+V\Phi(|\theta+120^\circ|)a^2r(g^2)^{NE}+V\Phi(|\theta+60^\circ|)a^2r(g^2)^{NW}+\sum_j P^2_{i-j}r(p)_j)/J\gamma\sum_j r(g^2)_j\right)^2;$$

$$\tau\frac{dr(g^3)_i}{dt}=-r(g^3)_i+\left((\sum_j W_{i-j}r(g^3)_j+V\Phi(|\theta+0^\circ|)a^3r(g^3)^W+V\Phi(|\theta-60^\circ|)a^3r(g^3)^{SW}+V\Phi(|\theta-120^\circ|)a^3r(g^3)^{SE}\right.$$

$$\left.+V\Phi(|\theta+180^\circ|)a^3r(g^3)^E+V\Phi(|\theta+120^\circ|)a^3r(g^3)^{NE}+V\Phi(|\theta+60^\circ|)a^3r(g^3)^{NW}+\sum_j P^3_{i-j}r(p)_j)/J\gamma\sum_j r(g^3)_j\right)^2;$$

$$\tau\frac{dr(p)_i}{dt}=-r(p)_i+\left((\sum_j W_{i-j}r(p)_j+\sum_j G^1_{i-j}r(g^1)_j+\sum_j G^2_{i-j}r(g^2)_j+\sum_j G^3_{i-j}r(g^3)_j+h_i)/J\gamma\sum_j r(p)_j\right)^2.$$

(6.1)

Here $r(g^1)_i$, $r(g^2)_i$ and $r(g^3)_i$ are the firing rates of the grid cell i from the first, second and third sets of grid cells correspondingly, whereas $r(p)_i$ is the firing rate of the place cell i. W_{i-j} is the weight of the recurrent connection from the grid/place cell j to the grid/place cell i, given by (4.9). P_{i-j} is the connection weight from the place cell j to the grid cell i and G_{i-j} is the connection weight from the grid cell j to the place cell i, both determined according to (4.9). a is the weight of the connection onto the grid cell i from the grid cell $r(g^n)^D$, where n is the set number and D gives the direction in which the cell are located from the cell i (the direction is determined relative to the axes of grid patterns generated by the set of grid cells). γ represents the strength of synapse from any grid/place cell onto a global inhibitory neuron for that set of grid/place cells, and J is the synaptic strength of the negative feedback from it. V is the speed and θ is the direction of the rat's movement. h_i is the external input to the place cell i. Function Φ describes the responses of head-direction cells in the following way:

$$\Phi(|\theta - \theta'|) = \begin{cases} \dfrac{2\cos(|\theta - \theta'| + 30^\circ)}{\sqrt{3}}, & |\theta - \theta'| \le 60^\circ \\ 0 \qquad otherwise \end{cases} \tag{6.2}$$

where θ' is a preferred angle of a particular head-direction cell and θ is an angle of rat's head direction. The equation (6.2) provides the form of the directional modulation of the inputs to each grid cell from its six neighbours necessary to perform path integration correctly. That is, this function describes the amplitude modulation required for the sum of the translation vectors produced by cell's neighbours (in the hexagonal grid) to equal the rat's actual translation.

6.3 Simulation of Gothard et al (1996b) place cells and Barry et al (2007) grid cells.

6.3.1 Simulation of the Gothard et al (1996b) place cell experiment

We simulate the grid cell - place model, given by equations (6.1), (6.2) and (5.4), in the situation of the Gothard et al. (1996b) experiments, in the same way as was done for the place cell model given by equation (4.16) in Chapter 5. Similarly, we use a 86x21 sheet of recurrently interconnected place cells that covers the full length of the track, such that the beginning of the track corresponds to the column 11 of the place cell sheet, and the end of the track to the column 76 of the sheet. Thus, at the start, the population activity bump of place cells is centered at the place cell which occupies 11^{th} position in the sheet, both horizontally and vertically. Again, only BVCs tuned to respond in the direction ahead of the rat are considered, and their amplitude is given by $A(d_i) = 3(1.218 - 0.0042d_i)$, as in section 5.3.2.

In addition to the place calls, and playing the same role as the asymmetric connections between them in the model in chapter 5, we also simulate three sets of 441 grid cells, each recurrently interconnected in the way that would result via Hebbian learning from the hexagonal topology of multiple firing fields of individual cells, see equation 6.1. All three sets have the same grid orientation, but different scaling, in accordance with recent physiological data (Barry et al., 2007). The grid scale of the medium set is 0.7188 of the large one, and the grid scale of the small set is 0.7188 of the medium one. The standard deviations of the individual firing fields of at the vertices of their grids scale accordingly, which also appears to be consistent with physiological data, and are as follows: 5cm, 7cm and 9.65cm.

Each set of grid cells makes synaptic projections onto the sheet of place cells, with the synaptic strengths given by a Gaussian function of the preferred locations of the grid and place cells in question. The variance of the Gaussian is equal to the average of the variances of the place and grid cell firing fields, and the peak value is equal to 2. In return, each set of grid cells receives synaptic connections from the place cells, which are described by the Gaussian with the same variance, but with the peak value equal to 6.

In addition to setting the strengths of these connections, a further assumption was made regarding synaptic transmission between the two layers: that only high firing rates propagated through these connections. Thus only firing rates exceeding a threshold r propagated between place cells and grid cells, where $r = r_{max} - 6$. The reason for this was to make sure the input between layers was spatially specific – i.e. only firing from the centres of the firing fields of place cells or grid cells should influence the representation in the other layer. There is some physiological evidence to support the idea that only spikes fired during periods of high-firing rate ("bursts" of spikes) are reliably transmitted by synapses in the hippocampal region (see Lisman, 1997, for a review).

As in the place cell only simulation in section 5.3.2, h_i in (6.1) represents the input solely from BVC inputs tuned to the boundary in front of the rat, given by (5.4), but is now increased by a factor 1.5 compared to the previous simulation, i.e. $A(d_i) = 4.5(1.218 - 0.0042d_i)$. The direction of the agent's movement $\theta = 0$ and the speed $V = 8$ across all trials. The time constant τ is set to 0.05, the strength of the synapse from any place cell onto the inhibitory neuron γ to 0.04, and the synaptic strength of the negative feedback J to 0.123, as in the place cell only simulation, above. All the simulations are done in MATLAB 7.1, using differential equation solver 'ode45'.

The model showed a behavior similar to the behavior of the first place-cell only model. The main difference was that this model required a stronger net external input for the activity bump to jump, making it start jumping further along the shortened track of the same length, when the mismatch signal was stronger than in the case of the first model. Correspondingly, the minimal length of the shortened track on which the jump occurred was smaller in the case of the second model. This is not surprising, since inputs from the three sets of grid cells are holding the bump in its original position. Therefore, in order for the bump to jump, the net external input to the place cells has to be stronger than the combined input from the three sets of grid cells.

On longer tracks the realignment was achieved via the bump translating through intermediate stages in the state space, with the speed of the translation increasing with the magnitude of the mismatch. When the place cell activity bump shifted due to external inputs, it dragged along the three grid cell activity bumps. On the other hand, when the bump jumped, it either caused the grid cell bumps to jump with it, or just shifted them until they aligned with its new location. Whether the former or the latter took place, depended, apart from the magnitude of the mismatch, on the strength of the connections from the place cells onto the grid cells. If the connections are comparatively weak, then the strength of place cell inputs is insufficient for the grid cell bumps to jump. Instead, they are translated through the intermediate stages with the speed increasing with the connection strength. When the latter become sufficiently strong, the grid cell activity bumps start to jump, with some initial delay after the jumping of place cell activity bump (Figure 28). The delay is needed to build up the place cell activity bump in its new position and thus to build up the strength of

the inputs to the grid cells. This time delay, again, decreases with the increasing strength of connections from place cells onto grid cells.

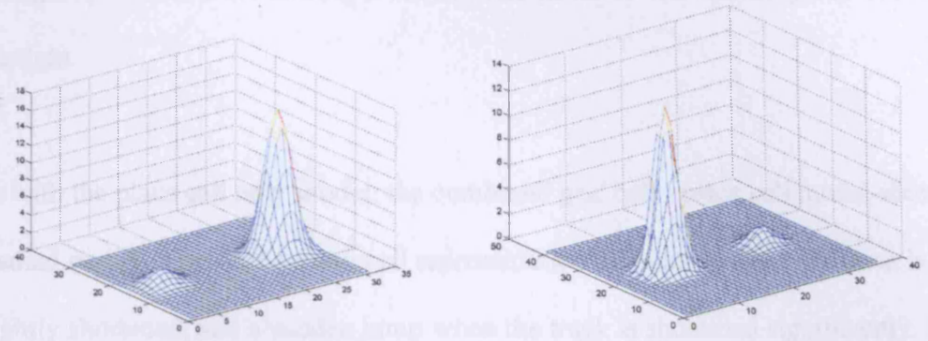

Figure 28. External inputs cause a realignment of place cell activity via activity bump jumping (*left*), which is followed, after some time delay, by jumping of the grid cell activity bump (shown for one set of grid cells, *right*).

Figure 29, below, shows simulation results, generated by (6.1), (6.2) and (5.4), for the original length of the track (160cm) and three equally spaced shortened versions: 134cm, 107cm and 80cm.

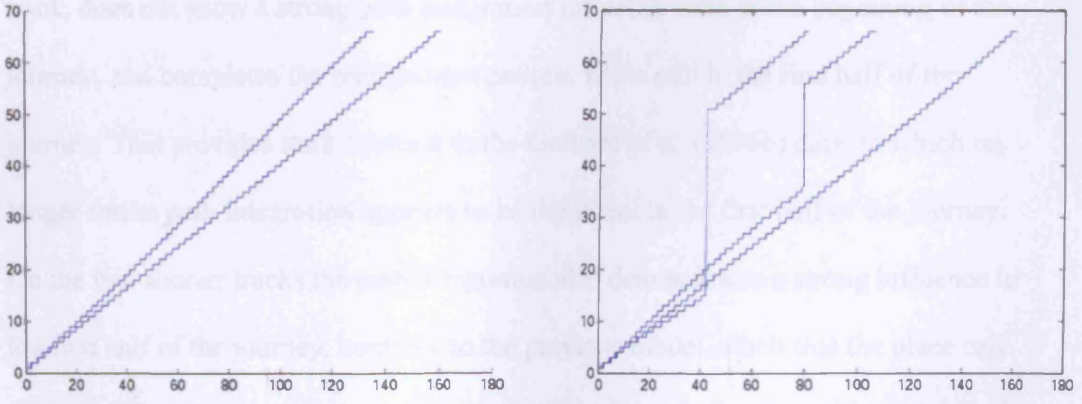

Figure 29. Realignment of the simulated place cell representation of location as track length varies in the combined grid cell-place cell model. Plots show position on the track on the *x* axis and place cells ordered by their location of peak firing on the full length track on the *y* axis. The blue line shows where each cell has its peak firing

location. Left plot shows the full length track (160cm) and the next longest track configuration. Right plot shows the full length track and the two shortest track configurations. Note the smooth transition shown on the left and the 'jump' shown on the right.

As with the place cell only model, the combined grid cell - place cell model shows gradual realignment of the place cell representation of location when the track is slightly shortened, and a sudden jump when the track is shortened significantly. See Figure 29. The most notable difference, though, is that the realignment happens much later on the track than in the case of the place cell model, even though for this model we increased A, the amplitude of the sensory input – BVCs from ahead of the rat, in (5.4) by a factor of 1.5 . When the track is slightly shortened, in the beginning of the journey the activity bump behavior appears to be dominated by the PI inputs, and then, closer to the middle of the track, visual inputs start playing a more prominent role. The realignment gets completed when the rat is already deep into the second half of the track. On the other hand, the place cell model, when on the same shortened track, does not show a strong path integration influence even in the beginning of the journey, and completes the realignment process while still in the first half of the journey. This provides stark contrast to the Gothard et al. (1996b) data, in which on longer tracks path integration appears to be dominant in the first half of the journey. On the two shorter tracks the path integration also demonstrates a strong influence in the first half of the journey, contrary to the previous model, albeit that the place cell firing profile of the representative rat A appears to jump before the mid-point (see Figure 20).

6.3.2 More detailed simulation of Gothard et al (1996b).

After detailed analysis of the results of the model simulations, it was found that on the two shortest tracks the place cell activity bump was continuously changing in height in an oscillatory manner, up to the point of a jump (but not after the jump). The amplitude of those oscillations was quite large, and as a result large oscillations appeared in place fields of individual cells, thus corrupting them. Especially the cells that are active in the central region of the track were affected. Analyzing the behavior of the model, we found that, when mismatched visual inputs generated a second, smaller, activity bump in front of the first one on the place cell layer, this activity propagated further down to the layer of grid cells via place cell – grid cell connections, thus intervening with their operation.

In order to stop propagation of visual inputs to the grid cells, we raised the firing rate threshold, which place cells need to exceed in order to provide inputs to grid cells, to: $r = r_{max} - 4$, where r_{max} is the highest place cell firing rate at a particular time (the firing threshold for the grid cell to place cell connections remained at $r = r_{max} - 6$). In order to compensate for this input reduction, we increased the maximum value of the corresponding place cell – grid cell connection weights from 6 to 10. Other model parameters have not been changed, with the exception of the strength of connections from grid to place cells (G, below). This we systematically varied across different track lengths in order to investigate its influence on the behavior of the model. As we have seen from the two previous simulations, its presence or absence makes a big difference to the behavior of the model.

Figure 30 shows results of the simulation of the modified grid cell – place cell model, performed, like in the Gothard et al. (1996b) experiment, on five different track lengths - varying from 160 to 80cm in steps of 20cm.

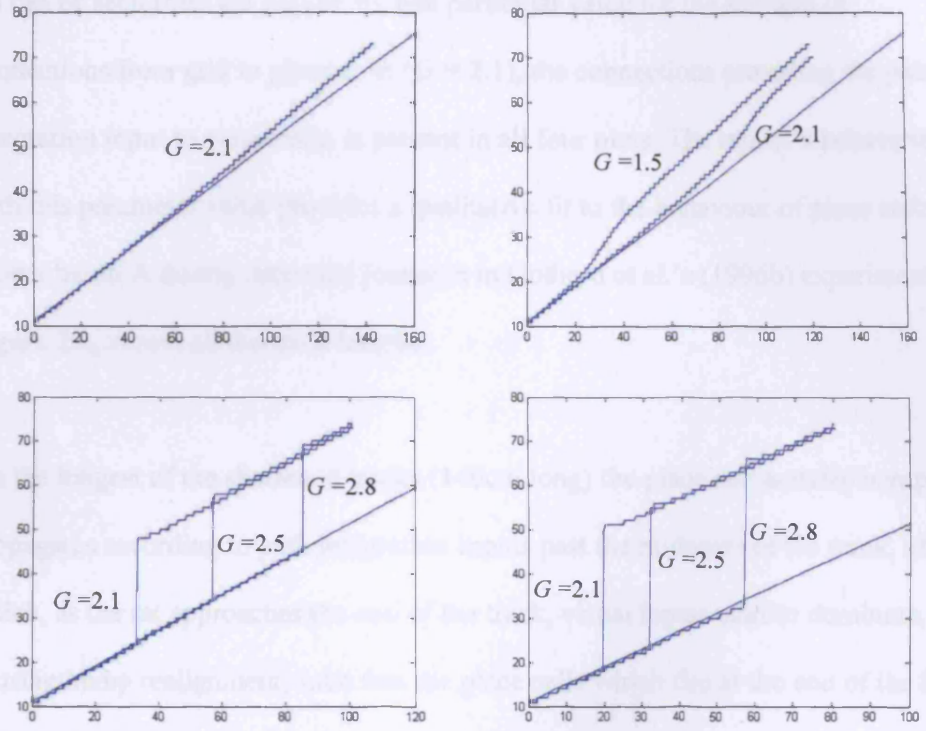

Figure 30. Realignment of the simulated place cell representation of location as track length varies in the combined grid cell-place cell model. Plots show position on the track on the *x* axis and the relevant place cells ordered by their location of peak firing on the full length track (160cm) on the *y* axis. The 11th place cell in columns 11-76 have firing peaks evenly distributed along the track, and these are shown against their column number (see also Figures 24 and 29). Each blue graph represents a particular simulation and shows where each cell has its peak firing location in that simulation. The straight blue line in each plot represents, for reference purposes, ideal peak firing locations of the place cells on the full length track. The plots show how the behaviour of the model changes when the strength of projections from grid to place cells, and

also the track length, are varied. Top Left) track length l = 140cm; projection strength G = 2.1; Top Right) l = 120cm; G = 1.5, 2.1. Bottom Left: l = 100cm; G = 2.1, 2.5, 2.8; Bottom Right: l = 80cm; G = 2.1, 2.5, 2.8

As can be seen from the Figure 30, one particular value for the strength of connections from grid to place cells (G = 2.1), the connections providing the path integration input to place cells, is present in all four plots. The model's behaviour with this parameter value provides a qualitative fit to the behaviour of place cells shown by rat A during outbound journeys in Gothard et al.'s (1996b) experiment (see Figure 20), across all the track lengths.

On the longest of the shortened tracks (140cm long) the place cell activity bump propagates according to path integration inputs past the midpoint of the track, after which, as the rat approaches the end of the track, visual inputs start to dominate, causing bump realignment, such that the place cells which fire at the end of the full length track (those in column 76) fire when the rat reaches the end of the shortened track.

On the second longest of the shortened tracks (120cm long), the path integration input (with G = 2.1) also manages to drive the bump past the midpoint (i.e. the pattern of place cell firing remains locked to the distance travelled from the starting box rather than the distance to the end ahead of the rat until after halfway down the track). Soon after the mid-point of the track, since this track is shorter than the previous one, strong sensory inputs coupled with a large mismatch between internal representation and external information, generate quite a rapid realignment of the activity profile. Notably, similar rapid continuous realignment of the activity profile of Gothard et al's

rat A takes place on the shortened track of similar length, and not on any other one, like in our simulations. However, in our case the phase of rapid realignment did not last sufficiently long for complete realignment of the place cells firing pattern to the reference frame of the track ahead. Thus place cells in columns 71-76 had not fired by the time the rat reached the end of the track. The sensory inputs near to the end of the track have higher amplitude than those near the middle (see BVC tuning curves, Figure 22). Thus it maybe that either the connections from place cells to grid cells should be strengthened, or the firing rate threshold for synaptic transmission should be reduced, so that sensory inputs near the end of the track can force the grid cell representation to realign more quickly, via their effect on place cell firing. The second line in the plot demonstrates that, if path integration inputs are not sufficiently strong ($G = 1.5$ here), in principle the realignment may begin long before the midpoint of the track, even right in the beginning.

On the third longest of the shortened tracks (100cm long), simulations with $G = 2.1$ show a discontinuous jump in the place cell activity profile occurring in the first half of the track. Parameter values $G = 2.5$ and $G = 2.8$ also were tested, showing that the greater the influence of path integration on place cell firing (i.e., the higher the G value was), the latter along the track the jump happened. For example, with $G = 2.1$, the jump happened at 1/3 of the track length, whereas with $G = 2.5$ soon after the midpoint, and with $G = 2.8$ already near the end of the track. This is not surprising, since the stronger are the PI inputs, the stronger BVC inputs are required in order to shift the bump. And the stronger ones are those tuned to shorter distances.

On the fourth longest of shortened tracks the same three values of G (21, 2.5, 2.8) were simulated. Like on the previous track, the activity realignment took place via a

discontinuous jump of the activity bump for all three *G*s, with the jump occurring later on the track the stronger the value of G (i.e., the greater the influence of path integration on place cell firing). On this track length (80cm) all three jumped significantly earlier than on the 100cm track. This could be explained by the fact that the position of the jump relative to the boundary in front was approximately the same as on the 100cm track. This is because it is the boundary in front, not the one behind, which explains the behaviour of the model, since this is the boundary that generates BVC inputs to the place cells in our model which cause the deviation from the pure effects of path integration.

Interestingly enough, qualitatively similar behaviour of the activity profile of the place cells was recorded in Gothard et al.'s representative rat A during outbound journeys. Thus, on the two least-severely shortened tracks (140 cm and 120 cm), the activity profile re-aligns smoothly from the reference frame of the box to that of the end of the track to which the rat is running, and does so after the midpoint of the track. Equally, on the more severely shortened tracks (100cm and 80cm) the activity profile "jumps" discontinuously from the reference frame of the box to that of the rest of the track. The activity profile in the experimental data also appears to make the jump during the first half of the more severely shortened tracks, see Figure 20. In general, whether the bump shifts or jumps during the realignment, is determined by the magnitude of the mismatch between the internal representation and external sensory inputs. The place cells have symmetrical recurrent connection which allows only one stable activity bump at a time. When the second bump appears due to strong sensory inputs, the first either dissolves, if the distance between the two is too large, or 'flows' into the new one, if the two are sufficiently close to link up.

Figure 31. Firing profiles of four outbound-selective cells (1, 2, 3, 4) shown for all five lengths of outbound journey (running direction is indicated by the arrow). The horizontal lines represent the track, and the small rectangles represent the box. Cell 1 fired immediately after the rat exited the box, cell 2 fired farther away from the box, cell 3 fired approximately halfway between the box and the end of the track and cell 4 fired close to the end of the trackl. Adapted from Gothard et al., (1996b).

As can be seen from Figure 31, the firing field of cell 2 shrank progressively as the box moved closer to the end of the track. The firing rate of this cell was very low on box4-out trials and vanished on box5-out trials. Cell 3 showed decreased firing rate on box3-out trials and did not fire on box4-out and box5-out trials. Cells 1 and 4, which fired near the ends of the track, did not show such modulation of firing rate and firing field size with track length.

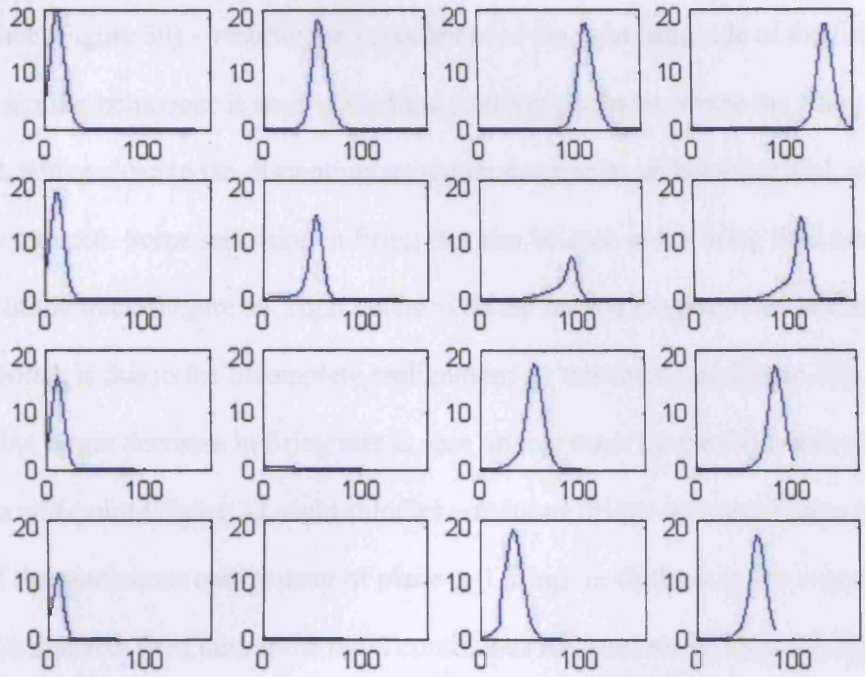

Figure 32. Firing profiles of four illustrative simulated place cells shown for four out of five lengths of outbound journey (the familiar 160cm track, 120cm, 100cm, 80cm). The top row corresponds to the full length track, the second from the top to the second longest of the shortened tracks, the second from bottom to the second shortest track and the bottom row to the shortest track. The first cell (left column) fired soon after the journey start, the fourth cell fired not far from the end of the track (right column), and the firing locations of second and third cells are approximately equally spaced between the locations of the first and the fourth ones (middle columns).

The plots of simulated place cell firing fields on the different track lengths qualitatively resemble those of Gothard et al. (1996b). The firing fields centred towards the start and end of the track (Figure 32, left and right columns respectively) maintain their location relative to the nearest end of the track across the different track lengths. On the shortest track, the firing field near the start of the track (Figure

32, left column) overlaps the point at which the discontinuous realignment of firing takes place (Figure 30) – resulting in curtailment of the right hand side of the firing field. A similar behaviour is seen in Gothard et al's experiment, where the firing rate of cell 2, active close to the discontinuous realignment point on box4-out trial, is strongly reduced. Some reduction in firing can also be seen in the firing field near to the end of the track (Figure 32, right column) on the second longest of shortened tracks, which is due to the incomplete realignment on this track (see Figure 30). A similar but larger decrease in firing rate is seen on this track for the field centred just after the mid-point (Figure 32, right-middle) – reduced firing corresponding to the point of the continuous realignment of place cell firing. In Gothard et al's experiment, the cell 3 that also fired during the rapid continuous realignment on the same type of track, demonstrates a substantial decrease in firing rate as well.

The firing field centred just before the middle of the track shows the greatest changes in firing rate as the track progressively shrinks (Figure 32, left-middle column). This firing field completely overlaps the point of place cell realignment on the shortest two tracks. As the realignment happens this cell ceases firing – it is one of those cells that were skipped during the discontinuous realignment. The rapid re-appearance of the bump of place cell activity following discontinuous realignment can be seen in the firing field centred just after the mid-point of the track (Figure 32, right-middle) – the firing field on the shortest track has a sharp cut off at the left side , which is due to the near instantaneous bump appearance in this location.

One aspect of the simulated place cell firing fields not seen in the examples shown by Gothard et al. is that of a cell whose firing is reduced on the second longest of shortened tracks but which recovers on the shorter tracks (Figure 32, right-middle

column). This can happen in the simulations because the realignment point occurs later (past the midpoint) on the longer tracks - affecting the firing of place fields centred there, but occurs earlier (before the midpoint) on the shortest tracks, allowing firing fields located past the midpoint to fire normally. Although the experimental data shows a similar tendency for early realignment on shorter tracks, it is not clear whether the same reduction and recovery of firing is seen in experimental data from individual trials. The Gothard et al's cell 3 fires earlier on the full length track (around the midpoint) than our cell 3 does, and the cell in our simulations that fires at the same location on the full track as the Gothard et al's cell3, ceases firing on the two shortest tracks as well. On the other hand, the figures shown by Gothard et al. (1996b) average the data over several runs, so that such effects would be obscured by any run-by-run variability in the realignment point.

The observed tendency for the realignment point to shift earlier on shorter tracks (in simulation and experiment) is in apparent contradiction to the observation of Redish et al. (2000) – that the realignment point tends to occur a fixed time after the start of a run, rather than a fixed distance. However, it is also true that rats run faster on longer tracks than on shorter ones (which is not simulated here). This leaves scope for either interpretation to be true, and indicates that further investigation is required for resolution of this point.

What happens to the grid cells during the place cell realignment? This experiment (recording grid cells in the situation of Gothard et al, 1996b) has not yet been performed, to our knowledge. However the model presented here makes a clear prediction: because we assume that place cell firing is used to reset the otherwise path-integration driven firing of grid cells. Thus, there should be a smooth

compression of the grid in the region of the smooth realignment of place cell firing on the slightly shortened tracks, and a significant disruption or discontinuity in firing of grid cells in the location of the abrupt realignment of place cell firing on the shortest tracks.

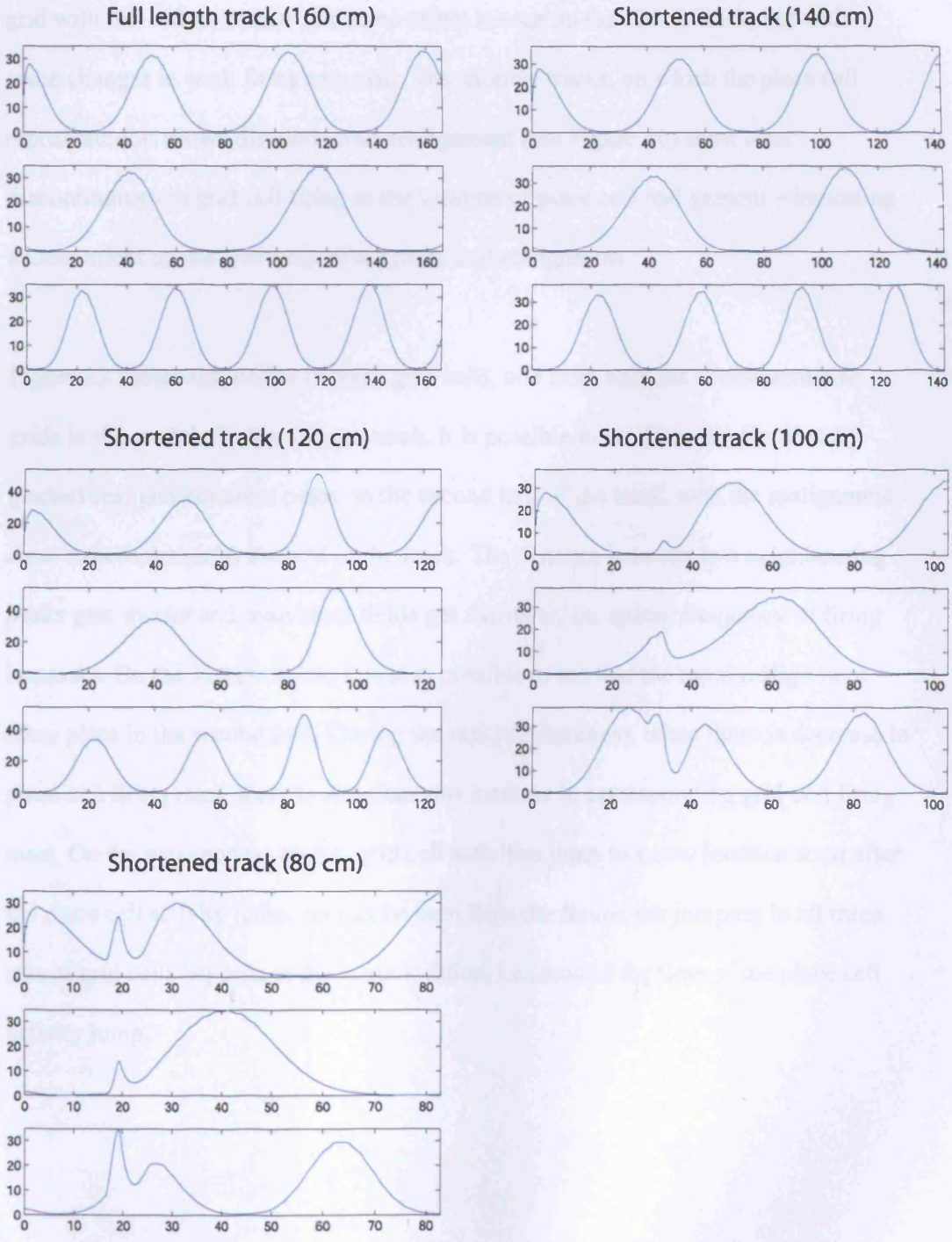

Figure 33. Firing fields of three simulated grid cells from the three sets with different sizes in the model. Each plot corresponds to a simulation on the track length shown above the plot, with the same cells shown in the same rows in each plot. Smooth distortion of the grids is seen on the 140cm track (cf. location of final bump in each grid with the 160cm track). The same effect is seen on the 120cm track, but with some changes in peak firing rate also. The shortest tracks, on which the place cell representation shows discontinuous realignment (see Figure 30) show clear discontinuities in grid cell firing at the location of place cell realignment – indicating a clear effect on the grid cells of the place cell realignment.

Figure 33 shows simulation of three grid cells, one from each set of different size grids in the model. On the 140 cm track, it is possible to see from the plot that a gradual realignment takes place on the second half of the track, with the realignment close to completion by the end of the track. The distance between two neighbouring peaks gets shorter and individual fields get narrower, i.e. spatial frequency of firing increases. On the 120 cm track, it is also possible to see that the rapid realignment takes place in the second half. During the rapid realignment, when there is decrease in place cell firing rates, there is simultaneous increase in corresponding grid cell firing rates. On the two shortest tracks, grid cell activities jump to a new location soon after the place cell activity jump. As can be seen from the figure, the jumping in all three sets of grid cells happens at the same location, i.e., around the time of the place cell activity jump.

These results provide a clear experimental prediction of the model, although the problems of averaging experimental data trial-by-trial, when the location of place cell realignment may vary from trial to trial will need to be borne in mind.

6.3.3 Simulation of the Barry et al. (2007) grid cell experiment

An interesting experiment, involving recordings from grid cells, was recently performed by Barry et al (2007). During the experiment they changed the shape and size of an environment in a way similar to the experimental studies of O'Keefe and Burgess (1996), while recording grid cell responses. When the original environment was compressed, a partial compression of grid-like firing patterns of grid cells occurred. See Figure 34.

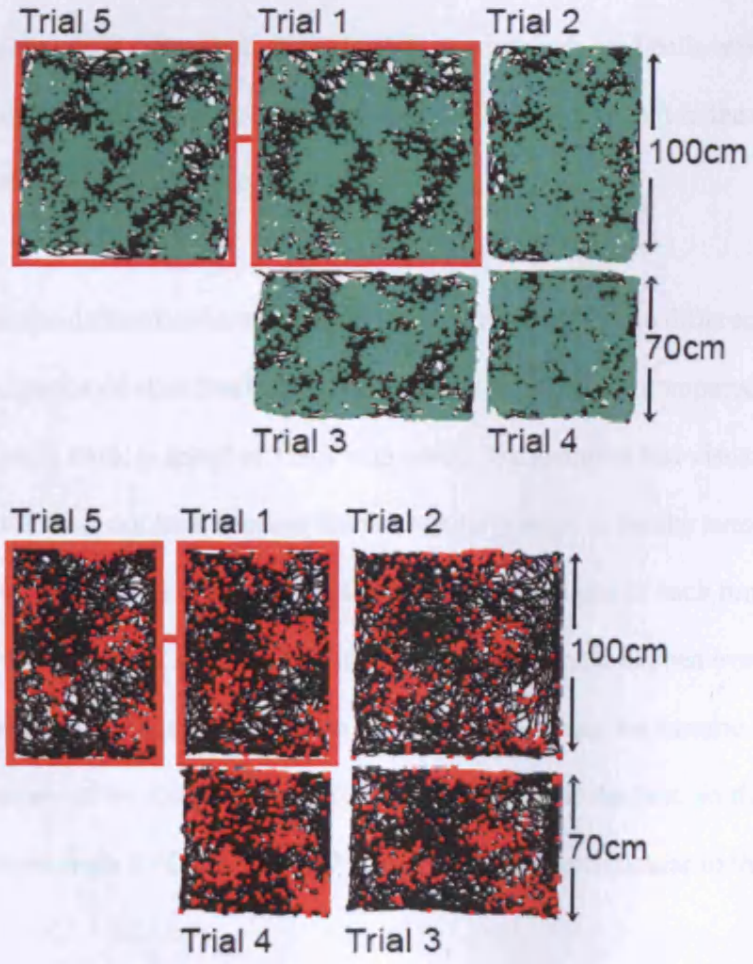

Figure 34. Examples of the deformation of the grid-like firing pattern of an entorhinal grid cell when the familiar environment for the rat (Trials 1 and 5: square box above, rectangular box, below) is changed in size and shape (Trials 2-4). The grid squashes (above and below), or stretches (below) by approximately 50% of the change in the size of the environment, although the initial amount of squashing is nearer to 80% and reduced with repeated exposure to the manipulation. Adapted from (Barry et al., 2007).

We attempted to simulate these experiments with our model, using the same parameters as above, but this time allowing the 'rat' to move randomly within a rectangular environment. A constant speed of movement was used, with direction varying smoothly from one time-step to the next. The connections between BVCs and place cells, place cells and grid cells and between grid cells were configured for a square environment, modelling the familiar environment in the experiments of Barry et al. (2007) shown in top half of Figure 34.

Some differences in our simulations are required by the different behavioural situation of slow freely-moving foraging within a box compared to repeated runs on a linear track (a speed of $V = 2$ was used). We assumed that visual inputs dominate in this case, not least because the rat regularly stops to eat the randomly scattered food rewards (on a linear track these are placed at the end of each run). And the realignment in accordance with visual inputs should happen every time the rat stops, which it does regularly, while foraging. In addition, we assume that the rat is equally aware of the distances to all four walls making up the box, so that each place cell gets input from BVCs tuned to all four directions perpendicular to the box walls.

Since place cells get inputs from BVC inputs from all four walls in these simulations, the amplitude of each is simply $A(d_i) = 1.218 - 0.0042d_i$, see Section 5.3.1. In addition, we assume that the four inputs are summed and then threshold at the level of place cell synapses, so as to get rid of the ridges associated with each BVC leaving only firing generated by the overlap of more than one BVC, thus giving a relatively localised sensory input to the place cells. Since the threshold level is high (at 0.4 below maximum summed firing rate found in the box), this threshold input is then amplified by a factor of 12.

Our interpretation that visual resetting of grids dominates the influence of path integration during free foraging is supported by the following observation. If path integration has an effect comparable to the BVC induced resetting, we would expect individual grid nodes shifting according to the direction in which the rat had most recently run – maintaining the distance from the wall behind the rat. In time-averaged data, firing fields in the middle of the box would appear blurry or stretched out. Yet we do not see anything like this in the data. On the contrary, not that much blurring of individual nodes is observed, they appear to be pretty localised. Specifically, the nodes, associated with the centre of the environment typically preserve their central position across various box configurations.

Each time the rat stops, our model resets itself in accordance with visual inputs, thus allowing for correction of accumulated error. Also, if some error accumulated along a particular direction of rat movement, it will get corrected when the rat changes its direction to an orthogonal one, since now there is no path integration influence opposing the influence of the external inputs on the location of activity along the earlier direction. While foraging inside the box, the rat turns regularly, and therefore

path integration inputs may only be dominant for a very short time span. The stronger are the visual inputs that place cells receive, the higher is their firing rate and thus the inputs they provide to grid cells, allowing them to have stronger control over grid cells. If for some reasons visual inputs degrade, path integration will start to play a more important role in the firing of both grid cells, and also of place cells via their input from grid cells.

Figures 35 and 36 below show illustrative examples of the firing of place cells and grid cells in the simulation of the Barry et al. (2007) experiment. As we discussed above, the main effect is a smooth stretching and squashing of the firing patterns of both place cells and grid cells in response to the stretching or squashing of the environment. When the box width was reduced to 70% of its width in the familiar square configuration, the width of the grids (i.e., distance between grid nodes in that direction) reduced to 83% of their size in the familiar square environment, i.e. a reduction of 57% of the reduction of box. When the box was expanded to 143% of its width in the familiar square configuration, the grids expanded to 124% of their width in the familiar square environment, i.e. an expansion of 56% of the expansion of the box. This is a good qualitative match to the experimentally observed 49% of the environmental deformation (Barry et al., 2007). No discontinuous changes in firing were seen, in contrast to those seen in Gothard et al.'s run-by-run deformation of a linear track. I consider the causes of the reduction in grid cell deformation with repeated experience of the shape manipulation, seen in the experiment but not simulated in the model, in the General discussion chapter.

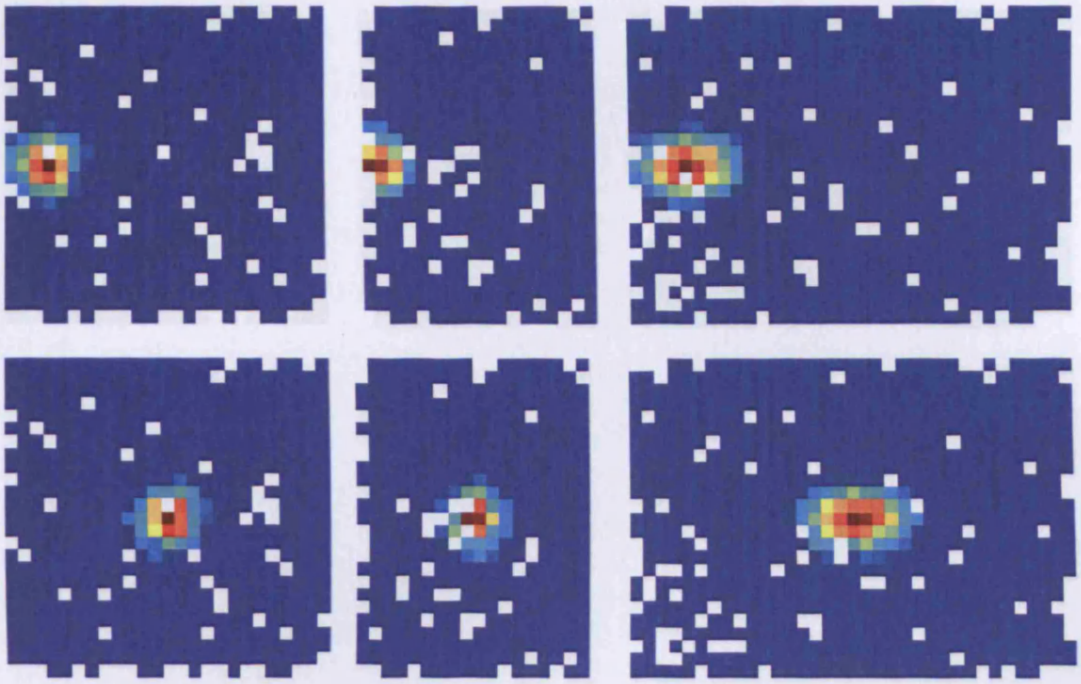

Figure 35. Examples of simulated place cells in the combined model, with place fields near to the edge (above) or centre of the environment (below). The square environment is 'familiar' in the sense that the models connections were set up to be consistent with this environment. The place fields squash and stretch with the deformation of the environment, emulating the behaviour seen by O'Keefe and Burgess (1996).

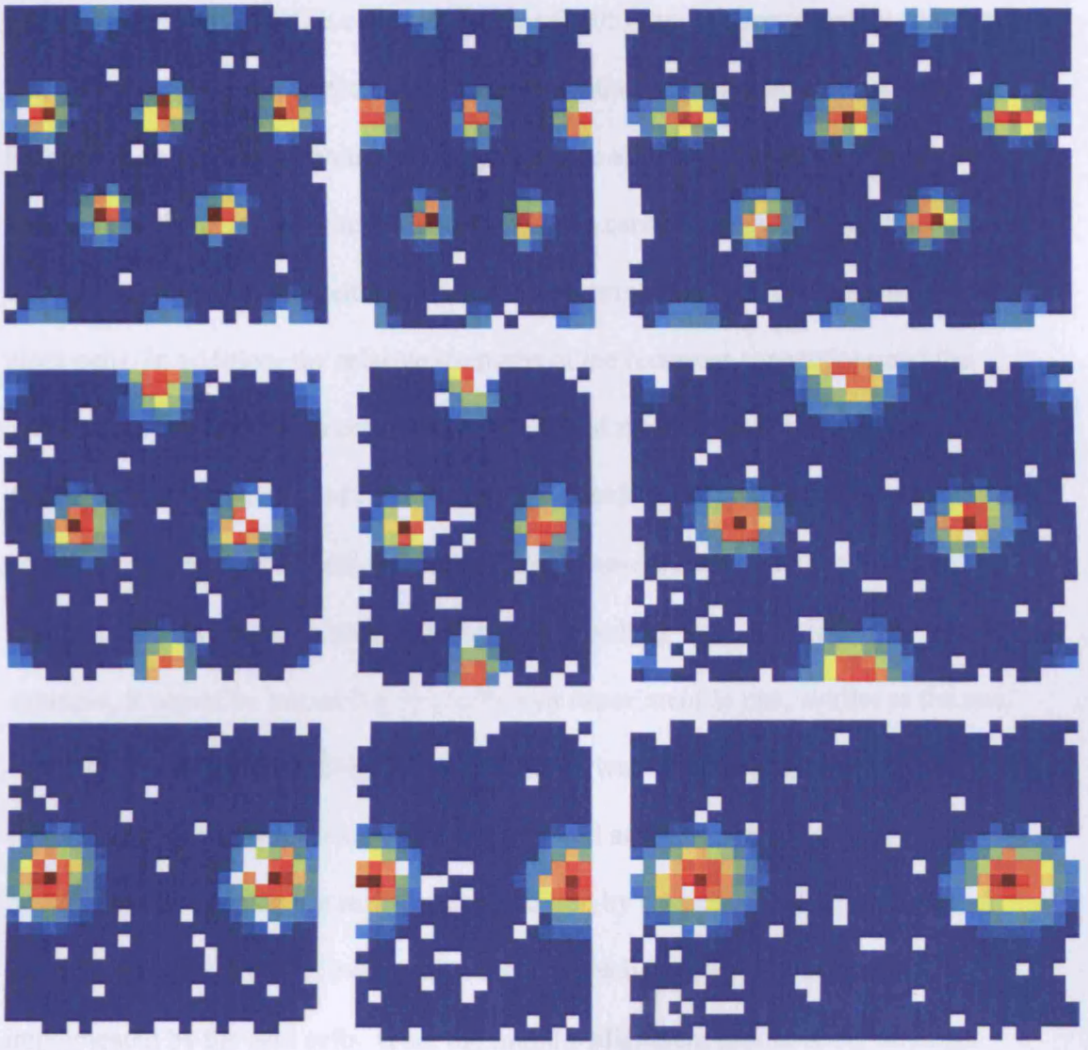

Figure 36. Examples of simulated grid cells in the combined model (small scale grid above; medium scale middle; large scale below). The square environment is 'familiar' in the sense that the models connections were set up to be consistent with this environment. The grid-like firing patterns squash and stretch with the deformation of the environment, emulating the behaviour seen by Barry et al (2007).

6.4 Modeling place cells and grid cells: interim conclusions.

I have shown, by simulation, that a combined place cell - grid cell model

of the type proposed by O'Keefe and Burgess (2005) can be approximately consistent with the observed experimental data. Performing these simulations enabled many of the precise assumptions behind this proposal to be specified. I specifically noted that the shape of the BVC input to place cells must be carefully chosen to be consistent with the operation of the continuous attractor recurrent network implemented by the place cells. In addition, the relative strengths of the recurrent connections and the connections between place cells and grid cells and those from BVCs to place cells directly affect the amount of deformation in O'Keefe and Burgess (1996)/ Barry et al (2007) experiments and the time course of realignment in Gothard et al (1996b) experiments. The model is able to make experimentally testable predictions. For example, it would be interesting to conduct an experiment in rats, similar to the one of Gothard et al, but recording from grid cells as well as place cells. It would be interesting to see how the realignment of grid cell activity takes place. It should be possible to test whether the realignment is driven by a conflict in which perceptual input from ahead of the rat eventually resets the path integrative mechanism implemented by the grid cells. If so, the initial realignment should occur amongst place cells, and earlier in some than others (as some may happen to have stronger BVC inputs from ahead than others), while the grid cell activity should realign later and coherently (the coherence ensured by their recurrent connectivity).

7. General discussion.

The use of computational modeling has allowed us to further understand some of the neuronal mechanisms behind eye movement control, and how this mechanism can go

wrong. I also used computational modeling to investigate the neural bases of processing of whole body motion relative to the external world. In both cases internal movement-related signals interact with external, perceptual, signals to determine position. On a more general level, it has become obvious that estimation of location needs to take into account both motion-related and perceptual information. Using perceptual information alone would be effortful and slow – having to observe the effects of motion so as to calibrate it. This would, for example, greatly restrict the speed of eye-movements. In addition, it would fail during any temporary absence of stable perceptual landmarks. Equally, relying on motion related information alone would rapidly accumulate error which must be corrected by perceptual input.

In both the oculomotor system for eye movement and the hippocampal system for processing self-location, study of the dynamics and stability of attractor representations proved useful. Our proposed model of the saccadic system is more physiologically plausible than the previous non-linear dynamics model by Broomhead et al (2000), and explicitly contains the pause cells. The model demonstrates that burst neurons with overlapping sigmoidal response functions do indeed show 'on' and 'off' responses similar to the ones found experimentally (Van Gisbergen et al, 1981), when inhibited by the pause cells. By varying the strength of the burst neurons' inhibition by the pause cells and the strength of the mutual inhibition between the burst cells, the model can generate the behavior observed in such clinical disorders as microsaccadic flutter and ocular flutter. However, it cannot simulate the whole frequency range of oscillations observed in microsaccadic flutter. Nevertheless, this problem can be resolved if inhibitory burst neurons are explicitly included in the model, which would make it even more physiologically realistic. Incorporating a pair of inhibitory burst neurons in the current model to allow

pathological off responses to be simulated would allow oscillations to develop directly through a Hopf bifurcation and also through a pitchfork bifurcation followed by a Hopf bifurcation. This would give rise to a system able to generate microsaccadic oscillations, as well as jerk nystagmus waveforms (Akman et al, 2005).

Moving on to the hippocampus, the initial self location model involved only place cells and perceptual (BVC) inputs to them in addition to recurrent connections between them. Neurophysiological findings during the course of my work indicated a slightly different model, in which the place cells, with their BVC inputs, work in tandem with 'grid cells' in entorhinal cortex which provide the substrate for path integration via recurrent connectivity. The grid cell – place cell model presented in this work is the first to properly integrate perception and motion inputs to place cell and grid cell firing. It allows investigation of the hypothesis that grid cells and place cells combine to represent the animal's current location as a compromise between perceptual and path integrative information. The fact that the model reproduces well the firing rate data from the experiments of Gothard et al (1996) and Barry et al (2007) supports the plausibility of the hypothesis. The model also makes neuronal firing predictions that could be tested in future animal studies in order to further verify the specific implementation of the hypothesis that we explored. In addition to neuron firing predictions, future work could also use the model to make predictions for behavioral studies, e.g. as Hartley, Trinkler and Burgess (2004) did in predicting search patterns in spatial memory using the perceptual-only BVC model of place cell firing, but now also including grid cell-mediated path integration. Subsequently, if the model proves to be correct, it could be used to design behavioral experiments for testing for the earliest stages of Alzheimer's disease, which starts in the entorhinal cortex (Braak and Braak, 1991).

Below I consider further the implications of the ongoing development of a model of the hippocampal processing of self-motion. The combined grid cell – place cell model seems to be an advance on the place cell only model, not only because grid cells actually exist and must serve some purpose, but also because it is easier to see how this system could arise from an unsupervised learning rule. This will be a promising area for future development of the model, see below.

7.1 Future work: Plasticity/learning of connections, and remapping.

The analysis and simulations presented here involve pre-configured patterns of connections. I did not address how these patterns arise, either during development or during experience of a particular environment. Some authors assume that the basic connections supporting path integration are indeed pre-configured or "hard-wired," presumably by some developmental rather than genetic process (McNaughton et al., 2006) which I return to in the General Discussion. However, it seems likely that at least the connections between place cells and grid cells are learned during the initial exposure to a novel environment. That is, connections will be formed between those place cells and grid cells which happen to fire in the same location on first exposure to an environment, presumably via some unsupervised Hebbian learning rule. In this way, an appropriate set of grid cells can provide input to a place cell (all those with grid nodes overlapping with the place field) so as support continued firing of the place cell when sensory input is not available. In return, an appropriate set of place cells can provide input to a grid cell (all those with place fields overlapping the

various nodes of the grid) so as to ensure that the grid-like firing pattern remains stable relative to the environment.

The simulation of experience-dependent connection weight modification will be an important aspect of future work as it may potentially explain some interesting aspects of the experimental data. Most notably, the squashing or stretching of grids observed by Barry et al. (2006) only occurs when a familiar environment is deformed. When the rat is taken from a familiar environment and put into a new environment of different size or shape, no stretching or squashing is seen (Barry et al., 2006; supplementary information). According to the model, deformation of the environment causes deformation of the grid-like firing pattern of grid cells because it changes the BVC inputs to place cells and the place cells affect grid cell firing via the connections from place cells to grid cells. When the rat is put into a novel environment place cells typically adopt a new firing pattern in which a new subset of place cells are active, and those cells which are active in both environments have unrelated firing fields (a phenomenon know as "remapping," Bostock et al., 1991; a randomly selected 30% of place cells appear to be active in a given environment, with 9% active in two distinct environment Guzowski et al., 1999). Thus, the exposure to a new environment, of whatever size or shape, will not cause deformation of the grid, as largely different place cells from those with connections learned in the familiar environment will now be active. New connections from these cells to grid cells will be learned as the new environment becomes familiar.

The possible plasticity of connections between place cells and grid cells may also explain the slow variation observed in both place cell firing and grid cell firing over multiple trials in which an environment's shape or size is altered. The initial response

of place cells and grid cells to variations in shape or size is parametric, as shown by O'Keefe and Burgess (1996) for place cells and Barry et al (2007) for grid cells, and simulated above. However, after repeated exposure to this manipulation over several days, the place cells begin to remap (Lever et al., 2002); eventually firing differently in the two environmental configurations, and the extent of deformation of the grids begins to reduce (Barry et al., 2007). These two findings may result from the grid cells having a tendency to produce grid-like firing patterns with a specific spatial scale (determined by the recurrent connections they receive). After deformation of a familiar environment, the grids are deformed by the input from place cells: forcing the firing of each node to occupy specific locations to match the new positions of firing of the place cells from which the grid cell receives connections. However, "remapping" of the pattern of place cell firing so that different cells fire in the differently shaped environmental configurations would allow grid cells to fire at a spatial scale consistently with the input received both via recurrent connections and via connections from place cells. In return, grid cells may have a tendency to fire at nearer to their natural spatial scale in the deformed environment than would be consistent with their place cell inputs. Such a tendency would introduce a conflict between the path-integrative input to place cells (from grid cells) and the perceptual input to place cells (from boundary vector cells), and this might be the cause of the slow remapping of place cells observed by Lever et al. (2002).

The above discussion explains the apparent contradiction between the squashing and stretching observed by Barry et al. (2006) and the absence of this effect reported by Hafting et al. (2005) when the same grid cells were recorded in a large cylinder and in a small cylinder. Crucially, the rats were already familiar with both cylinders, and presumably had different place cell representations for each.

7.2 Do grid cell and place cell representations complement each other?

What does the discovery of grid cells contribute to the continuous attractor models of path integration amongst place cells? The continuous attractor models of place cell firing had been proposed by Zhang (1996) and Samsonovich and McNaughton (1997) long before the discovery of grid cells in 2005, see Chapter 4. The grid cell firing patterns are strongly suggestive of providing a continuous attractor mechanism for path integration, and have been assumed to support this aspect of the preceding models, see Fuhs and Touretzky (2006), McNaughton et al. (2006) and Chapter 6. What benefit do they bring?

There are three differences between the grid cell representation of space and the place cell representation of space which have obvious implications of the formation of appropriate recurrent connections for a continuous attractor. First, grid cells fire within a regularly repeating array of locations across an environment, whereas most place cells fire in a single location. Second, grid cells are topographically organised so that physically nearby cells have similar (but offset) firing locations (Hafting et al., 2005), whereas place cells are not topographically organised (O'Keefe et al., 1998; Redish et al., 2001). Third, grid cells do not remap between different environments: the relative locations of the firing patterns of different grid cells do not change (Fyhn et al., 2007), whereas place cells often do remap between very different environments (Bostock et al., 1991; Wills et al., 2005; Fyhn et al., 2007). All of these differences would facilitate the formation of recurrent connections capable of supporting path integration amongst grid cells compared to place cells. These connections are presumably formed during development via an unsupervised activity-dependent

learning. For grid cells, the connection weight between two cells could be adjusted when the rat is in multiple locations across a single environment and when it is in different environments, and will involve physically nearby cells. For place cells, there will be far fewer opportunities to adjust such a connection weight due to the single firing location and remapping between environments (which implies that different weights are required for continuous attractors in different environments), and would involve well separated cells. The requirement for place cell continuous attractor models to have different patterns of connections in different environments is not insurmountable, see Samsonovich and McNaughton (1997), but the advantage of the grid cell representation in this regard is clear. See O'Keefe and Burgess (2005) for further discussion.

The existence of a place cell representation separate from the grid cell continuous attractor also has advantages in terms of the ease of association of locations to sensory input (e.g., BVCs) and to 'output' functions such as identifying specific locations with their contents or likely positive or negative outcomes (i.e., "goals" or places to avoid). Thus the existence of a separate place cell representation allows the BVCs to be summed and thresholded before contributing to the continuous attractor. This may make the resetting of the continuous attractor path integration more precise compared to direct input of BVCs to a place cell continuous attractor. In addition, the mediation of path integration by recurrent connections between grid cells leaves the recurrent connections between place cells in region CA3 free for other purposes. These include the formation of different continuous attractors for different environments. Thus the place cells can remap between different environments, and perform pattern completion within these remapped representations to accommodate minor sensory changes or cue removal (Wills et al., 2005; Nakazawa et al., 2002) on

the basis of the CA3 recurrent connections, independent of the recurrent connections between grid cells. Given that the grid cell representation does not remap, which facilitates development of appropriate recurrent connections for path integration, it is useful to have a separate place cell representation to which to associate goal locations, for two reasons. First, the place cells tend to code for single locations, enabling unambiguous representation of a single goal location. Second, the place cell representations remap, allowing different goal locations to be represented in different environments.

7.3 Relation to alternative models of path integration.

7.3.1 The Droulez and Berthoz continuous attractor model.

The vast majority of models of the path integration component of place cell firing, and of the firing of grid cells *per se*, follow the idea of the creation of a continuous attractor for firing patterns by an appropriate organisation of recurrent connections. These in turn follow the model of Droulez and Berthoz (1991) of the superior colliculus: shifting a bump of activity around a sheet of cells by asymmetric recurrent connections between neighbouring cells. In the superior colliculus, the location of the bump of activity reflects eye position, whereas in the hippocampus it reflects the animal's location within the environment. Thus, in Droulez and Berthoz's model, the strength of the asymmetric recurrent connections must follow the angular velocity of the eye, while in place cell or grid cell models it must follow the velocity of the animal. The relative strengths of the symmetric and asymmetric interactions between cells determine the speed with which the bump of activity shifts, as laid out in Zhang's theoretical paper (Zhang, 1996).

7.3.2 The grid cell driven model of Sheynikhovich et al.

Sheynikhovich et al (in prep) propose a model for spatial updating in which path integration is performed by different groups of grid cells. Each group contains recurrently interconnected cells with the same specific spatial frequency and orientation of firing fields, with different groups having different frequencies and orientations (although recent data suggests that the grids of all cells within one hemisphere actually have the same orientation, Barry et al., 2007). Visual inputs are provided directly to grid cells (not via place cells as in our model), and anchor their firing patterns to the environment. Place cells are recurrently interconnected, and are driven only by feed-forward inputs from different groups of grid cells. The visual input in the model is represented exclusively by a snapshot of the environment, subsequently processed by a large set of orientation-sensitive visual filters. The agent's allocentric position and head direction are extracted from visual inputs by matching the currently perceived snapshot (represented by the responses of the visual filters to the input image) with multiple snapshots stored in memory during exploration.

Sheynikhovich et al argue in their paper that since it is 'simpler and biologically more plausible' to explain experimental data with their visual snapshot matching approach, then there is no need for complex geometrical feature extracting mechanisms, like the one involving BVCs. Yet their proposed approach to visual information processing also appears to be fairly complicated, and perhaps not that physiologically plausible, since many different snapshots of the environment need to be stored in memory during initial exploration. On the other hand, neurons with firing patterns resembling those of BVCs have been found in subiculum (Lever in Barry et al, 2006) and in entorhinal cortex (Soldstat, Moser and Moser, pers. com. to NB; Csicsvari, pers. com.

to NB). In addition, some experiments have shown barriers to influence place cell firing (Muller and Kubie, 1987) and search location in the water maze (Maurer and Derivaz, 2000) even when made of transparent material. In our model, partial grid squashing/stretching (around half of the environment deformation, see Barry et al, 2007) is achieved due to the specific properties of BVC response curves. Sheynikhovich et al do simulate some place fields which stretch when a familiar environment is deformed. However, they do not provide any squashing/stretching simulation results for grid cells, so it is not yet clear whether their visual snapshot approach can account for the phenomenon observed by Barry et al.

7.3.3 The Byrne et al spatial memory and imagery model.

One exception to the standard continuous attractor model is provided by the model of human spatial memory and imagery by Byrne et al (2007), which addresses the relationships between long-term memory, short term memory and imagery, and between egocentric and allocentric and visual and idiothetic representations. According to the authors, the functional architecture of the model was largely informed by thinking about imagery and planning in human spatial memory. Long-term spatial memory is modelled within medial-temporal allocentric representations, and short-term memory is modelled as egocentric parietal representations within the 'parietal window' circuit, driven by perception, retrieval, and imagery. The medial-temporal place cell representation of location functions as a continuous attractor, due to the presence of recurrent connections, much like the preceding models. However, in Byrne et al.'s model, place cells form part of a recurrent circuit containing Boundary Vector Cells (in parahippocampal cortex) and visual texture cells (in perirhinal cortex). Thus the activity of place cells, BVCs and texture cells all

influence each other and form a single continuous attractor for all three types of information. The connections weights involved are learned during exploration of a familiar environment, so that only combined representations consistent with being at a single location in that environment are included in the continuous attractor.

Encoding from short-term into long-term memory (bottom-up path), as well as retrieval from long-term into short-term memory (top-down path), requires translation between egocentric and allocentric representations. The egocentric-to-allocentric transformation is accomplished in the model by a circuit that combines head direction information with egocentric spatial input from the parietal window. The transformation circuit, assumed to be supported by neurons in the retrosplenial and posterior parietal cortices, is comprised of a set of N identical neural subpopulations, each tuned to a specific head direction. Each subpopulation encodes a rotated egocentric map consistent with the direction of its preferred heading. Thus, connections between the parietal window and any one of the transformation subpopulations are weighted such that a rotated version of the egocentric spatial information contained in the parietal window is projected onto that transformation sublayer. The model has 20 such sublayers, corresponding to evenly spaced allocentric directions. Each transformation sublayer then projects an identical copy of its activation pattern onto the layer of BVCs. By setting connections from the layer of head direction cells to the transformation neurons such that only the sublayer corresponding to the current head direction is active, the transformation from egocentric to allocentric coordinates is accomplished. During the allocentric-to-egocentric transformation, the allocentric BVC representation of the environment is projected identically onto each of the transformation sublayers. Each of these identical representations would be rotated through different angles by the weights

from the sublayers to the parietal window, but gaiting by the head direction system allows only the correct sublayer to maintain sufficient activity to drive parietal window neurons. The proposed mechanism is supported by the finding of posterior parietal 'gain field' neurons, whose firing is tuned to respond to specific egocentric locations but which is also modulated by orientation within the world (Snyder et al, 1998).

Spatial updating in the model is performed by manipulating egocentric parietal representations according to idiothetic information. Rotational and forward-translational egomotion signals act upon the egocentric parietal window representation of space via different mechanisms. In the case of rotation, the egomotion signal drives continuous updating of head direction cell activity, thus rotating the image that is projected into the parietal window from the BVCs. For the case of forward translation, the egomotion signal gates the top-down connections from the parietal transformation layer to the parietal window such that the 'normal' top-down weights connecting these regions are down regulated, whereas a second, alternate set of top-down weights are up regulated.

When there is no forward velocity signal, the normal top-down connections perform reconstruction of a head-centered egocentric representation of the model's current spatial surrounding in the parietal window by using information from place cell activity. Once up regulated by the velocity signal, the alternate set of top-down connections performs an almost identical function, except that the representation of space reconstructed in the parietal window is shifted backwards slightly in the model's egocentric space. When the next bottom-up phase begins, the shifted spatial information in the parietal window is transmitted through the transformation and BVC layers to activate place cells corresponding to the location slightly ahead of the

current one. This process is repeated during the next top-down/bottom-up cycle, and so on until there is no longer a velocity signal. This mechanism results in a regular updating of the model's internal representation of its space location.

Byrne et al assume a single spatial updating mechanism for both parietal and medial temporal representations, whereas our model implies that the updating can be performed separately for the two representations. Although our interpretation requires two separate updating mechanisms, their utility can be justified, since there are many spatial tasks for which only short-term egocentric memory is sufficient. Such tasks could be accomplished faster and with less resource if the updating took place locally within parietal cortex by the mechanism proposed by Byrne and Becker (2004), without the need to engage long term memory. On the other hand, continuous allocentric updating could also be done locally within the medial temporal lobe, sending spatial information to the parietal window only when there is a need for read-out into short-term egocentric memory, thus making the updating process easier and faster. This would also help to reduce an error that would otherwise accumulate due to the repeated rotational allocentric-egocentric transformations supporting updating in the Byrne et al model. If the number of transformation sublayers is 20, as in the Byrne et al model, this error could be considerable, since two closest alternative sublayer representations differ by 18 degrees. At the same time, the number of sublayers, which would enable sufficiently accurate spatial updating, does not appear to be physiologically plausible. In addition, since the spatial updating process in the model is not continuous, but cycling, forward translation modulation by the speed value may take place only during a top-down part of the cycle, so that a continuously varying speed of movement would generate additional error.

Finally, the recently discovered grid cells (Hafting et al., 2005) have striking spatial correlates of firing which are highly suggestive of an involvement in path integration (McNaughton et al., 2006). In addition, lesions to parietal and hippocampal areas have dissociable effects on path integration in rats – suggesting that both areas support distinct path integration mechanisms rather than combining to support a single mechanism (Save, Gauzzelli, Poucet, 2001). Both of these finding support our hypothesis of a local medial-temporal mechanism for allocentric updating, without denying the existence of parallel egocentric mechanisms in parietal or retrosplenial areas.

7.3.4 The oscillatory interference model of Burgess et al.

A completely different alternative to any of the above continuous attractor approaches has recently been proposed, in which grid cell firing is assumed to reflect an interference pattern between two or more sub-threshold oscillations in the cell's membrane potential (Burgess et al., 2007). This model builds upon an earlier model of the "theta-phase precession" seen in place cell firing (O'Keefe and Recce, 1993; Lengyel et al., 2003). A baseline oscillation at the frequency of the theta rhythm of the EEG interferes with a dendritic membrane potential oscillation which increases in frequency above theta frequency as a result of synaptic input to the dendrite. This synaptic input is assumed to be both cosine tuned to a preferred heading direction and proportional to running speed. Thus the envelope of the interference pattern, which varies with the phase difference between the two oscillations (i.e., the integral of their frequency difference), will vary with distance travelled in the preferred direction. The spatial array of grid cell firing locations corresponds to the product of several interference patterns with preferred directions differing by multiples of 60°

The oscillatory interference model offers an alternative to the continuous attractor mechanisms for path integration discussed here: using phase differences to integrate velocity encoded as frequency differences. Which mechanism turns out to represent the best model for grid cell firing will be determined by experimental evidence. However, the two mechanisms need not be incompatible. For example, the mechanism of the oscillatory interference model appears to be compatible with the basic oscillatory properties of the stellate cells in medial entorhinal layer II (Giocomo et al., 2007), and the presence of neurons whose firing rate reflects head-direction and running speed in the deeper layers of mEC (Sargolini et al., 2006). Thus, the oscillatory interference mechanism may provide initial grid-like firing patterns which enable the appropriate recurrent connections to develop via some unsupervised (e.g. Hebbian) learning process. In return, evidence for the effects of recurrent connections between grid cells includes the fact that all of the grid-like firing patterns, at least those from the same hemisphere, have the same orientation, and have clustered spatial scales (Barry et al., 2007).

8. References.

Abadi, R.V., Scallan, C. and Clement, R.A. (2000) The characteristics of dynamic overshoots in square-wave jerks, and in congenital and manifest latent nystagmus. *Vis. Res.* 40: 2813-2829.

Abadi RV, Gowen E (2004) Characteristics of saccadic intrusions. Vision Res 44: 2675-2690

Akman OE, Broomhead DS, Abadi RV, Clement RA (2005) Eye movement instabilities and congenital nystagmus can be predicted by a nonlinear model of the saccadic system. J Math Biol. 51: 661-694 (2005)

Alyan S, McNaughton BL (1999) Hippocampectomized rats are capable of homing by path integration. Behav Neurosci 113: 19-31.

Amaral DG, Witter MP (1989) The three-dimensional organization of the hippocampal formation: a review of anatomical data. Neuroscience 31: 571-591

Ashe J, Hain TC, Zee DS, Schatz NJ (1991) Microsaccadic flutter. Brain 114: 461-472.

Bahill AT, Clark MR, Stark L (1975) The main sequence, a tool for studying human eye movements. Math Biosci 24:191-204

Barry C, Hayman R, Burgess N, Jeffery KJ (2007). Experience-dependent rescaling of entorhinal grids. Nature Neurosci 10: 682-684.

Barry C, Lever C, Hayman R, Hartley T, Burton S, O'Keefe J, Jeffery KJ, Burgess N (2006) The boundary vector cell model of place cell firing and spatial memory. Reviews in the Neurosciences 17(1-2), 71-79

Bostock E, Muller RU, Kubie JL (1991) Experience-dependent modifications of hippocampal place cell firing. Hippocampus 1: 193-205.

Braak H, Braak E. Neuropathological stageing of Alzheimer-related changes. Acta Neuropathol (Berl). 1991 Jan 1; 82(4):239-59.

Broomhead DS, Clement RA, Muldoon MR, Whittle JP, Scallan C, Abadi RV (2000) Modelling of congenital nystagmus waveforms produced by saccadic system abnormalities. Biol Cybern 82: 391-399

Burgess N (2006) Computational models of the spatial and mnemonic functions of the hippocampus. In: The Hippocampus. Eds: P. Andersen, T. Bliss, J. O'Keefe and R.G.M. Morris. Pp. 715-749. O.U.P.

Burgess N, O'Keefe J (2003) Spatial Models of the Hippocampus, in: *The Handbook of Brain Theory and Neural Networks*, 2nd Edition. Ed: Arbib M A, pp. 539-543. MIT press.

Burgess N, Barry C, O'Keefe J (2007) An oscillatory interference model of grid cell firing. Hippocampus, 17: 801-812

Burgess N, Recce M, O'Keefe J (1994) A model of hippocampal function. Neural Networks 7:1065–1081.

Byrne P, Becker S (2004) Modelling mental navigation in scenes with multiple objects. Neural Computation 16(9):1851-1872

Byrne P, Becker S, Burgess N (2007) Remembering the past and imagining the future: a neural model of spatial memory and imagery. Psychol Rev 114: 340-375

Cacucci F, Lever C, Wills TJ, Burgess N, O'Keefe J. 2004. Theta modulated place-by-direction cells in the hippocampal formation in the rat. J Neurosci 24:8265–8277

Carpenter RHS (1988) Movements of the Eyes. 2nd Edition. Pion Limited, London. p 70-72

Cressant A, Muller RU, Poucet B (1997) Failure of centrally placed objects to control the firing fields of hippocampal place cells. Journal of Neuroscience 17: 2531-2542

Dayan P, Abbott LF (2001) Theoretical Neuroscience. The MIT Press.

Debanne D, Gahwiler BH, Thompson SM (1998) Long-term synaptic plasticity between pairs of individual CA3 pyramidal cells in rat hippocampal slice cultures. J Physiol (Lond) 507: 237–247

Dhillon A, Jones RS (2000) Laminar differences in recurrent excitatory transmission in the rat entorhinal cortex in vitro. Neuroscience 99: 413-422

Doiron B, Longtin A, Berman N, Maler L (2000) Subtractive and divisive inhibition: Effect of voltage-dependent inhibitory conductances and noise. Neural Computation 12:1-22

Droulez J, Berthoz A (1991) A neural network model of sensoritopic maps with predictive short-term memory properties. Proceedings of the National Academy of Sciences 88:9653-9657

Etienne AS, Jeffery KJ. Path integration in mammals Hippocampus. 2004;14(2):180-92

Etienne AS, Maurer R, Seguinot V (1996) Path integration in mammals and its interaction with visual landmarks. J Exp Biol 199: 201-209

Fuhs MC, Touretzky DS (2006) A spin glass model of path integration in rat medial entorhinal cortex. J Neurosci 26: 4266-4276.

Fyhn M, Hafting T, Treves A, Moser MB, Moser EI (2007) Hippocampal remapping and grid realignment in entorhinal cortex. Nature 446:190-4.

Gancarz G, Grossberg G (1998) A neural model of the saccade generator in the reticular formation. Neural Networks 11: 1159-1174

Germroth P, Schwerdtfeger WK, Buhl EH (1991) Ultrastructure and aspects of functional organization of pyramidal and nonpyramidal entorhinal projection neurons contributing to the perforant path. J Comp Neurol 305: 215—231

Giocomo, LM, Zilli, EA, Fransen, E, Hasselmo, ME Temporal frequency of subthreshold oscillations scales with entorhinal grid cell field spacing. Science 315: 1719-1722.

Goodridge JP, Taube JS (1995) Preferential use of landmark navigational system by head direction cells in rats. Behav Neurosci 109:49-61

Gothard KM, Skaggs WE, Moore KM, McNaughton BL (1996a) Binding of hippocampal CA1 neural activity to multiple reference frames in a landmark-based navigation task. J Neurosci 16:823-35

Gothard KM, Skaggs WE, McNaughton BL (1996b) Dynamics of mismatch correction in the hippocampal ensemble code for space: interaction between path integration and environmental cues. J Neurosci 16:8027-40

Guzowski JF, McNaughton BL, Barnes CA, Worley PF (1999) Environment-specific expression of the immediate-early gene Arc in hippocampal neuronal ensembles. Nat Neurosci. 2: 1120-4.

Hafting T, Fyhn M, Molden S, Moser M-B, Moser EI (2005) Microstructure of a spatial map in the entorhinal cortex. Nature 436: 801-806

Hartley T, Burgess N, Lever C, Cacucci F, O'Keefe J (2000) Modeling place fields in terms of the cortical inputs to the hippocampus. Hippocampus 10:369–379

Helmholtz, H. von (1924). Treatise on physiological optics. (J. P. Southall, Ed). New York: Dover. (Original work published 1866).

Hopfield JJ (1982) Neural networks and physical systems with emergent collective computational abilities. Proc Natl Acad Sci U S A. 79: 2554-8.

Kali S, Dayan P (2000) The Involvement of Recurrent Connections in Area CA3 in Establishing the Properties of Place Fields: A Model. J. Neurosci. 20: 7463-7477

Laptev D, Akman O, Clement R (2006) Stability of the saccadic oculomotor system. Biol Cybern. 95: 281-7.

Lebedev S, Gelder PV, Tsui WH (1996) Square-root relations between main saccadic parameters. Invest Ophthalmol Vis Sci 37, 2751-2758

Leigh RJ and Zee DS (1999) The Neurology of Eye Movements. 3rd Edition. Oxford University Press, Oxford. p 91-92

Lengyel M, Szatmary Z, Erdi P (2003) Dynamically detuned oscillations account for the coupled rate and temporal code of place cell firing. Hippocampus 13: 700-714.

Lever C, Wills T, Cacucci F, Burgess N, O'Keefe J (2002) Long-term plasticity in hippocampal place-cell representation of environmental geometry. Nature 416: 90-4.

Lingenhohl K, Finch DM (1991) Morphological characterization of rat entorhinal neurons in vivo: soma-dendritic structure and axonal domains. Exp Brain Res 84: 57–-74

Lisman JE (1997) Bursts as a unit of neural information: making unreliable synapses reliable. Trends. Neurosci. 20:38-43

Markus EJ, Barnes CA, McNaughton BL, Gladden VL, Skaggs WE (1994) Spatial information content and reliability of hippocampal CA1 neurons: Effects of visual input. Hippocampus 4: 410-421

Maurer, R. and Derivaz, V., 2000. Rats in a transparent Morris water maze use elemental and configural geometry of landmarks as well as distance to the pool wall. *Spatial Cognit. Computat.* 2, pp. 135–156.

McNaughton BL, Battaglia FP, Jensen O, Moser EI, Moser MB (2006). Path integration and the neural basis of the 'cognitive map'. Nat.Rev.Neurosci 7: 663-678

McNaughton BL, Chen LL, Markus EJ (1991) "Dead reckoning", landmark learning, and the sense of direction: a neurophysiological and computational hypothesis. J Cognit Neurosci 3:190-202

Mel BW (1993) Synaptic integration in an excitable dendritic tree. J Neurophysiol 70: 1086—1101

Mel BW (1994) Information processing in dendritic trees. Neural Computation 6: 1031-1085

Miller, K.D. (1996) Synaptic economics: competition and cooperation in synaptic plasticity. Neuron 17:371-374.

Miller JM, Robins D (1992). Extraocular muscle forces in alert monkey. Vision Res, vol 32, isu 6, pgs 1099-1113.

H. Mittelstaedt and M.L. Mittelstaedt, Mechanismen der Orientierung ohne richtende Aussenreize, *Fortschr. Zool.* 21 (1973), pp. 46–58.

H. Mittelstaedt, Triple-loop model of path control by head direction and place cells, *Biol. Cybern.* 83 (2000), pp. 261–270.

Mizumori SJY, Williams JD (1993) Directionally selective mnemonic properties of neurons in the lateral dorsa l nucleus of the thalamus of rats. J Neurosci 13:4015-4028

Morris RG, Garrud P, Rawlins JN, O'Keefe J (1982) Place navigation impaired in rats with hippocampal lesions. Nature 297:681-683.

Muller, R. U., and J. L. Kubie (1987). The effects of changes in the environment on the spatial firing of hippocampal complex-spike cells. J. Neurosci. 7:1951-1968.

Naka KI, Rushton WA (1966) S-potentials from colour units in the retina of fish. J Physiol 185: 584-599

Nakazawa K, Quirk MC, Chitwood RA, Watanabe M, Yeckel MF, Sun LD, Kato A, Carr CA, Johnston D, Wilson MA, Tonegawa S (2002) Requirement for hippocampal CA3 NMDA receptors in associative memory recall. Science 297: 211-8.

O'Keefe J (1976) Place units in the hippocampus of the freely moving rat. Exp Neurol 51:78–109

O'Keefe (2007) Hippocampal Neurophysiology in the Behaving Animal. The Hippocampus Book (Chapter 11). Editors: Per Andersen, Richard Morris, David Amaral, Tim Bliss and John O'Keefe. Oxford University Press. 2007

O'Keefe J, Burgess N (1996) Geometric determinants of the place fields of hippocampal neurons. Nature 381:425–428

O'Keefe J, Burgess N (2005) Dual phase and rate coding in hippocampal place cells: theoretical significance and relationship to entorhinal grid cells. Hippocampus 7: 853-866

O'Keefe J, Burgess N, Donnett JG, Jeffery KJ, Maguire EA (1998) Place cells, navigational accuracy, and the human hippocampus. Philos Trans R Soc Lond B Biol Sci. 353:1333-40.

O'Keefe J, Dostrovsky J (1971) The hippocampus as a spatial map. Preliminary evidence from unit activity in the freely-moving rat. Brain Res 34:171–175

O'Keefe J, Nadel L (1978) The hippocampus as a cognitive map. Oxford: Oxford University Press.

O'Keefe J, Recce ML (1993) Phase relationship between hippocampal place units and the EEG theta rhythm. Hippocampus 3: 317-330

Optican LM, Zee DS (1984) A hypothetical explanation of congenital nystagmus. Biol Cybern 70: 291-302

Parron C, Save E (2004) Evidence for entorhinal and parietal cortices involvement in path integration in the rat. Exp Brain Res 159: 349–359

Ramat SJ, Leigh J, Zee DS, Optican LM (2005) Ocular oscillations generated by coupling of brainstem excitatory and inhibitory saccadic burst neurons. Exp Brain Res 160:89-106

Redish AD, Rosenzweig ES, Bohanick JD, McNaughton BL, Barnes CA (2000) Dynamics of hippocampal ensemble activity realignment: time versus space. Journal of Neuroscience 20:9298-9309

Redish AD, Battaglia FP, Chawla MK, Ekstrom AD, Gerrard JL, Lipa P, Rosenzweig ES, Worley PF, Guzowski JF, McNaughton BL, Barnes CA (2001) Independence of firing correlates of anatomically proximate hippocampal pyramidal cells. J Neurosci. 21: RC134.

Redish AD, Touretzky DS (1998) "The Role of the Hippocampus in Solving the Morris Water Maze". Neural Computation 10(1): 73-112

Samsonovich A, McNaughton BL (1997) Path integration and cognitive mapping in a continuous attractor neural network model. J Neurosci 17:5900–5920

Sargolini F, Fyhn M, Hafting T, McNaughton BL, Witter MP, Moser MB, Moser EI (2006). Conjunctive representation of position, direction, and velocity in entorhinal cortex. Science, 312: 758-762

Save E, Nerad L, Poucet B (2000) Contribution of multiple sensory information to place field stability in hippocampal place cells. Hippocampus 10:64-76.

Save, E., Guazzelli, A., and Poucet, B. 2001. Dissociation of the effects of bilateral lesions of the dorsal hippocampus and parietal cortex on path integration in the rat. *Behav. Neurosci.* 115:1212 -1223.

Scudder CA, Kaneko CRS, Fuchs AF (2002) The brainstem burst generator for saccadic eye movements. A modern synthesis. Exp Brain Res 142: 439-462

Skaggs WE, Knierim JJ, Kudrimoti HS, McNaughton BL (1995) A model of the neural basis of the rat's sense of direction. In: Advances in neural information processing systems 7 (Tcsauro G, Tourctzky DS, Leen TK, eds), p 173-180. Cambridge, Massachusetts: MIT.

Snyder L, Grieve K, Brotchie P, Andersen R (1998) Separate body- and world-referenced representations of visual space in parietal cortex. Nature 394: 887–891.

Sparks DL (2002) The brainstem control of saccadic eye movements. Nat Neurosci Rev 3: 952-964

Steffenach H-A, Witter MP, Moser M-B, Moser EI (2005) Spatial memory in the rat requires the dorsolateral band of the entorhinal cortex. Neuron 45: 301—313

Stringer SM, Trappenberg TP, Rolls ET, de Araujo IET (2002a) Self-organizing continuous attractor networks and path integration: one-dimensional models of head direction cells. Network: Computation in Neural Systems 13: 217-242.

Stringer SM, Rolls ET, Trappenberg TP, de Araujo IET (2002b) Self-organizing continuous attractor networks and path integration: two-dimensional models of place cells. Network: Computation in Neural Systems 13: 429-446.

Taube JS (1998) Head direction cells and the neurophysiological basis for a sense of direction. Prog Neurobiol 55: 225-256

Taube JS, Muller RU, Ranck JB Jr (1990a) Head-direction cells recorded from the postsubiculum in freely moving rats. I. Description and quantitative analysis J Neurosci 10:420–435

Taube JS, Muller RU, Ranck JB Jr (1990b) Head-direction cells recorded from the postsubiculum in freely moving rats. II. Effects of environmental manipulations J Neurosci 10:436–447

Van Gisbergen JAM, Robinson DA, Gielen S (1981) A quantitative analysis of generation of saccadic eye movements by burst neurons. J Neurophysiol 45: 417-442

Verdaasdonk BW, Koopman HFJM, Gils SA van, Helm CT van der (2004) Bifurcation and stability analysis in musculoskeletal systems: a study in human stance. Biol Cybern 91, 48-62

Whishaw IQ, Hines DJ, Wallace DG. Dead reckoning (path integration) requires the hippocampal formation: evidence from spontaneous exploration and spatial learning tasks in light (allothetic) and dark (idiothetic) tests. Behav Brain Res. 2001 Dec 14;127(1-2):49-69.

Wilson HR (1999) Spikes, Decisions and Actions. The dynamical foundations of neuroscience. Oxford University Press, Oxford. p 126

Zee DS, Robinson DA (1979) A Hypothetical Explanation of Saccadic Oscillations. Ann Neurol 5: 405 – 414

Zhang K (1996) Representation of spatial orientation by the intrinsic dynamics of the head-direction cell ensemble: a theory. J Neurosci 16:2112–2126